The biomechanics of lumbar total disc replacement impingement: *In silico* Investigations of polyethylene damage modes of lumbar total disc replacement

A dissertation

Submitted to the Faculty

of

Drexel University

by

Steven Anthony Rundell

In partial fulfillment of the

Requirements for the degree

of

Doctor of Philosophy

December 2010

Dedication

This dissertation is dedicated to my loving, beautiful wife, my son Jake, and unborn daughter.

Acknowledgements

Special thanks to Dr. Jorge Isaza, his family, and Stevie Guillory for their incredible hospitality. My visits to Baton Rouge and long conversations with Dr. Isaza regarding spine biomechanics gave way to many of the studies performed in this dissertation.

I would like to thank and acknowledge my academic advisor, Dr. Steven Kurtz, who provided me with valuable mentorship and guidance throughout the duration of my PhD work.

Thanks to Dr. Judd Day for his co-authorship and willingness to partake in long technical conversations in order to ensure the quality and novelty of the performed studies.

I would also like to acknowledge my committee members, Dr. Todd Doehring, Dr. Fred Allen, Dr. Rami Seliktar, and Dr. Sorin Siegler for providing valuable insight and critique of the performed work, which has ultimately vastly improved its quality and importance.

Thanks to Stephanie Siskey for all of her help with finite element pre and post processing. Additional thanks to Exponent's visual communications department (Chirs Espinosa, Gil Matityahu, Eric Wysocki, and Mike Drzal) for their help with 3D CAD surface repair.

Last but not least, I would like to acknowledge my fellow graduate students. Specifically, thanks to Ryan Baxter, Dan MacDonald, and Dave Jaekel. The journey towards a PhD can be trying, but having good friends to commiserate with made the hard times bearable.

Table of Contents

List of Tables

List of Figures

Abstract

The biomechanics of lumbar total disc replacement impingement: *In silica* Investigations of polyethylene damage modes of lumbar total disc replacement

Steven Anthony Rundell

Discogenic lower back pain results in a substantial reduction in the quality of life and affects a significant portion of the world's population. Currently, the gold standard for surgical intervention involves removing the lumbar intervertebral disc, which is thought to be causing the pain and fusing the adjacent bony vertebrae. This practice has existed for almost a century, and generally results in successful clinical outcomes. However, the lack of flexibility at the fused segment may lead to degenerated discs at adjacent levels. As a result, disc replacement technologies have been introduced as a motion preserving alternative to spinal fusion. Like preceding hip and knee replacements, these devices typically involve articulating bearing surfaces, which pose the potential for similar clinical failure modalities. Specifically, impingement of these devices can lead to accelerated polyethylene wear. Despite the relatively recent introduction of these devices, osteolysis has been reported in a small number of cases. Therefore, a better understanding of the biomechanical environment associated with impingement is needed in order to properly assess device performance. The current dissertation outlines several studies, which evaluated the biomechanics of total disc replacement. Specifically, an *in situ* model

of lumbar total disc replacement impingement was generated and validated based on clinical data from retrieved implants. The clinical parameters associated with impingement sensitivity were also determined in order to provide better guidance to both clinicians and designers.

Introduction

Low back pain is the fifth most common reason for all physician visits in the United States[1]. Americans spend approximately $50 billion per year on treatment for low back pain[1]. There are several potential underlying causes of low back pain, which include degenerative processes. Specifically, degeneration of the intervertebral disc, or degenerative disc disease (DDD), can result in chronic low back pain in some patients. This process has been characterized by a disruption of the normal annular fibers, reduction in water content, increase in collagenous tissue, narrowing of the disc space, and development of osteophytes. These changes result in the inability of the disc to maintain its mechanical function, and are associated with discogenic low back pain.

Treatment options for chronic discogenic low back pain typically initiate with physical therapy and pharmaceuticals. However, persistent pain may require surgical intervention. In general, lumbar spinal surgery often includes removal of either bony or soft tissue components which are thought to be causing the pain. This type of surgery is generally referred to as a decompression. In cases of discogenic low back pain, the intervertebral disc itself will be removed. Once removed, bone grafts are inserted into the evacuated space to facilitate arthrodesis (fusion of the bones) of the affected segment. This practice was performed as early

---

[1] In Project Briefs: Back Pain Patient Outcomes Assessment Team (BOAT). In MEDTEP Update, Vol. 1 Issue 1, Agency for Health Care Policy and Research, Rockville, MD, Summer 1994.

as 1911 by Drs. Fred Albee and Russell Hibbs[2]. Complications associated with these early fusion procedures included infection, pseudoarthrosis, thrombosis, embolus, and death[3]. Subsequently, metallic instrumentation, such as interbody cages, were introduced as a means of facilitating fusion between the bones[4]. The first interbody cage, the Bagby and Kuslich implant (BAK), was approved for implantation in humans in the United States on September 20, 1996, by the Food and Drug Administration (FDA). A multi-center study (19 centers and 42 surgeons) was performed to evaluate the use of the BAK implant for treatment of discogenic low back pain, which documented a fusion rate of 91% with a pain reduction of 84% at two years post-op[5]. As a result, interbody fusion became the gold standard of treatment for surgical intervention of degenerative disc disease.

Despite generally positive clinical outcomes for spinal fusion, degeneration of the adjacent segments, often referred to as adjacent segment degeneration (ASD) has been reported in numerous studies[6-10]. The mechanisms responsible for the onset of ASD following fusion are not well understood, and complicated by the difficulty associated with early diagnosis of degenerative disc disease. It remains unknown if the long-term degenerative changes adjacent to fused segments are causally related to the fusion or simply the product of natural progression of disc disease[11]. Several studies have indicated the presence of an altered biomechanical environment after fusion, which may be responsible for ASD. Specifically, Kumar et al. (2001), indicated a greater occurrence of ASD in patients with post operative

sagittal plane abnormalities. Additionally, *in vitro* studies have indicated greater deformation in the segments adjacent to fused segments[12-15].

Recently, total disc replacement systems (TDRs) have been introduced as an alternative to fusion. These devices are intended to restore the disc height, maintain or correct segmental lordosis, and preserve segmental range of motion[16]. Biomechanical studies have documented a reduction in adjacent level effects after TDR when compared with fusion [12, 17]. Disc replacement procedures were initially performed in the 1950s. Ulf Fernstrom introduced a type of arthroplasty involving implantation of a spherical endoprothesis (stainless steel ball bearing) into the center of an evacuated disc. Specifically, Fernstrom implanted stainless steel ball bearings following diskectomy, or for painful disc disease, and termed this procedure disc arthroplasty[18]. Fernstrom's intention was to provide a motion-preserving safer alternative to fusion, which he anticipated would prevent or forestall degenerative changes at the adjacent levels. However, the general lack of biomechanical knowledge at the time likely contributed to subsidence of these devices and consequent loss of the restored disc height.

Currently, almost 60 years later, there are two total disc replacements approved for implantation in the United States, and several more undergoing pre-clinical testing. The approved implants include a mobile (Charite, Depuy Spine) or fixed (Prodisc, Synthes Spine) polyethylene (PE) bearing surface between two cobalt chrome alloy endplates. The SB Charite artificial disc was invented by Kurt Shellnack, M.D., and Karin Buttner-Janz, M.D., Ph.D. at the Charite Center for Musculoskeltal surgery. In

general, its design consists of a mobile, or floating, polyethylene core with symmetric inferior and superior domed surfaces that articulate with two metallic footplates. The mobile core is free to rotate and translate, which provides a mobile center of rotation, which is thought to be consistent with the kinematics of the intact disc[19]. The SB Charite III was first commercialized by Waldemar Link GmbH and Co. in 1987. Since that time it has been used in multiple clinical trials[20-26]. Two FDA Investigational Device Exemption studies were performed[27, 28], which indicated that at 24 months post-op motion was maintained or restored, disc height was restored, and subsidence was significantly less then when compared with a BAK cage.

Unlike the Charite's mobile bearing design, the Prodisc consists of a fixed bearing surface. Specifically, a polyethylene core insert conforms and locks into the inferior metallic footplate. The superior face of the polyethelyene core is a domed surface that articulates with the conforming superior metallic footplate. It was originally conceived of by Thierry Marnay, M.D., in 1989. The Prodisc was approved by the FDA for implanation in the United States in 2006. Several clinical studies, which have evaluated the Prodisc's safety and efficacy have been performed[29-33]. In general, the clinical results suggest that, for the appropriate patient population, the Prodisc results are comparable or better than fusion.

Despite generally positive clinical results, complications have been reported. Due to the articulating polyethylene surfaces present in both FDA approved lumbar TDR designs, there is the potential for polyethylene wear debris. Specifically,

impingement of these devices has been observed clinically[34-36], and shown to result in damage to the polyethylene. Polyethylene wear debris is a well-documented clinical failure mode in both total knee and hip replacements. The particles associated with polyethylene wear can elicit an inflammatory response, which can result in periprosthetic osteolysis. This has lead to clinical failure of the knee and hip prostheses through aseptic loosening. Similarly, for TDRs, excessive wear of the polyethylene and associated osteolysis has been reported in a small number of cases [34, 37-40]. These data indicate the importance of understanding the long-term clinical wear performance of lumbar TDRs, especially since they are often indicated for young, active patients[41].

Determining the clinical wear performance of total disc replacement devices utilizing pre-clinical protocols can be extremely difficult due to the spine's complex loading environment, large variations in patient morphology and tissue properties, and disparity in surgical technique. Assessing this wide range of parameters using a combination of cadaveric and wear-testing techniques would be prohibitively complicated and costly. Finite element models pose an alternative to cadaveric experimentation that allows for the ability to control variation, and test for a wide range of parameters without excessive time and monetary cost[42, 43]. However, careful validation of these models is required to ensure that the results can be interpreted as predictive and indicative of what is happening in the real world. Specifically, the outcome measures provided by these analyses must be associated with known physical outcomes to ensure and quantify the level of predictability.

The primary objective of the current dissertation was to develop, verify, and validate a finite element model of *in situ* total disc replacement in order to characterize and understand the sensitive parameters of TDR impingement.

In chapter 1 of the current dissertation, the development and validation of a lumbar single motion segment finite element is introduced. Additionally, the sensitivity to nucleus replacement moduli is evaluated. In chapter 2, the finite element model is used to evaluate the very first disc replacement technology, the Fernstrom sphere, at varying levels of implant subsidence. Both PEEK and cobalt chrome spheres were evaluated. In chapter 3, a modern TDR fixed bearing technology was evaluated with specific attention to loading of the bony endplates and facet contact forces. Chapter 4 introduces a simple sagittal balance loading paradigm and evaluates the impingement risk associated with disc height distraction for both a mobile and fixed bearing TDR. Chapter 5 details the development of case-specific models based on the clinical scenarios from retrieved implants. Outputs from these analyses were compared with the retrieved implants. Significant correlations were found between the retrieved implant's rim penetration rate and peak contact stress from the finite element model. In the final chapter, the validated model of TDR impingement was used to determine the impingement risk associated with several parameters.

References

1. Hart, L.G., R.A. Deyo, and D.C. Cherkin, *Physician office visits for low back pain. Frequency, clinical evaluation, and treatment patterns from a U.S. national survey.* Spine (Phila Pa 1976), 1995. **20**(1): p. 11-9.
2. White, A.H., R.H. Rothman, and C.D. Ray, *Lumbar spine surgery : techniques & complications*1987, St. Louis: Mosby. xvi, 587 p.

3. Wiltberger, B.R., *Surgical Treatment of Degenerative Disease of the Back.* J Bone Joint Surg Am, 1963. **45**: p. 1509-16.
4. Bagby, G.W., *Arthrodesis by the distraction-compression method using a stainless steel implant.* Orthopedics, 1988. **11**(6): p. 931-4.
5. Kuslich, S.D., et al., *The Bagby and Kuslich method of lumbar interbody fusion. History, techniques, and 2-year follow-up results of a United States prospective, multicenter trial.* Spine (Phila Pa 1976), 1998. **23**(11): p. 1267-78; discussion 1279.
6. Aota, Y., K. Kumano, and S. Hirabayashi, *Postfusion instability at the adjacent segments after rigid pedicle screw fixation for degenerative lumbar spinal disorders.* J Spinal Disord, 1995. **8**(6): p. 464-73.
7. Etebar, S. and D.W. Cahill, *Risk factors for adjacent-segment failure following lumbar fixation with rigid instrumentation for degenerative instability.* J Neurosurg, 1999. **90**(2 Suppl): p. 163-9.
8. Frymoyer, J.W., et al., *Disc excision and spine fusion in the management of lumbar disc disease. A minimum ten-year followup.* Spine (Phila Pa 1976), 1978. **3**(1): p. 1-6.
9. Guigui, P., et al., *[Long-term outcome at adjacent levels of lumbar arthrodesis].* Rev Chir Orthop Reparatrice Appar Mot, 1997. **83**(8): p. 685-96.
10. Hambly, M.F., et al., *The transition zone above a lumbosacral fusion.* Spine (Phila Pa 1976), 1998. **23**(16): p. 1785-92.
11. Hilibrand, A.S. and M. Robbins, *Adjacent segment degeneration and adjacent segment disease: the consequences of spinal fusion?* Spine J, 2004. **4**(6 Suppl): p. 190S-194S.
12. Panjabi, M., et al., *Multidirectional testing of one- and two-level ProDisc-L versus simulated fusions.* Spine, 2007. **32**(12): p. 1311-9.
13. Panjabi, M.M., *Hybrid multidirectional test method to evaluate spinal adjacent-level effects.* Clin Biomech (Bristol, Avon), 2007. **22**(3): p. 257-65.
14. Panjabi, M., et al., *Hybrid testing of lumbar CHARITE discs versus fusions.* Spine (Phila Pa 1976), 2007. **32**(9): p. 959-66; discussion 967.
15. Goel, V.K., et al., *Effects of charite artificial disc on the implanted and adjacent spinal segments mechanics using a hybrid testing protocol.* Spine (Phila Pa 1976), 2005. **30**(24): p. 2755-64.
16. Mayer, H.M. and A. Korge, *Non-fusion technology in degenerative lumbar spinal disorders: facts, questions, challenges.* Eur Spine J, 2002. **11 Suppl 2**: p. S85-91.
17. Auerbach, J.D., et al., *Evaluation of spinal kinematics following lumbar total disc replacement and circumferential fusion using in vivo fluoroscopy.* Spine, 2007. **32**(5): p. 527-36.
18. Fernstrom, U., *Arthroplasty with intercorporal endoprothesis in herniated disc and in painful disc.* Acta Chir Scand Suppl, 1966. **357**: p. 154-9.
19. Link, H.D., *History, design and biomechanics of the LINK SB Charite artificial disc.* Eur Spine J, 2002. **11 Suppl 2**: p. S98-S105.

20. David, T., *Lumbar disc prosthesis. Surgical technique, indications and clinical results in 22 patients with a minimum of 12 months follow-up.* Eur Spine J, 1993. **1**(4): p. 254-9.
21. Griffith, S.L., et al., *A multicenter retrospective study of the clinical results of the LINK SB Charite intervertebral prosthesis. The initial European experience.* Spine (Phila Pa 1976), 1994. **19**(16): p. 1842-9.
22. Cinotti, G., T. David, and F. Postacchini, *Results of disc prosthesis after a minimum follow-up period of 2 years.* Spine (Phila Pa 1976), 1996. **21**(8): p. 995-1000.
23. Zeegers, W.S., et al., *Artificial disc replacement with the modular type SB Charite III: 2-year results in 50 prospectively studied patients.* Eur Spine J, 1999. **8**(3): p. 210-7.
24. Sott, A.H. and D.J. Harrison, *Increasing age does not affect good outcome after lumbar disc replacement.* Int Orthop, 2000. **24**(1): p. 50-3.
25. Lemaire, J.P., et al., *Clinical and radiological outcomes with the Charite artificial disc: a 10-year minimum follow-up.* J Spinal Disord Tech, 2005. **18**(4): p. 353-9.
26. Putzier, M., et al., *Charite total disc replacement--clinical and radiographical results after an average follow-up of 17 years.* Eur Spine J, 2006. **15**(2): p. 183-95.
27. McAfee, P.C., et al., *A prospective, randomized, multicenter Food and Drug Administration investigational device exemption study of lumbar total disc replacement with the CHARITE artificial disc versus lumbar fusion: part II: evaluation of radiographic outcomes and correlation of surgical technique accuracy with clinical outcomes.* Spine (Phila Pa 1976), 2005. **30**(14): p. 1576-83; discussion E388-90.
28. Blumenthal, S., et al., *A prospective, randomized, multicenter Food and Drug Administration investigational device exemptions study of lumbar total disc replacement with the CHARITE artificial disc versus lumbar fusion: part I: evaluation of clinical outcomes.* Spine (Phila Pa 1976), 2005. **30**(14): p. 1565-75; discussion E387-91.
29. Tropiano, P., et al., *Lumbar disc replacement: preliminary results with ProDisc II after a minimum follow-up period of 1 year.* J Spinal Disord Tech, 2003. **16**(4): p. 362-8.
30. Bertagnoli, R., et al., *Lumbar total disc arthroplasty in patients older than 60 years of age: a prospective study of the ProDisc prosthesis with 2-year minimum follow-up period.* J Neurosurg Spine, 2006. **4**(2): p. 85-90.
31. Bertagnoli, R. and S. Kumar, *Indications for full prosthetic disc arthroplasty: a correlation of clinical outcome against a variety of indications.* Eur Spine J, 2002. **11 Suppl 2**: p. S131-6.
32. Delamarter, R.B., et al., *ProDisc artificial total lumbar disc replacement: introduction and early results from the United States clinical trial.* Spine (Phila Pa 1976), 2003. **28**(20): p. S167-75.

33. Mayer, H.M., et al., *Minimally invasive total disc replacement: surgical technique and preliminary clinical results.* Eur Spine J, 2002. **11 Suppl 2**: p. S124-30.
34. Kurtz, S.M., et al., *Polyethylene wear and rim fracture in total disc arthroplasty.* Spine J, 2007. **7**(1): p. 12-21.
35. Choma, T.J., et al., *Retrieval analysis of a ProDisc-L total disc replacement.* J Spinal Disord Tech, 2009. **22**(4): p. 290-6.
36. Kafer, W., et al., *Posterior component impingement after lumbar total disc replacement: a radiographic analysis of 66 ProDisc-L prostheses in 56 patients.* Spine, 2008. **33**(22): p. 2444-9.
37. Kurtz, S.M., et al., *Analysis of a retrieved polyethylene total disc replacement component.* Spine J, 2005. **5**(3): p. 344-50.
38. Punt, I.M., et al., *Complications and reoperations of the SB Charite lumbar disc prosthesis: experience in 75 patients.* Eur Spine J, 2008. **17**(1): p. 36-43.
39. van Ooij, A., et al., *Polyethylene wear debris and long-term clinical failure of the Charite disc prosthesis: a study of 4 patients.* Spine, 2007. **32**(2): p. 223-9.
40. van Ooij, A., F.C. Oner, and A.J. Verbout, *Complications of artificial disc replacement: a report of 27 patients with the SB Charite disc.* J Spinal Disord Tech, 2003. **16**(4): p. 369-83.
41. Siepe, C.J., et al., *Total lumbar disc replacement in athletes: clinical results, return to sport and athletic performance.* Eur Spine J, 2007. **16**(7): p. 1001-13.
42. Rundell, S.A., et al., *Total disc replacement positioning affects facet contact forces and vertebral body strains.* Spine, 2008. **33**(23): p. 2510-7.
43. Rundell, S.A., et al., *Effect of nucleus replacement device properties on lumbar spine mechanics.* Spine (Phila Pa 1976), 2009. **34**(19): p. 2022-32.

1. Effect of Nucleus Replacement Device Properties on Lumbar Spine Mechanics

Abstract

Nucleus pulposus replacements are interventional therapies that restore stiffness and height to mildly degenerated intervertebral discs. Currently a wide variety of nucleus replacement technologies with a large range of mechanical properties are undergoing pre-clinical testing. The objective of the current study was to determine the biomechanical effects of nucleus replacement technology for a variety of implant moduli. We hypothesized that there would be an optimal modulus for a nucleus replacement that would provide loading in the surrounding bone and annulus similar to the intact state. A FEM of L3-L4 was created and validated using range of motion, disc pressure, and bony strains from previously published data. The intact model was altered by changing the mechanical properties of the nucleus pulposus to represent a wide range of nucleus replacement technologies (E= 0.1, 1, 4, and 100 MPa). All of the models were exercised in compression, flexion, extension, lateral bending, and axial rotation. Vertebral body strain, peak annulus fibrosus shear strain, initial bone remodeling stimulus, range of motion, and center of rotation was analyzed. A nucleus replacement modulus of 1 and 4 MPa resulted in vertebral body strains similar to the intact model. The softest device indicated increased loading in the AF and bone resorption adjacent to the implant. Areas of strain maxima and bone formation were observed adjacent to the implant for the stiffest device. The current study predicted an optimal nucleus replacement of 1 to 4 MPa. An overly stiff implant could result in subsidence, which would preclude the benefit of disc

height increase or restoration. Conversely, an overly soft implant could accelerate a degenerative cascade in the annulus.

Introduction

The current gold standard treatment for degenerative disc disease (DDD) continues to be lumbar spinal fusion. However, the potential for development of adjacent level disease has been shown both in vitro and clinically[1-5]. Adjacent level disease may be partly related to the effect of an altered biomechanical environment caused by fusion. Recently, total disc and nucleus replacement systems have been introduced as an alternative to fusion. These devices have the potential to relieve pain while maintaining motion, which may result in a lower likelihood of adjacent level disease[5, 6].

In contrast with total disc arthroplasty, in which both the nucleus pulposus and annulus fibrosus are replaced, nucleus pulposus replacements are intended to maintain as much of the annulus fibrosus as possible. These devices are early-stage therapeutic treatment for patients suffering mild to moderate DDD, and can be implanted in a minimally-invasive surgical fashion. A large variety of these devices are currently undergoing clinical and pre-clinical testing. Materials used in these devices include cobalt chrome (Fernstrom ball – historically stainless steel), PEEK (Nubac; Pioneer), polyurethane (Dascor; Disc Dynamics), silicone (PNR; TranS1), and hydrolyzed polyacrylonitrile (PDN; Raymedica)[7]. Furthermore, some of these devices are composites of polymer and fiber reinforcement. The mechanical properties of these materials and constructs vary substantially. Confined

compression testing of a nucleus pulposus replacement hydrogel material resulted in apparent moduli between 0.55 and 4.28 megapascals (MPa), depending on the applied load[8]. A separate study reported apparent moduli of a hydrogel material under confined compression from 0.19 to 12.7 MPa depending on the stiffness of the confining material[9]. The tangential modulus for an injectable polyurethane material is in the range of 3.3 to 5.4 MPa at 5 to 20% strain, respectively (information provided by Disc Dynamics, Inc.). These modulus values are similar to values measured for human nucleus pulposus tissue[10],[11]. The modulus for unfilled and carbon-fiber reinforced PEEK has been documented to vary between 3 and 12 gigapascals (GPa)[12], which is three orders of magnitude stiffer than the previously mentioned elastomer devices, and falls in the range of cancellous to cortical bone[13]. The modulus for cobalt chrome is even greater at approximately 210 GPa. It is important to choose appropriate geometric and material properties for these devices since they will govern load sharing with the vertebral endplates and annulus fibrosus under physiologic loading.

Implantation of an overly stiff device could lead to implant subsidence through overloading of the endplate, while a very soft implant could lead to bone resorption from underloading. An example of a stiff device resulting in subsidence is the Fernstrom ball where after 2 years of follow up subsidence of 1 to 3 mm was documented [14]. It was indicated in a later review that 88% of initial disc height restoration was lost at 4 to 7 years follow up[15]. Additionally, several studies have documented changes to the vertebral endplates and implant subsidence after

implantation of a prosthetic nucleus device[14, 16, 17]. In one such study, the authors indicated that the endplate remodeling was the result of an altered load distribution post implantation, and further indicated that the device was made less stiff in order to prevent or minimize these changes [16]. These data suggest that appropriate selection of the implant material modulus is important in restoring near physiologic loading, provided that minimizing the potential for endplate changes is a design objective for nucleus replacements.

Finite element (FE) models, when properly validated, provide a valuable tool for evaluating load distribution in the lumbar spine. Previous FE studies have evaluated the effects of fusion instrumentation, dynamic posterior stabilization devices, and total disc replacements on the load bearing characteristics of the lumbar spine[18-25]. In contrast, very few analytical studies have been reported on the evaluation of nucleus pulposus replacements. In a recent FE study, the authors evaluated a variety of nucleus replacement moduli from 0.5 to 100 MPa and determined that a modulus of 3 MPa for a fully conforming device provided physiological loading in the annulus[26]. The authors modeled the annulus and nucleus under compression, and therefore were unable to make any conclusions regarding ideal implant modulus with respect to the bony structures under a variety of loading conditions. Therefore, the objective of the current study was to evaluate a large range of nucleus replacement moduli under a variety of physiologic loading conditions using a validated FE model of an entire single functional spinal unit (L3-

L4).[27] We hypothesize that there will be an optimum nucleus modulus, which will restore physiologic load sharing with the annulus fibrosus and vertebral bodies.

Methods

A three-dimensional finite element model (FEM) of a ligamentous L3-L4 motion segment was generated from quantitative computed tomography (QCT) data of a cadaveric spine. The donor was a 78-year-old male who died from cardiac arrhythmia. The data set was taken from an Institutional Review Board-approved cadaveric study. The spine was chosen due to its lack of any bony or disc deformities, i.e, osteophytes or herniations. Hounsfield units were used as a surrogate for bone mineral density (BMD). The development of the model is described in greater detail in Appendix A, but is outlined, in part, in the following paragraphs.

A combination of automatic and manual image segmentation techniques (Analyze, AnalyzeDirect, Inc., Lenexa, KS) were used to extract detailed surfaces corresponding to the major bony structures of L3-L4. The software package allowed for automatic segmentation based on thresholding of the QCT grayscale values. The surfaces for the discs were based on These surfaces were imported into the commercial finite element mesh generation program, HyperMesh (Altair Inc., Troy, MI), and were discretized into a combination of tetrahedral elements for the bony structures and hexahedral elements for the intervertebral disc (IVD). The surfaces for the IVD were based on anatomic bony landmarks obtained from the segmentation. The nucleus pulposus was created to account for approximately 40% of the total volume[28]. The average disc height was measured to

be 12 mm. Major spinal ligaments (anterior longitudinal ligament, posterior longitudinal, intraspinatus, supraspinatus, intratransverse, facet capsule, ligamentum flavum) were implemented in the model using tension-only nonlinear springs. Shell elements were used to plate the exterior surface of the vertebral bodies and represented the cortex and bony endplate (Figure 1-1).

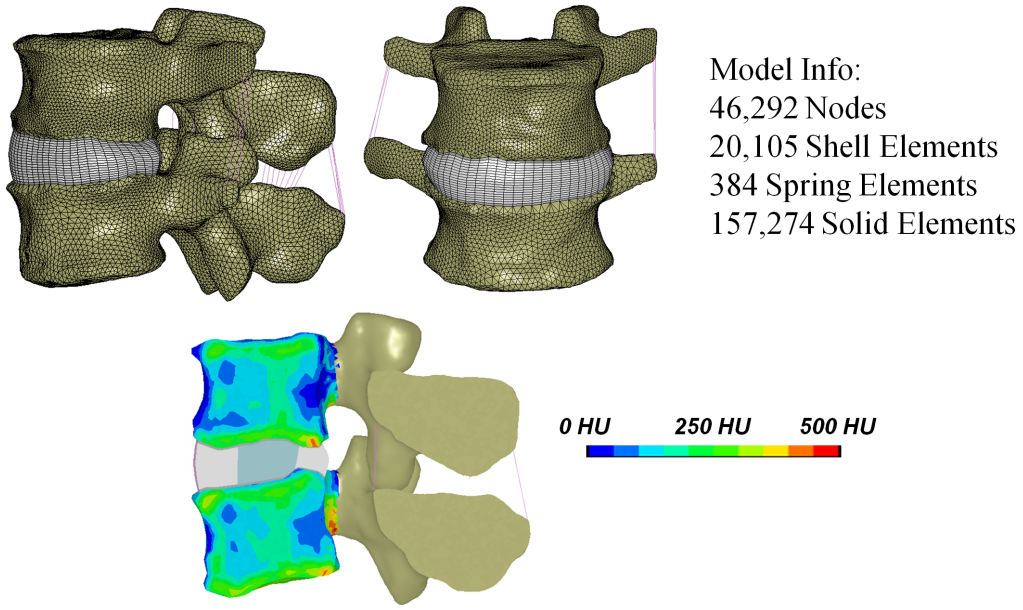

Figure 1-1. 3-D finite element model of a ligamentous L3-L4 motion segment. Sagittal cross-section depicts the contours of Houndsfield units, which were used as a surrogate for bone mineral density.

Bone mineral density (BMD)-dependent orthotropic material properties were assigned to the cancellous bone of the vertebral bodies. Custom software was written to apply the measured Hounsfield numbers from the QCT data to the nodal points within the finite element mesh. Similar methodology has been used to create models with heterogeneous bone properties of the tibia and femur.[29, 30] The quantitative relationship between bone mineral density and elastic modulus in cancellous vertebral

bone, as reported by Morgan et al., and Ulrich et al., was utilized to define a nonlinear relationship between bone mineral density and orthotropic elastic modulus.[31, 32] Elastic moduli within the vertebral body fell within what has been previously reported in the literature.[33-35] The remaining structures were assigned material properties from the literature and are depicted in Table 1-1. Frictionless contact was defined between the facets using a penalty-based contact algorithm.

Table 1-1. Summary of Element Type and Material Properties Used in the FE model

Component	Element type	Thickness or Cross-sectional area	Young's Modulus (MPa)	Poisson's ratio	Reference
Cortical Bone	Shell	0.4 mm	12,000	0.3	[13]
Vertebral Endplate	Shell	0.25 mm	1,000	0.2	[36]
Cancellous Bone	Tet	N/A	$4{,}730\rho^{1.56}$/ $1{,}987\rho^{1.56}$/ $1{,}357\rho^{1.56}$	0.2	[31, 32]
Posterior Elements	Tet	N/A	3,500	0.25	[37]
Annulus Fibrosus Ground Substance	Hex	N/A	1.36	0.45	[38]
Annulus Fibrosus Collagen Fibers	Fabric	N/A	Stress-Strain Curve		[39]
Nucleus Pulposus	Hex	N/A	K = 1666.7	incompressible	[13]
Ligaments	Spring	N/A	hyperelastic	N/A	[40, 41]
Cartilage Endplate	8-Noded Hex	N/A	24	0.4	[23]

Two separate analyses were performed in order to validate the results of the model. The first analysis involved applying a 1000 N compressive force to the intact model in order to simulate previously published experiments using cadaveric specimens.[42] The total vertical displacement of L3, intervertebral disc pressure, and

cortical and endplate first principal strains were compared between the FEM and the previously published experimental data.[42] A second validation study was performed by applying moments of 7.5 Nm along the three principal anatomic axes and comparing total range of motion (RoM) in flexion-extension, lateral bending, and axial rotation with previously published data.[43-48]

The effect of nucleus replacement properties on motion segment mechanics was evaluated in this study by adjusting the material properties of the nucleus pulposus in the intact FEM of L3-L4. The intact model consisted of a nucleus pulposus of incompressible fluid elements with a bulk modulus of 1667 MPa.[13] Separate models were created with linear elastic nucleus pulposus material properties with elastic moduli of 0.1, 1, 4, and 100 MPa and Poisson's ratios of 0.48, corresponding to a nearly incompressible material (a fully incompressible material has a Poisson's ratio of 0.5). The geometry of these nucleus replacement devices was the same of that of the intact nucleus pulposus. In all cases, there were no gaps at the interface of the nucleus and annulus, and the boundary of the two disc regions were tied together (i.e., displacement compatible). This resulted in a total of five models (intact, 0.1 MPa, 1 MPa, 4 MPa, and 100 MPa). All five models were exercised in compression (1,000 N), flexion (7.5 Nm), extension (7.5 Nm), axial rotation (7.5 Nm), and lateral bending (7.5 Nm) with a 1,000 N compressive follower load applied to the superior endplate of L3. This resulted in a total of 25 analyses (Table 1-2).

Table 1-2. Matrix depicting the analyses performed for all finite element models and modes of loading

	INTACT	IMPLANTED			
	Fluid; k = 1667 MPa	E = 0.1 MPa ν = 0.48	E = 1.0 MPa ν = 0.48	E = 4.0 MPa ν = 0.48	E = 100 MPa ν = 0.48
Compression	X	X	X	X	X
Flexion	X	X	X	X	X
Extension	X	X	X	X	X
Lateral Bending	X	X	X	X	X
Axial Rotation	X	X	X	X	X

The inferior endplate of L4 was fixed in space to provide an appropriate boundary condition. The value of peak maximum shear strain in the annulus fibrosus ground substance was extracted from each analysis. Vertebral body cancellous bone effective von Mises (VM) strains were also determined. Strain was chosen over stress due to the heterogeneous nature of the vertebral bone. Strain has been documented to have less dependence on the apparent density when compared with stress.[33] Von Mises strains were chosen in order to depict the distortional strains being experienced in the vertebral bodies after implantation of a nucleus replacement, and how this is affected by implant modulus. Von Mises yield criterion is often used to predict the yield point for bone.[49] The Von Mises strain is intended to qualitatively depict areas of the bone that may be most at risk of yielding after nucleus replacement. Range of motion (RoM) was defined as the total angular rotation of L3. The 3-D helical axis of rotation for L3 was also determined using methods previously described in the literature.[50],[51] The center of rotation (CoR) was reported as the point at which the helical axis of rotation crossed through the sagittal plane for flexion-extension, the axial plane for axial rotation, and the

coronal plane for lateral bending. The total resultant force passing through an axial cross-section at the mid intervertebral disc space of the annulus fibrosus was also reported.

Initial bone remodeling signal for the vertebral bodies was calculated for each node by applying the following equation, which used strain energy density (SED) results from the implanted and intact models [52]:

$$Signal = \frac{SED_{implanted} - SED_{natural}}{SED_{natural}}$$

It has been previously determined that an appropriate threshold for humans is 0.75.[53] Therefore, signal values greater than 0.75 were indicated as areas of increased bone formation, while areas below –0.75 were indicated as areas of bone resorption.

Results

Results from the validation analysis indicated reasonable agreement between the FEM and previously reported experimental data. The FEM was generally able to predict cortical and endplate strains within the ranges reported in the literature.[42] Typically, the FEM's results matched the trends demonstrated by the experimental median values (Figure 1-2). Additionally, the FEM predicted a disc pressure of 0.75 MPa and a total vertical displacement of 1.1 mm after application of 1000N of compression, which fell within the range of the experimentally reported values. Further validation indicated that the FEM predicted the total range of motion in flexion-extension, lateral bending, and axial rotation (Figure 1-3).

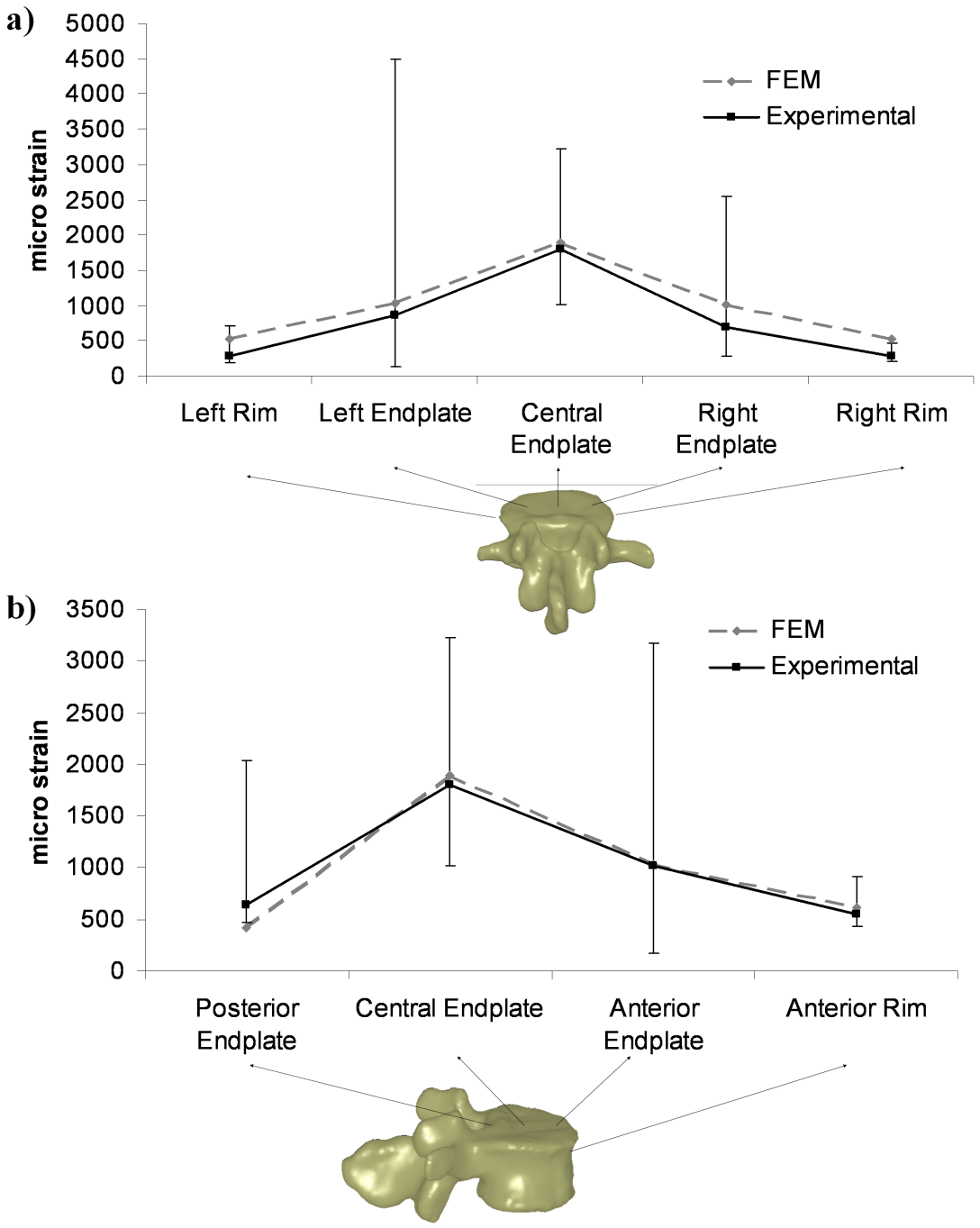

Figure 1-2. Graphs depicting 1st principal strains at various locations along the endplate and cortical rim between previously published experimental (Frei et al., 2001) and FEM results.

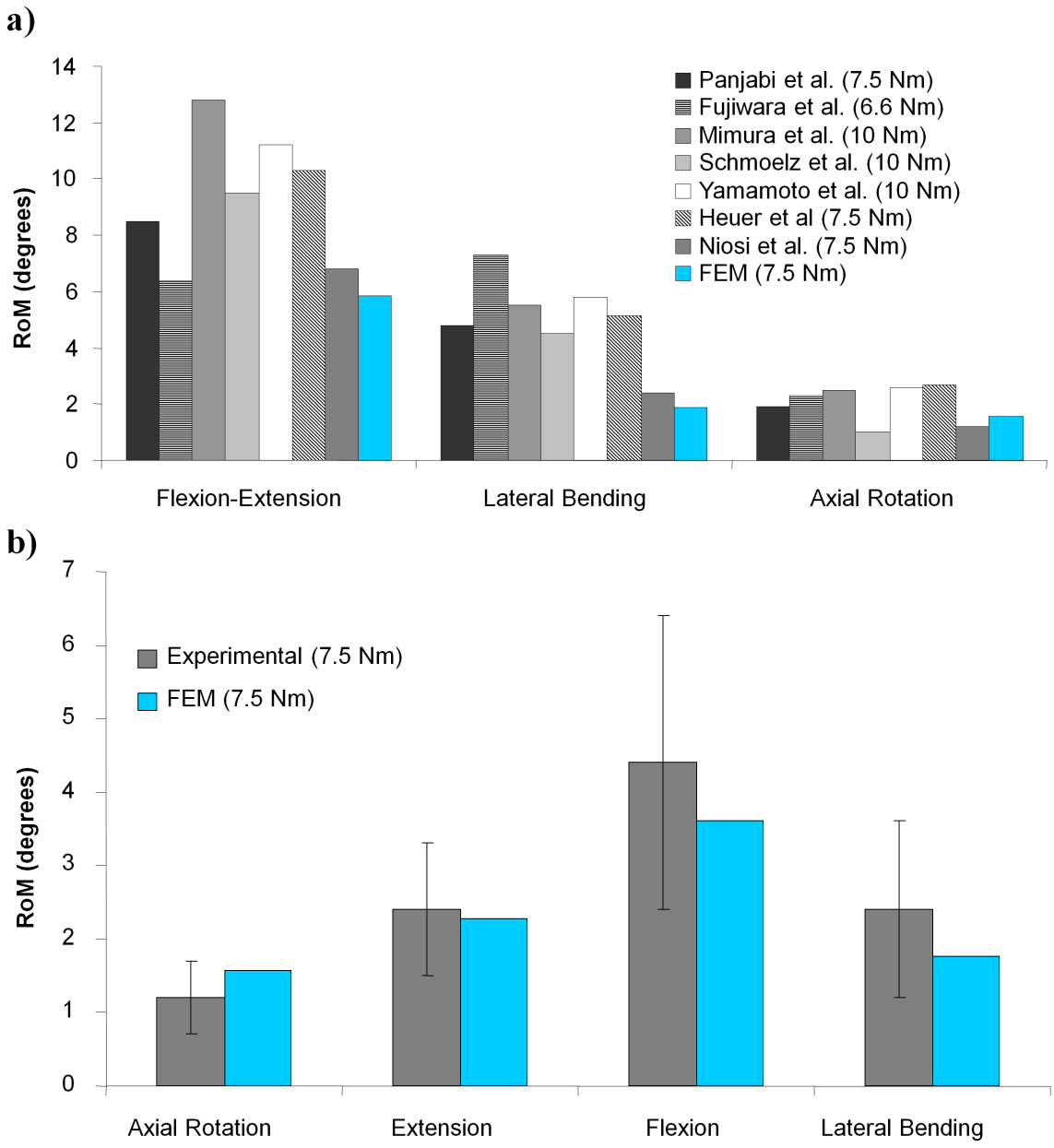

Figure 1-3. Bar graphs depicting comparisons of angular ranges of motion between the FEM versus several previously published values (a). A separate bar graph shows a comparison between the FEM and a specific set of experimental data (Niosi et al., 2006), which also includes ranges for the standard deviations (b).

Implantation of the lowest modulus nucleus replacement (0.1 MPa) increased the RoM in all modes of loading with the exception of lateral bending (Figure 1-4a). Stiffening of the implant lead to a progressive reduction in the RoM

with the most substantial reduction occurring for the 100 MPa modulus. The 1MPa and 4MPa models had the most similar RoMs to the intact model across all loading conditions. The peak maximum shear strain value in the annulus fibrosus corresponded with the trends in RoM (Figure 1-4b). The 0.1 MPa model experienced the greatest increase in peak maximum shear strain when compared with the intact model. All other nucleus replacement models resulted in a decrease of the peak maximum shear strain value in the annulus fibrosus compared to the intact model. The total resultant force experienced by the annulus increased for the 0.1 MPa model when compared with the intact model for all loading scenarios (Figure 1-4c). The resultant force in the annulus decreased to approximately 10% to 20% of the applied compressive follower load in the 100 MPa model compared to 60% to 70% for the intact model.

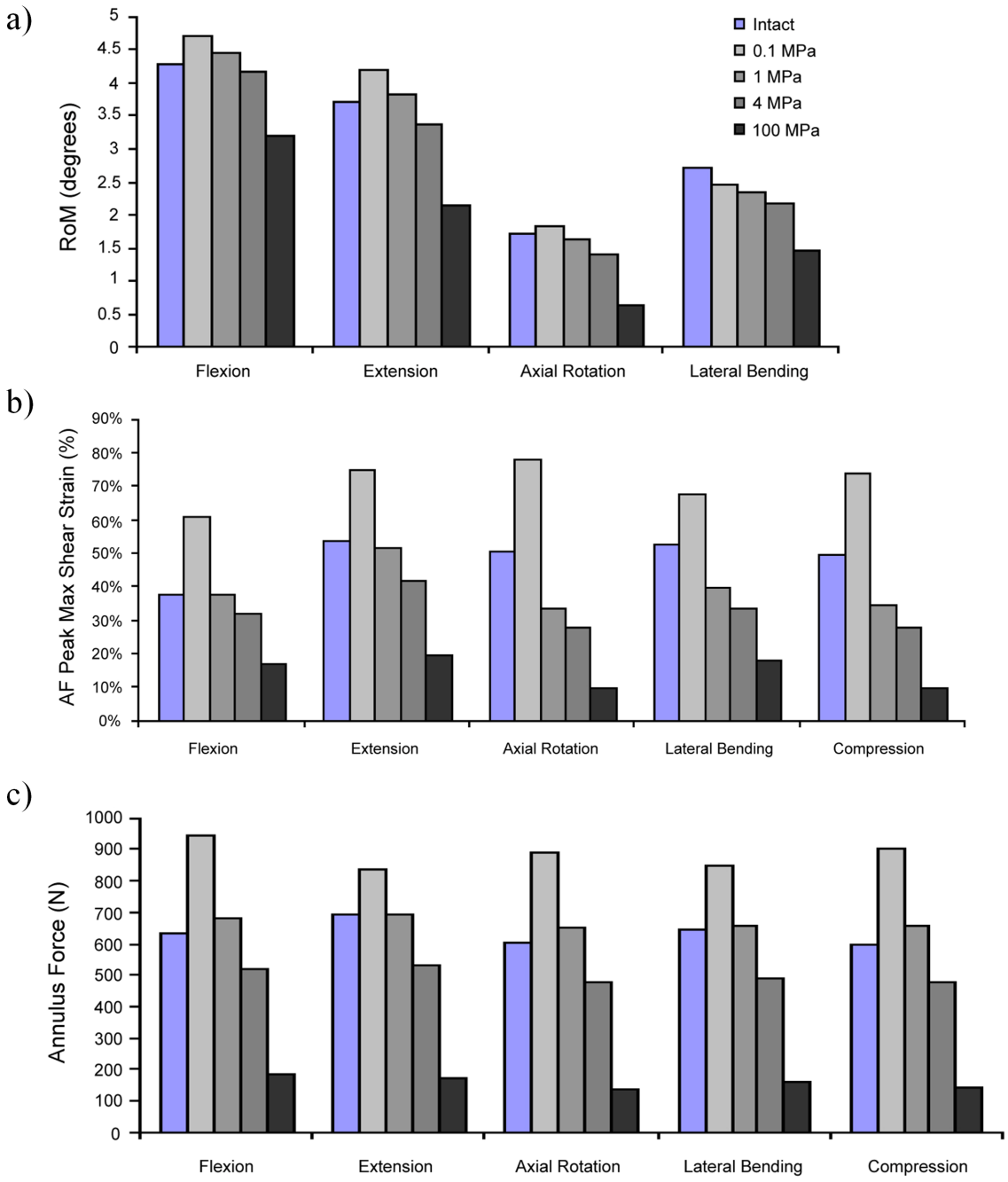

Figure 1-4. Bar graphs depicting the total RoM (a), annulus fibrosus (AF) peak maximum shear strains (b), and total resultant force through an axial cross-section of the AF (c) for all loading modes and models.

The CoRs for the flexion analyses remained at approximately the mid disc height and centerline of the vertebral bodies regardless of nucleus modulus (Figure

1-5a). Subtle alterations to the location of the CoR were observed during extension and lateral bending as a result of different nucleus moduli (Figure 1-5b,d). During both extension and lateral bending the CoR for the 100 MPa model moved towards the location of the nucleus. During axial rotation of the CoR for the intact, 1MPa and 4MPa models stayed in approximately the same location (Figure 1-5c), however, the 0.1 MPa model experienced a shift toward the sagittal midline of approximately 4 mm. The most substantial change in CoR location occurred during axial rotation of the 100 MPa model, which shifted from the right to the left side of the spinal canal.

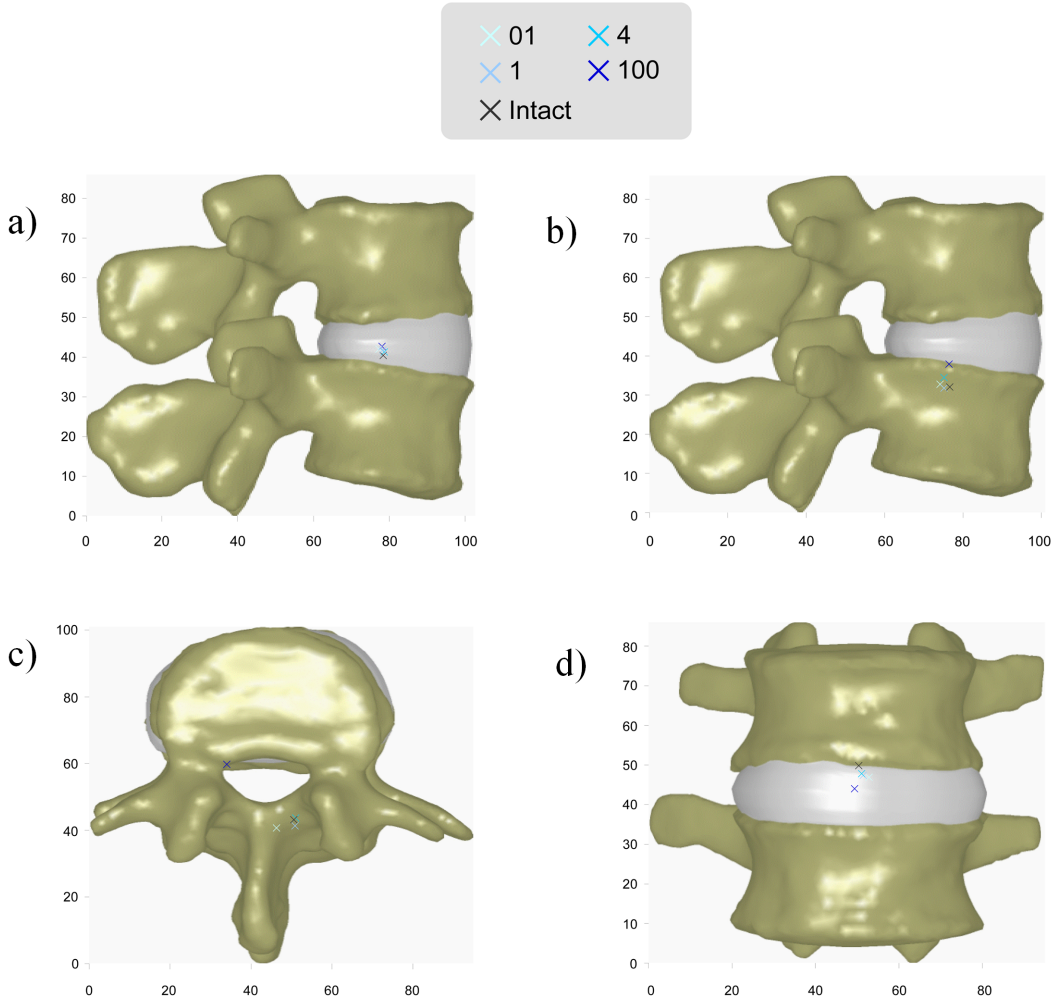

Figure 1-5. Graphs depicting the CoR for flexion (a), extension (b), axial rotation (c), and lateral bending (d).

Increases in strain maxima that corresponded to increases in implant modulus were observed in the vertebral bodies (Figure 1-6). Qualitatively, the 1MPa and 4MPa models demonstrated strain contours very similar to the intact model. The 100 MPa model indicated strain maxima located in the vertebral body as well as at the superior endplate of L4. The 0.1 MPa model demonstrated a reduction in strain maxima, particularly in the vertebral body of L4.

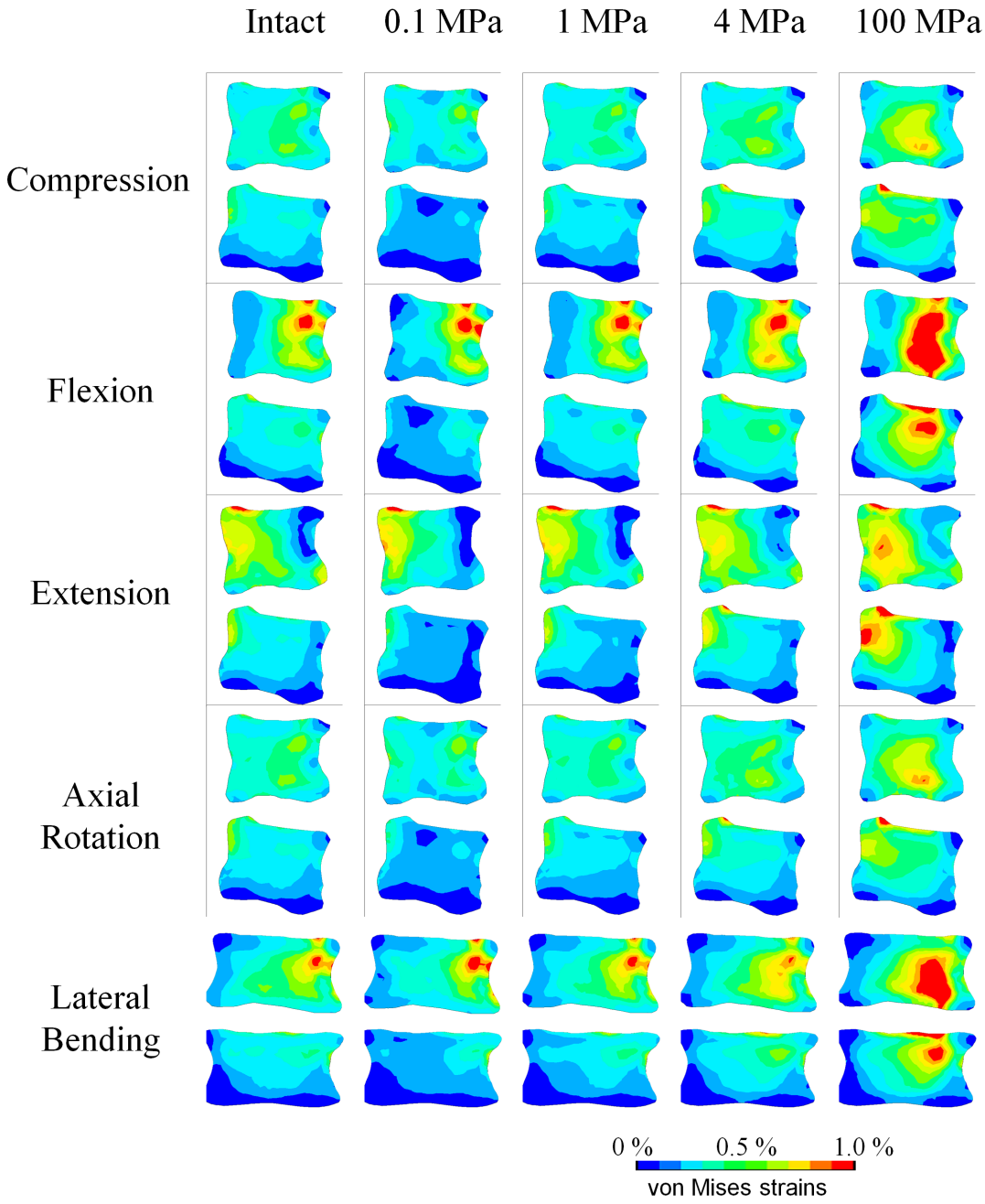

Figure 1-6. Effective (VM) strain contour plots of L3-L4 vertebral bodies at a sagittal or coronal cutplane

Initial bone remodeling stimulus results indicated bony resorption adjacent to the nucleus replacement for the 0.1 MPa model (Figure 1-7). Conversely, the 100

MPa model indicated large regions of bony formation signal throughout the central vertebral bodies, with bone resorption signal towards the perimeter of the vertebral bodies adjacent to the endplates. The 1 and 4 MPa models tended to have minimal initial remodeling signal with the exception of small areas of bone formation signal for the 4 MPa model.

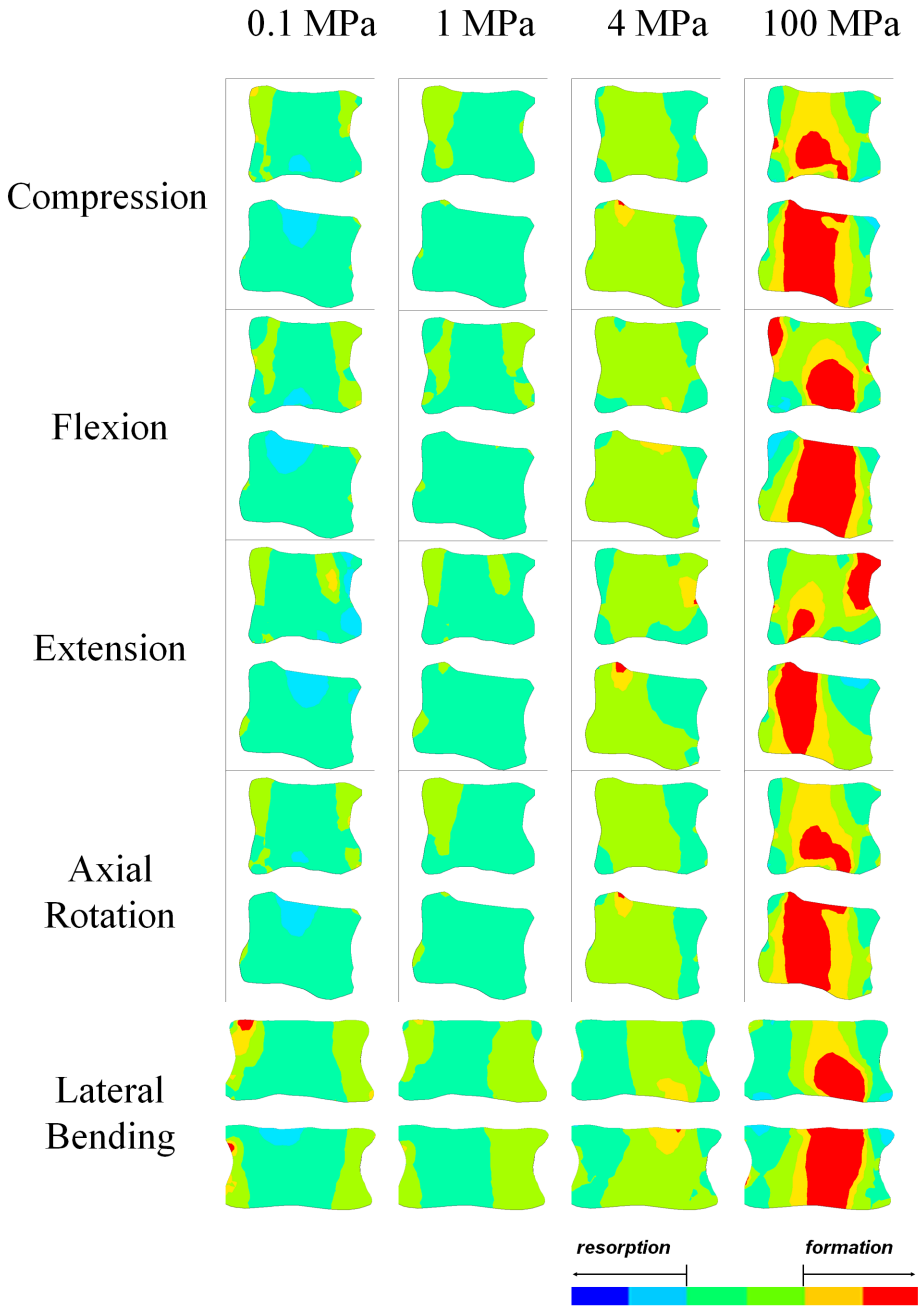

Figure 1-7. Initial remodeling stimulus contour plots of L3-L4 vertebral bodies at a sagittal or coronal cutplane. Areas of light blue and blue indicate bone resorption, green indicates no remodeling signal, and orange and red indicate bone formation.

Discussion

The results of this study suggest that, for a nucleus replacement with geometry identical to a physiologic nucleus pulposus, a modulus in the range of 1 to 4 MPa for a nearly incompressible material provides physiologic load sharing with the annulus and endplates. These findings were obtained with the assumption that the boundary of nucleus and annulus are perfectly conforming and that the boundary of the two disc regions are tied together. Under these key assumptions, the results indicate that the RoM was sensitive to changes in the nucleus modulus. This is consistent with an *in vitro* test that showed an increased RoM after nucleotomy.[54] The highest modulus material (100 MPa) resulted in a reduced range of motion, annulus peak max shear strain, and annulus force for all scenarios. Interestingly, implantation of the 0.1 MPa nucleus resulted in an increased range of motion for all modes of loading with the exception of lateral bending. Intuitively, it was expected that a low modulus nucleus replacement would result in an increased range of motion for all modes of loading. However, the increased load supported by the annulus for the 0.1 MPa model combined with the larger moment arm between the annulus reaction force and the CoR for lateral bending caused an effective stiffening of the motion segment. These data suggest that RoM, by itself, is not a sufficient metric to determine the biomechanical effect of a nucleus replacement device.

The current study predicted peak max shear strain values in the annulus for the intact group in the range of 30% to 60% with a 1000 N compressive follower load. This is consistent with results reported in a previously published FE study of 20% to 40% for a 500 N compressive follower load.[55] The peak maximum shear strain in the annulus increased in the 0.1 MPa model for all loading scenarios when compared with the intact

group. This corresponded to increased loading in the annulus. It has been previously shown that high loading in the annulus can distort the lamellae and result in tears.[56] While these tears may contribute to an inflammatory response and subsequent degeneration of the tissue[57, 58] they also place the disc at greater risk of prolapse by jeopardizing the structure responsible for retaining the nucleus. In the case of nucleus replacement, the risk of disc prolapse is replaced by the risk of implant extrusion.[59] Therefore, implantation of an overly soft (i.e. low modulus) nucleus replacement and subsequent increased strains in the annulus have the potential to promote disc degeneration, and may increase the likelihood of implant extrusion.

Contour plots of effective strain (Figure 6) contained numerical ranges from zero to one percent. One percent was chosen since it is the approximate yield strain of vertebral cancellous bone.[33] Contour plots of VM strain for the intact model (Figure 6) indicated effective (VM) strains under 1% in the cancellous bone, with the exception of small areas near the superior endplate of L3 in flexion, extension, and lateral bending. Strain maxima concentrations were observed adjacent to the disc for the 100 MPa modulus model, which differed from the diffuse strain distribution in the intact group. Concentrations in loading from a stiff interbody device, such as the Fernstrom ball, have been theorized to result in subsidence, which has been documented clinically[15]. Similar concentrated distributions of von Mises stress in the vertebral body have been reported in FE studies of interbody cages.[60],[21] These areas of load concentration may be correlated with the subsidence of interbody cages into the adjacent vertebral body, which has been well documented in clinical studies.[61, 62],[63],[64],[65] Subsidence of interbody cages does not necessarily require revision of the procedure, provided the

segment achieves fusion (which is promoted by removing the cartilaginous endplate and facilitating contact between bony surfaces). Unfortunately, this is not the case for certain arthroplasty procedures, in which maintenance of the cartilaginous endplate is performed to minimize subsidence. Furthermore, retaining the cartilaginous endplate is meant to facilitate the maintenance or increase in the height of the neuroforamen and intervertebral disc. Data from the current study indicated that an implant modulus of 100 MPa may be sufficiently stiff to cause subsidence similar to that seen for interbody cages and the Fernstrom sphere, which may preclude the benefit of initial disc height maintenance or increase.

Results from the bone remodeling analysis indicated that the 0.1 MPa model would experience initial bone resorption adjacent to the nucleus while the 100 MPa model would experience bone formation throughout the vertebral bodies. However, the high strain fields documented for the 100 MPa model make it difficult to determine whether or not the bone would yield prior to formation. Generally, there was little signal for either bone resorption or formation for the 1 and 4 MPa models. These data quantify the effect of changes in load distribution from the intact state after implantation of a variety of nucleus replacement moduli. McNally et al[66] showed specific patterns of loading in the vertebral bodies for clinically painful discs suggesting a relationship between abnormal loading and pain. It has been suggested that restoration of physiological loading in the vertebral bodies after either arthrodesis or arthroplasty will result in improved clinical success[67]. Based on these studies, our results indicate that moduli between 1 and 4 MPa for a nucleus replacement results in near physiologic loading in the vertebral bodies, which may result in an optimal overall motion segment

biomechanical environment and, ultimately, better long-term disc health and clinical outcomes.

The current study used a validated FE model of the spine, which shares certain limitations of previously published models [40, 41, 68]. The bone geometry and material properties were generated from a specific QCT data set of a single L3-L4 motion segment. While this may not be entirely representative of a wide patient population, it provides the ability to perform a well-controlled comparative study. Therefore, the data depicted in the current study should be interpreted as trends. Additionally, we maintained the disc height and annulus material properties for all of the scenarios tested. This was done in order to isolate the effects of the nucleus replacement moduli and eliminate confounding variables. Future studies should evaluate the effects of disc height and annular degeneration on nucleus replacement efficacy.

The results of this study are based upon the key assumptions that the nucleus replacement fills the entire nucleus cavity, and the interfaces are displacement compatible. Currently, our lab is investigating the effects of a sliding interface at the boundaries of the device and a circumferential void between the device and the annulus. Preliminary results from these analyses indicate that simulation of a frictionless contact interface at the device boundaries for a fully conforming device has a negligible effect on the results. However, a device that does not fully conform to the annular wall permits inward bulging of the inner annulus and associated increases in the maximum shear strain.

Results from this study indicate an optimal modulus between 1 and 4 MPa for a nearly incompressible material for use in a conforming and displacement compatible

nucleus replacement (i.e. no gaps between the nucleus and annulus, with the boundary of the two regions tied together). Moduli in this range resulted in physiologic loading in both the annulus and vertebral bodies. A modulus of 0.1 MPa indicated the risk for bony resorption in the adjacent bone and increased strains in the annulus, which could result in implant subsidence or extrusion, respectively. An implant with a modulus of 100 MPa resulted in high strain fields in the adjacent bone indicating an increased risk of subsidence similar to what is experienced clinically by interbody cages. The current study evaluated a variety of nucleus replacement moduli without adjusting the implant geometry, which varies substantially for the current designs. Future studies should evaluate the effects of a variety of implant geometries in order to determine an ideal size and shape for a nucleus replacement.

References

1. Kumar, M.N., A. Baklanov, and D. Chopin, *Correlation between sagittal plane changes and adjacent segment degeneration following lumbar spine fusion.* Eur Spine J, 2001. **10**(4): p. 314-9.
2. Pellise, F., et al., *Radiologic assessment of all unfused lumbar segments 7.5 years after instrumented posterior spinal fusion.* Spine, 2007. **32**(5): p. 574-9.
3. Schulte, T.L., et al., *Disc height reduction in adjacent segments and clinical outcome 10 years after lumbar 360 degrees fusion.* Eur Spine J, 2007.
4. Cunningham, B.W., et al., *Biomechanical evaluation of total disc replacement arthroplasty: an in vitro human cadaveric model.* Spine, 2003. **28**(20): p. S110-7.
5. Auerbach, J.D., et al., *Evaluation of spinal kinematics following lumbar total disc replacement and circumferential fusion using in vivo fluoroscopy.* Spine, 2007. **32**(5): p. 527-36.
6. Panjabi, M., et al., *Multidirectional testing of one- and two-level ProDisc-L versus simulated fusions.* Spine, 2007. **32**(12): p. 1311-9.
7. Coric, D. and P.V. Mummaneni, *Nucleus replacement technologies.* J Neurosurg Spine, 2008. **8**(2): p. 115-20.
8. Bertagnoli, R., et al., *Mechanical testing of a novel hydrogel nucleus replacement implant.* Spine J, 2005. **5**(6): p. 672-81.

9. Joshi, A., et al., *Functional compressive mechanics of a PVA/PVP nucleus pulposus replacement.* Biomaterials, 2006. **27**(2): p. 176-84.
10. Cloyd, J.M., et al., *Material properties in unconfined compression of human nucleus pulposus, injectable hyaluronic acid-based hydrogels and tissue engineering scaffolds.* Eur Spine J, 2007. **16**(11): p. 1892-8.
11. Johannessen, W. and D.M. Elliott, *Effects of degeneration on the biphasic material properties of human nucleus pulposus in confined compression.* Spine, 2005. **30**(24): p. E724-9.
12. Kurtz, S.M. and J.N. Devine, *PEEK biomaterials in trauma, orthopedic, and spinal implants.* Biomaterials, 2007. **28**(32): p. 4845-69.
13. Kumaresan, S., et al., *Contribution of disc degeneration to osteophyte formation in the cervical spine: a biomechanical investigation.* J Orthop Res, 2001. **19**(5): p. 977-84.
14. Fernstrom, U., *Arthroplasty with intercorporal endoprothesis in herniated disc and in painful disc.* Acta Chir Scand Suppl, 1966. **357**: p. 154-9.
15. Bono, C.M. and S.R. Garfin, *History and evolution of disc replacement.* Spine J, 2004. **4**(6 Suppl): p. 145S-150S.
16. Bertagnoli, R. and R. Schonmayr, *Surgical and clinical results with the PDN prosthetic disc-nucleus device.* Eur Spine J, 2002. **11 Suppl 2**: p. S143-8.
17. Allen, M.J., et al., *Preclinical evaluation of a poly (vinyl alcohol) hydrogel implant as a replacement for the nucleus pulposus.* Spine, 2004. **29**(5): p. 515-23.
18. Denoziere, G. and D.N. Ku, *Biomechanical comparison between fusion of two vertebrae and implantation of an artificial intervertebral disc.* J Biomech, 2006. **39**(4): p. 766-75.
19. Dooris, A.P., et al., *Load-sharing between anterior and posterior elements in a lumbar motion segment implanted with an artificial disc.* Spine, 2001. **26**(6): p. E122-9.
20. Polikeit, A., et al., *Factors influencing stresses in the lumbar spine after the insertion of intervertebral cages: finite element analysis.* Eur Spine J, 2003. **12**(4): p. 413-20.
21. Polikeit, A., et al., *The importance of the endplate for interbody cages in the lumbar spine.* Eur Spine J, 2003. **12**(6): p. 556-61.
22. Moumene, M. and F.H. Geisler, *Comparison of biomechanical function at ideal and varied surgical placement for two lumbar artificial disc implant designs: mobile-core versus fixed-core.* Spine, 2007. **32**(17): p. 1840-51.
23. Noailly, J., D. Lacroix, and J.A. Planell, *Finite element study of a novel intervertebral disc substitute.* Spine, 2005. **30**(20): p. 2257-64.
24. Rohlmann, A., et al., *Comparison of the effects of bilateral posterior dynamic and rigid fixation devices on the loads in the lumbar spine: a finite element analysis.* Eur Spine J, 2007. **16**(8): p. 1223-31.
25. Rohlmann, A., T. Zander, and G. Bergmann, *Comparison of the biomechanical effects of posterior and anterior spine-stabilizing implants.* Eur Spine J, 2005. **14**(5): p. 445-53.

26. Meakin, J.R., *Replacing the nucleus pulposus of the intervertebral disk: prediction of suitable properties of a replacement material using finite element analysis.* J Mater Sci Mater Med, 2001. **12**(3): p. 207-13.
27. Rundell, S.A., J.D. Auerbach, and S.M. Kurtz, *Total Disc Replacement Positioning Affects Facet Contact Forces and Vertebral Body Strains.* Spine, 2008. **33**: p. In Press.
28. White, A.A., Panjabi, M.M.,, *Clinical Biomechanics of the Spine, 2nd ed.*1990, Philadelphia-Toronto: J.B. Lippincott Company.
29. Yosibash, Z., et al., *A CT-based high-order finite element analysis of the human proximal femur compared to in-vitro experiments.* J Biomech Eng, 2007. **129**(3): p. 297-309.
30. Sawatari, T., et al., *Three-dimensional finite element analysis of unicompartmental knee arthroplasty--the influence of tibial component inclination.* J Orthop Res, 2005. **23**(3): p. 549-54.
31. Ulrich, D., et al., *The ability of three-dimensional structural indices to reflect mechanical aspects of trabecular bone.* Bone, 1999. **25**(1): p. 55-60.
32. Morgan, E.F., H.H. Bayraktar, and T.M. Keaveny, *Trabecular bone modulus-density relationships depend on anatomic site.* J Biomech, 2003. **36**(7): p. 897-904.
33. Kopperdahl, D.L. and T.M. Keaveny, *Yield strain behavior of trabecular bone.* J Biomech, 1998. **31**(7): p. 601-8.
34. Mosekilde, L. and C.C. Danielsen, *Biomechanical competence of vertebral trabecular bone in relation to ash density and age in normal individuals.* Bone, 1987. **8**(2): p. 79-85.
35. Hansson, T.H., T.S. Keller, and M.M. Panjabi, *A study of the compressive properties of lumbar vertebral trabeculae: effects of tissue characteristics.* Spine, 1987. **12**(1): p. 56-62.
36. Silva, M.J., T.M. Keaveny, and W.C. Hayes, *Load sharing between the shell and centrum in the lumbar vertebral body.* Spine, 1997. **22**(2): p. 140-50.
37. Polikeit, A., L.P. Nolte, and S.J. Ferguson, *The effect of cement augmentation on the load transfer in an osteoporotic functional spinal unit: finite-element analysis.* Spine, 2003. **28**(10): p. 991-6.
38. Schmidt, H., et al., *Application of a new calibration method for a three-dimensional finite element model of a human lumbar annulus fibrosus.* Clin Biomech (Bristol, Avon), 2006. **21**(4): p. 337-44.
39. Shirazi-Adl, A., A.M. Ahmed, and S.C. Shrivastava, *Mechanical response of a lumbar motion segment in axial torque alone and combined with compression.* Spine, 1986. **11**(9): p. 914-27.
40. Rohlmann, A., et al., *Analysis of the influence of disc degeneration on the mechanical behaviour of a lumbar motion segment using the finite element method.* J Biomech, 2006. **39**(13): p. 2484-90.
41. Schmidt, H., et al., *Application of a calibration method provides more realistic results for a finite element model of a lumbar spinal segment.* Clin Biomech (Bristol, Avon), 2007. **22**(4): p. 377-84.

42. Frei, H., et al., *The effect of nucleotomy on lumbar spine mechanics in compression and shear loading.* Spine, 2001. **26**(19): p. 2080-9.
43. Yamamoto, I., et al., *Three-dimensional movements of the whole lumbar spine and lumbosacral joint.* Spine, 1989. **14**(11): p. 1256-60.
44. Mimura, M., et al., *Disc degeneration affects the multidirectional flexibility of the lumbar spine.* Spine, 1994. **19**(12): p. 1371-80.
45. Panjabi, M.M., et al., *Mechanical behavior of the human lumbar and lumbosacral spine as shown by three-dimensional load-displacement curves.* J Bone Joint Surg Am, 1994. **76**(3): p. 413-24.
46. Fujiwara, A., et al., *The effect of disc degeneration and facet joint osteoarthritis on the segmental flexibility of the lumbar spine.* Spine, 2000. **25**(23): p. 3036-44.
47. Schmoelz, W., et al., *Dynamic stabilization of the lumbar spine and its effects on adjacent segments: an in vitro experiment.* J Spinal Disord Tech, 2003. **16**(4): p. 418-23.
48. Niosi, C.A., et al., *Biomechanical characterization of the three-dimensional kinematic behaviour of the Dynesys dynamic stabilization system: an in vitro study.* Eur Spine J, 2006. **15**(6): p. 913-22.
49. Nagaraja, S., T.L. Couse, and R.E. Guldberg, *Trabecular bone microdamage and microstructural stresses under uniaxial compression.* J Biomech, 2005. **38**(4): p. 707-16.
50. Spoor, C.W. and F.E. Veldpaus, *Rigid body motion calculated from spatial co-ordinates of markers.* J Biomech, 1980. **13**(4): p. 391-3.
51. Challis, J.H., *A procedure for determining rigid body transformation parameters.* J Biomech, 1995. **28**(6): p. 733-7.
52. Weinans, H., et al., *Sensitivity of periprosthetic stress-shielding to load and the bone density-modulus relationship in subject-specific finite element models.* J Biomech, 2000. **33**(7): p. 809-17.
53. Kerner, J., et al., *Correlation between pre-operative periprosthetic bone density and post-operative bone loss in THA can be explained by strain-adaptive remodelling.* J Biomech, 1999. **32**(7): p. 695-703.
54. Heuer, F., et al., *Stepwise reduction of functional spinal structures increase range of motion and change lordosis angle.* J Biomech, 2007. **40**(2): p. 271-80.
55. Schmidt, H., et al., *Intradiscal pressure, shear strain, and fiber strain in the intervertebral disc under combined loading.* Spine, 2007. **32**(7): p. 748-55.
56. Adams, M.A. and W.C. Hutton, *Gradual disc prolapse.* Spine, 1985. **10**(6): p. 524-31.
57. Goel, V.K., et al., *Interlaminar shear stresses and laminae separation in a disc. Finite element analysis of the L3-L4 motion segment subjected to axial compressive loads.* Spine, 1995. **20**(6): p. 689-98.
58. Meakin, J.R., J.E. Reid, and D.W. Hukins, *Replacing the nucleus pulposus of the intervertebral disc.* Clin Biomech (Bristol, Avon), 2001. **16**(7): p. 560-5.
59. Klara, P.M. and C.D. Ray, *Artificial nucleus replacement: clinical experience.* Spine, 2002. **27**(12): p. 1374-7.

60. Kumar, N., et al., *Analysis of stress distribution in lumbar interbody fusion.* Spine, 2005. **30**(15): p. 1731-5.
61. Bartels, R.H., R.D. Donk, and T. Feuth, *Subsidence of stand-alone cervical carbon fiber cages.* Neurosurgery, 2006. **58**(3): p. 502-8; discussion 502-8.
62. Gercek, E., et al., *Subsidence of stand-alone cervical cages in anterior interbody fusion: warning.* Eur Spine J, 2003. **12**(5): p. 513-6.
63. Barsa, P. and P. Suchomel, *Factors affecting sagittal malalignment due to cage subsidence in standalone cage assisted anterior cervical fusion.* Eur Spine J, 2007. **16**(9): p. 1395-400.
64. Choi, J.Y. and K.H. Sung, *Subsidence after anterior lumbar interbody fusion using paired stand-alone rectangular cages.* Eur Spine J, 2006. **15**(1): p. 16-22.
65. Beutler, W.J. and W.C. Peppelman, Jr., *Anterior lumbar fusion with paired BAK standard and paired BAK Proximity cages: subsidence incidence, subsidence factors, and clinical outcome.* Spine J, 2003. **3**(4): p. 289-93.
66. McNally, D.S., et al., *In vivo stress measurement can predict pain on discography.* Spine, 1996. **21**(22): p. 2580-7.
67. Mulholland, R.C., *The myth of lumbar instability: the importance of abnormal loading as a cause of low back pain.* Eur Spine J, 2008. **17**(5): p. 619-25.
68. Noailly, J., et al., *How does the geometry affect the internal biomechanics of a lumbar spine bi-segment finite element model? Consequences on the validation process.* J Biomech, 2007. **40**(11): p. 2414-25.

2. Biomechanical Evaluation of a Spherical Lumbar Interbody Device at Varying Levels of Subsidence

Abstract

Ulf Fernström implanted stainless steel ball bearings following discectomy, or for painful disc disease, and termed this procedure disc arthroplasty. Today, spherical interbody spacers fabricated are clinically available, however, there remains a paucity of clinical and biomechanical data for these devices. The current study utilized a validated nonlinear 3-D finite element model (FEM) of a single lumbar motion segment (L3-L4) to evaluate the implantation of a spherical interbody device with and without subsidence. The primary objective of the current study was to evaluate the biomechanics of a spherical interbody implant. It was hypothesized that implantation of a spherical interbody implant, with combined subsidence into the vertebral bodies, would result in similar ranges of motion (RoM) and facet contact forces (FCFs) when compared with an intact condition. A secondary objective of this study was to determine the effect of using a PEEK versus a cobalt chrome (CoCr) implant on vertebral body strains. We hypothesized that the material selection would have a negligible effect on vertebral body strains since both materials have elastic moduli substantially greater than the annulus. A FEM of L3-L4 was created and validated using range of motion, disc pressure, and bony strain from previously published data. Virtual implantation of a spherical interbody device was implanted with 0, 2, and 4 mm of subsidence. The model was exercised in compression, flexion, extension, axial rotation and lateral bending. The RoM,

vertebral body effective (von Mises) strain, and facet contact forces were reported. Implantation of a PEEK implant resulted in slightly lower strain maxima when compared with a CoCr implant. For both materials the peak strain experienced by the underlying bone was reduced with increasing subsidence. All levels of subsidence resulted in range of motion and facet contact forces similar to the intact model. The results suggest that a simple spherical implant design is able to maintain segmental RoM and provide minimal differences in FCFs. Large areas of von Mises strain maxima were generated in the bone adjacent to the implant regardless of whether the implant was PEEK or CoCr.

Introduction

Despite the resurgent interest in lumbar disc arthroplasty, these procedures were initially performed in the 1960s. Ulf Fernström implanted stainless steel ball bearings following discectomy, or for painful disc disease, and termed this procedure disc arthroplasty[1]. At that time, persistent low back pain was prevalent following discectomy of a herniated or painful disc. While combining discectomy with fusion improved clinical results there was an increased risk of infection, pseudoarthrosis, thrombosis, embolus, and death[2]. More recently, fusion has been associated with adjacent level disc degeneration, which may be the result of an altered biomechanical environment[3-5]. Therefore, Fernström introduced a type of arthroplasty involving implantation of a spherical endoprothesis (stainless steel ball bearing) into the center of an evacuated disc. The intention of such a procedure was

to provide a motion-preserving alternative to fusion, which would potentially prevent or forestall degenerative changes at the adjacent levels.

The Fernström prosthesis has been criticized for having a high subsidence risk[6, 7]. However, subsidence has also recently been documented as a complication following modern total disc replacements (TDRs) for both mobile and fixed core implants[8-10]. However, very few biomechanical studies have been performed to determine the cause and factors associated with TDR subsidence. Two year follow-up performed by Fernström revealed indentation of the implant into the endplates ranging from 1 to 3 mm[1]. Two-year clinical follow up of a modern, fixed core TDR implanted in athletes demonstrated subsidence of the implants 2 to 3 mm in 30% of the patients occurring during the first three months[11]. For this modern TDR design, up to 5 mm of subsidence was considered "minor" and was not judged to have an adverse effect on the clinical outcome. A different study involving a modern, elastomeric nucleus replacement documented endplate changes following implantation, which the authors attributed to loading of the endplate by the implant [12]. Despite these endplate changes, the authors documented favorable clinical results in 88% of their patients after 1 to 2 years. Thus, several contemporary studies indicate that the levels of subsidence documented by Fernström are also observed with modern spinal arthroplasty technologies. Furthermore, initial subsidence of disc arthroplasty devices may be unavoidable, and does not appear to necessarily predict poor clinical results, provided the subsidence equilibrates after an initial period without further, long-term unstable loss of disc height or neural

foramina. Fernström indicated that indentation of the implant into the endplate prevented ventral and dorsal slipping while still allowing bending movements, suggesting that initial subsidence of the device may improve its functionality.

Complications reported by Fernström included expulsion of the device in one case (0.7%) and temporary paresis of the peroneus in another case (0.7%) after two years. Interestingly, there were no observations made regarding the facets at the index level. However, a later clinical study which evaluated spherical interbody implants after 10 to 20 years of implantation reported the need for subsequent fusion as a result of facet arthrosis in 10% of patients treated for degenerated disc disease, and none for those treated for a protruding disc[13]. In modern fixed or mobile bearing TDRs, facet arthrosis at the implanted level may occur in approximately a third of the patients after three years regardless of TDR type[14]. Several contemporary studies have also documented facet joint triggered low back pain as a complication associated with modern TDRs[11, 15, 16]. It is unclear what contributes to the prevalence of facet arthrosis post TDR, and it is further complicated by the difficulty to diagnose the disease in its early stages. However, several studies have hypothesized or demonstrated altered facet loading following implantation of modern TDRs[17-22], which may be attributed to changes in the center of rotation or removal of associated soft tissue structures, such as the anterior longitudinal ligament and most of the annulus. Since the Fernström prosthesis can be implanted without resection of the anterior longitudinal ligament, and the center of rotation will inherently be near the center of the disc, loading in

the facets may be similar to the pre-implanted condition. However, no biomechanical studies have quantified facet loading after implantation of a spherical interbody device.

Long-term follow up of patients implanted with a Fernström sphere was performed at 10 to 20 years by Mckenzie [13]. He reported good or excellent clinical outcomes in 83% of patients treated for disc protrusions and 75% for those treated for disc pain. These results are similar to a recent clinical study involving a contemporary, mobile bearing disc arthroplasty, which indicated good or excellent results in 82% of patients approximately 13 years post implantation. Despite certain similarities in clinical outcomes between the Fernström sphere and modern technologies, the device has not been widely used clinically. Today, spherical interbody spacers fabricated from PEEK or CoCr are clinically available, however, there remains a paucity of clinical and biomechanical data for these devices.

The primary objective of the current study was to evaluate the biomechanics of a spherical interbody implant using a previously validated finite element model (FEM) of a single lumbar motion segment. It was hypothesized that implantation of a spherical interbody implant, with combined subsidence into the vertebral bodies, would result in similar ranges of motion (RoM) and facet contact forces (FCFs) when compared with an intact condition. A secondary objective of this study was to determine the effect of using a PEEK versus a cobalt chrome (CoCr) implant on vertebral body strains. We hypothesized that the material selection would have a

negligible effect on vertebral body strains since both materials have elastic moduli substantially greater than the annulus.

Methods

A three-dimensional finite element model (FEM) of a ligamentous L3-L4 motion segment was generated from quantitative computed tomography (QCT) data of a cadaveric spine. The donor was a 78-year-old male who died from cardiac arrhythmia. The data set was taken from an Institutional Review Board-approved cadaveric study. The spine was chosen due to its lack of any bony or disc deformities, i.e, osteophytes, herniations, or degenerative disc disease. Hounsfield units were used as a surrogate for bone mineral density (BMD). Elastic moduli within the vertebral body fell within what has been previously reported in the literature.[23-25] The development of the model has been previously described, but will be outlined below[22]. A combination of automatic and manual image segmentation techniques (Analyze, AnalyzeDirect, Inc., Lenexa, KS) were used to extract detailed surfaces corresponding to the major bony structures of L3-L4. The software package allowed for automatic segmentation based on thresholding of the QCT grayscale values. These surfaces were imported into the commercial finite element mesh generation program, HyperMesh (Altair Inc., Troy, MI), and were discretized into a combination of tetrahedral elements for the bony structures and hexahedral elements for the intervertebral disc (IVD). The central portion of the IVD, approximately 40% of the volume[26], was designated to be the nucleus pulposus (NP), while the remaining volume was considered the annulus fibrosus. Major spinal ligaments (anterior longitudinal ligament, posterior longitudinal, intraspinatus, supraspinatus, intratransverse, facet capsule, ligamentum flavum) were implemented in the model using

tension-only nonlinear springs. Shell elements were used to plate the exterior surface of the vertebral bodies and represented the cortex and bony endplate (Figure 1-1).

Bone mineral density (BMD)-dependent orthotropic material properties were assigned to the cancellous bone of the vertebral bodies. Custom software was written to apply the measured Hounsfield numbers from the QCT data to the nodal points within the finite element mesh. Similar methodology has been used to create models with heterogeneous bone properties of the tibia and femur.[27, 28] The quantitative relationship between bone mineral density and elastic modulus in cancellous vertebral bone, as reported by Morgan et al., and Ulrich et al., was utilized to define a nonlinear relationship between bone mineral density and orthotropic elastic modulus.[29, 30] Elastic moduli within the vertebral body fell within what has been previously reported in the literature.[23-25] The remaining structures were assigned material properties from the literature and are depicted in Table 1-1. Frictionless contact was defined between the facets using a penalty-based contact algorithm.

Two separate analyses were performed in order to validate the results of the model. The first analysis involved applying a 1000 N compressive force to the intact model in order to simulate previously published experiments using cadaveric specimens.[31] The total vertical displacement of L3, intervertebral disc pressure, and cortical and endplate first principal strains were compared between the FEM and the previously published experimental data.[31] A second validation study was performed by applying moments of 7.5 Nm along the three principal anatomic axes and comparing total range of motion (RoM) in flexion-extension, lateral bending, and axial rotation with previously published data.[32-37]

A virtual implantation of a 16 mm diameter sphere was performed on the intact model, which resulted in a total distraction of 4 mm. The 16 mm diameter sphere was chosen in order to simulate subsidence of the implant of 2 mm into each endplate without reducing the total disc height beyond the intact state (12 mm). To simulate subsidence, two additional models were created with total subsidence of the implant into the vertebral bodies of 2 and 4 mm distributed equally between the superior and inferior endplates (Figure 2-1). The initial forces and stresses in the annulus and ligaments were set to zero at the fully distracted state for all models. This was done to isolate the effect of facet joint distraction and endplate-implant loading for different levels of subsidence. Subsidence of the implant was applied symmetrically between the inferior and superior endplate. The nucleus and cartilaginous endplate was removed within the nuclear cavity. For the cases of 2 and 4 mm of subsidence, vertebral bone was removed to accommodate for the implant geometry. A layer of shell elements representing the bony endplate was maintained between the implant and vertebral body at all levels of subsidence. The heterogeneous modulus of the underlying cancellous bone was not altered for the different levels of subsidence. Frictionless contact was defined at the implant-endplate interfaces as well as between the implant and the interior surface of the annulus fibrosus. To determine the sensitivity to friction both flexion and extension was applied to the 4 mm of subsidence model with a coefficient of friction of 0.5. These results indicated a less than 10% difference in the total flexion-extension range of motion when compared with the frictionless model. The spherical implant was modeled using material properties for PEEK (E = 4 GPa, n = 0.46) and cobalt chrome Alloy (E = 200 GPa, n = 0.3).

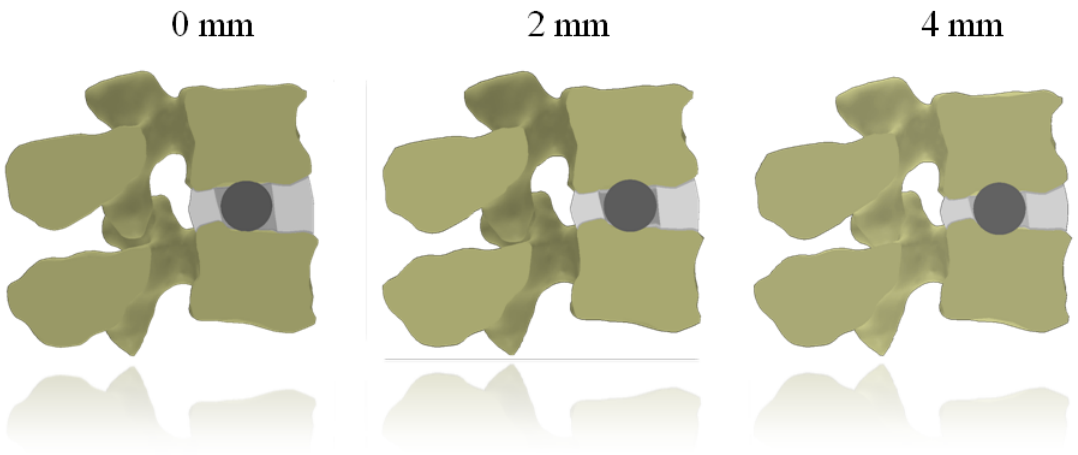

Figure 2-1. Fernstrom spheres were virtually implanted in order to depict three levels of subsidence. The figure depicts sagittal cross-sections of the three models, which consisted of 0 mm of implant subsidence (left), 2 mm of implant subsidence (center), and 4 mm of implant subsidence (right)

A compressive follower load of 500 N was applied to the intact, implanted with 0mm subsidence, implanted with 2 mm subsidence, and implanted with 4 mm subsidence with both a PEEK and cobalt chrome alloy implant. A combination of a compressive follower load (500 N) and flexion (7.5 Nm), extension (7.5 Nm), lateral bending (7.5 Nm), and axial rotation (7.5 Nm) was applied to all models with the implant modeled as PEEK. Rotational loading was applied via a moment at the center of mass of the superior endplate of L3, which was modeled as a rigid body. There were no constraints applied to any of the rotational or translational degrees of freedom of the L3 superior endplate. The inferior endplate of L4 was constrained in all degrees of freedom to provide an appropriate boundary condition. All models were solved using the commercial finite element modeling software LS-Dyna (LSTC, Livermore, CA).

Vertebral body cancellous bone effective von Mises (VM) strains were determined. Strain was chosen over stress due to the heterogeneous nature of the

vertebral bone. Strain has been documented to have less dependence on the apparent density when compared with stress.[23] Von Mises strain was chosen in order to depict the distortional strain being experienced in the vertebral bodies after implantation of a spherical implant. Von Mises yield criterion is often used to predict the yield point for bone.[38] The Von Mises strain is intended to qualitatively depict areas of the bone that may be most at risk of yielding after device implantation. Range of motion (RoM) was defined as the total angular rotation of L3. The total facet contact force (FCF) was defined as the sum of all nodal contact forces for both the left and right facet.

Results

In our validation analyses, the model was generally able to predict cortical and endplate strains within the ranges reported in the literature.[31] Typically, the model's results matched the trends demonstrated by the experimental median values (Figure 1-2). Additionally, the model predicted a disc pressure of 0.75 MPa and a total vertical displacement of 1.1 mm after application of 1000N of compression, which fell within the range of the experimentally reported values. Further validation indicated that the model predicted the total range of motion in flexion-extension, lateral bending, and axial rotation (Figure 1-3a, b).

When analyzing the Fernström prosthesis, peak effective strain in the cancellous bone during compression occurred just beneath the surface adjacent to the endplate-implant interface with values of 0.48%, 12.9%, and 14.7% for the intact, implanted with PEEK and 0 mm subsidence, and implanted with CoCr and 0 mm subsidence, respectively. Peak effective strain reduced to 4.0% and 4.6% at 2

mm of subsidence for the PEEK and CoCr implants, respectively. At 4 mm of subsidence the peak effective strain was 2.7% and 3.0% for the PEEK and CoCr implants, respectively. Compressive loading resulted in strain maxima at the implant-endplate interface for both a CoCr and PEEK implant (Figure 2-2). Qualitatively, the PEEK implant resulted in a slight decrease in the size of the strain maxima. Both the PEEK and CoCr implants resulted in a decrease in strain maxima with increasing subsidence. During 0 mm of subsidence the strain maxima occurred directly adjacent to the implant. At 2 mm of subsidence the strain maxima in the superior vertebrae radiated out from the anterior and posterior portions of the endplate-implant interface, which resulted in an area of reduced strain maxima near the most superior portion of the implant. At 4 mm of subsidence the strain maxima occurred at the anterior and posterior portions of the endplate-implant interface in both the superior and inferior vertebral bodies.

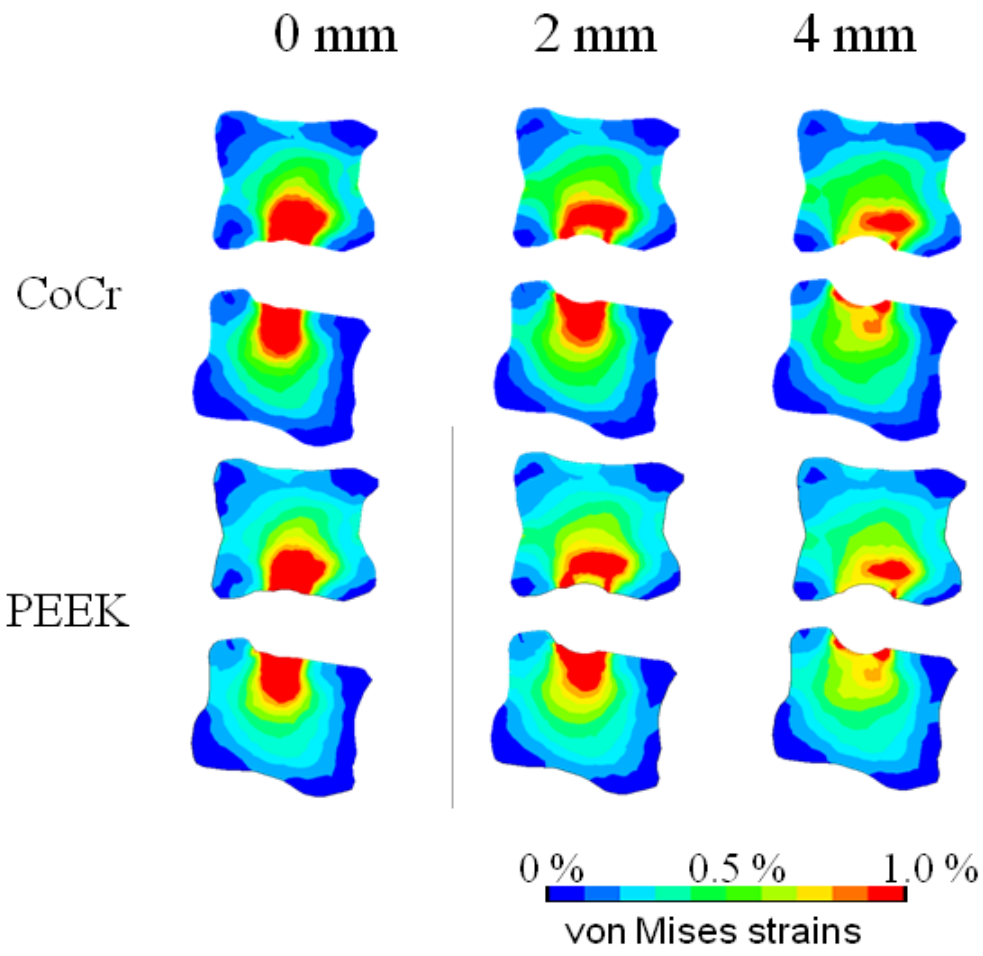

Figure 2-2. Effective (VM) strain contour plots of L3-L4 vertebral bodies at a sagittal cutplane for three levels of implant subsidence. The images on top depict the models implanted with CoCr sphere, and the images on the bottom depict the models implanted with a PEEK implant.

Increased subsidence of the device from 0 to 4 mm resulted in a progressive decrease of the RoM (Figure 2-3). Implantation with 0 mm of subsidence resulted in an increased RoM for all modes of loading compared to the intact model. These increases ranged from 80% during axial rotation to 10% during flexion (Table 2-1). Subsidence of 2 mm resulted in increased RoM for all modes of loading with the exception of flexion. The increased range of motion during 2 mm of subsidence was greatest during extension (31%). Subsidence of the implant at 4 mm resulted in a

decreased RoM for all modes of loading when compared with the intact model from -32% to -3%.

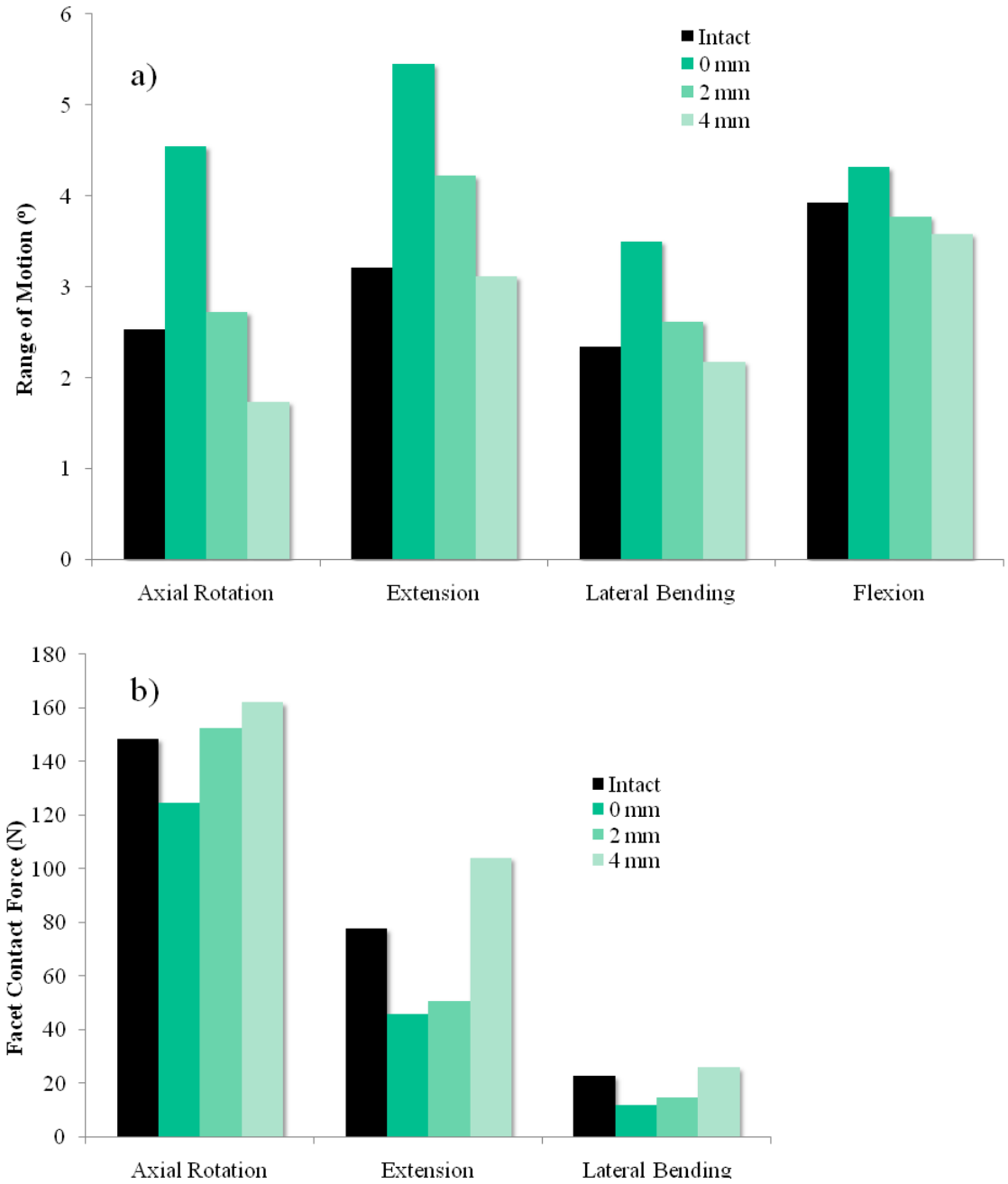

Figure 2-3. Bar graphs depicting the total angular RoM (a) and total facet contact force (b) for all loading modes and models.

Table 2-1. Tables representing the percentage change of RoM (a) and FCF (b) for the implanted models compared to the intact model.

a)

	Axial Rotation	Extension	Lateral Bending	Flexion
0mm	80%	70%	50%	10%
2mm	8%	31%	12%	-4%
4mm	-32%	-3%	-6%	-9%

b)

	Axial Rotation	Extension	Lateral Bending
0mm	-16%	-41%	-48%
2mm	3%	-35%	-37%
4mm	9%	34%	14%

FCFs in the intact model were greatest during axial rotation (148 N), less in extension (77 N), and the least during lateral bending (22.5 N). Flexion resulted in distraction of the facets for both the implanted and intact models. Facet contact forces tended to increase with increasing subsidence of the device from 0 to 4 mm (Figure 6b). 0 mm of subsidence resulted in a decreased FCF for all modes of loading between -16% and -48% when compared with the intact model (Table 2b). 2 mm of subsidence resulted in a small increase in FCF during axial rotation (3%), but decreased FCF during extension (-35%) and lateral bending (-37%) when compared to the intact model. FCFs increased at 4 mm of subsidence for all modes of loading between 9% and 34% when compared with the intact model.

Contours of von Mises strain in the cancellous bone of the vertebral bodies indicated values below 1% for the intact model with the exception of a small area near the ALL attachment during extension (Figure 2-4). Implantation of a PEEK spherical implant resulted in increased strain maxima adjacent to the implant-endplate interface for all modes of loading and levels of subsidence. Qualitatively, areas of strain maxima tended to decrease with increasing levels of implant subsidence. Areas of strain maxima tended to be larger in the superior vertebrae when compared with the inferior during 4 mm of subsidence. During compression, flexion, axial rotation, and lateral bending the areas of strain maxima were localized to the area adjacent to the endplate-implant interface. However, during extension, the strain maxima in the superior vertebra was continuous with the maxima observed near the ALL insertion site.

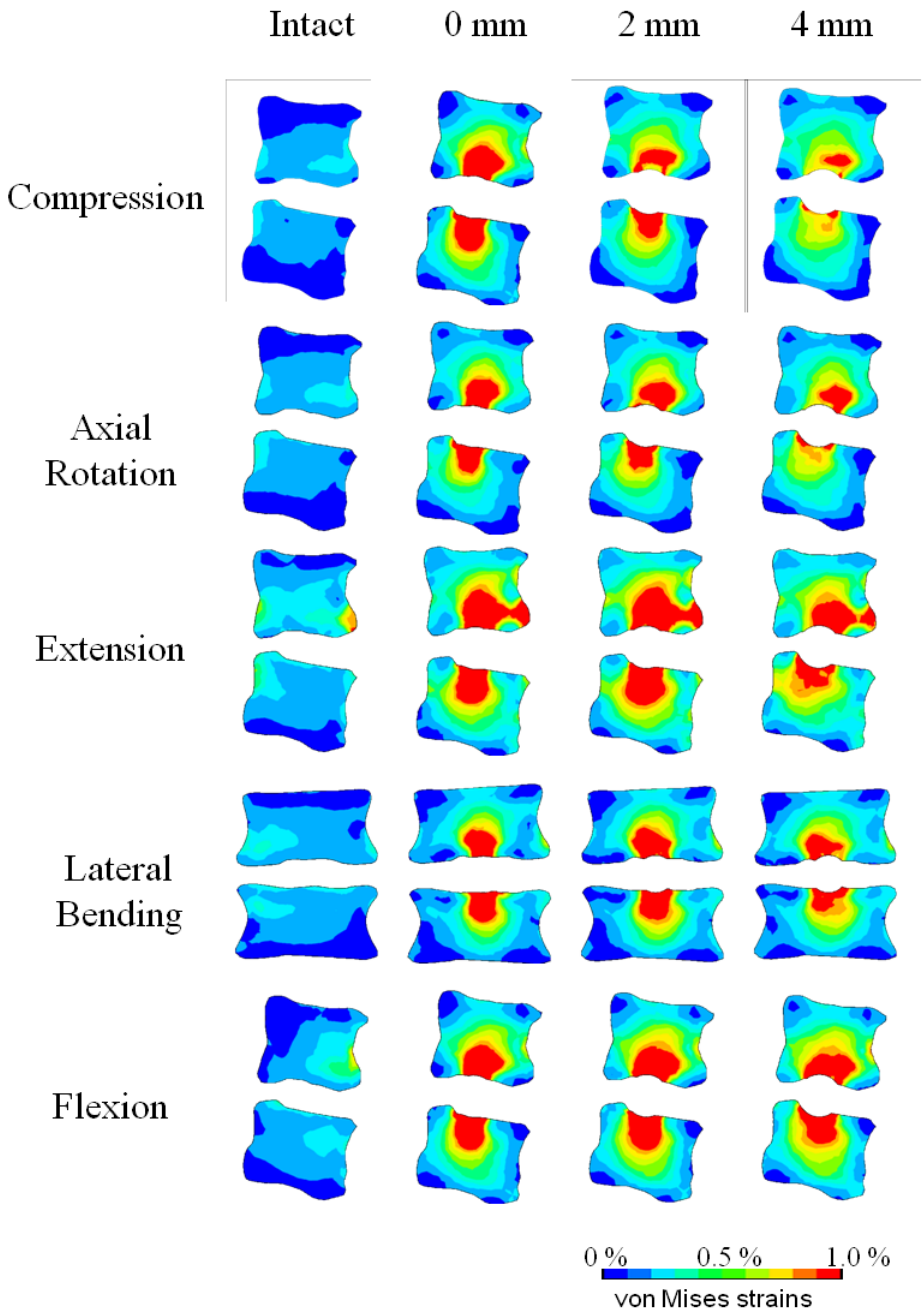

Figure 2-4. Effective (VM) strain contour plots of L3-L4 vertebral bodies at a sagittal or coronal cutplane for all modes of loading and models.

Discussion

The current study evaluated the differences in PEEK and CoCr implants on von Mises strain in the vertebral cancellous bone. Radiolucent PEEK implants provide the ability to visualize the surrounding bone and soft tissues during diagnostic imaging, but the biomechanical effects are not fully understood. We hypothesized that use of a PEEK versus a CoCr Fernström prosthesis would have a negligible effect on bone strains. However, we noticed a small reduction in the peak strain values. Results from the current study indicated increased peak von Mises strain in the vertebral body cancellous bone for CoCr implant (14.7%) compared to a PEEK implant (12.9%) when no subsidence of the device was modeled. This is consistent with results from a previous finite element study that documented a reduction in endplate stresses between a PEEK and titanium interbody spacer[39]. The authors of the previous study concluded that the reduced stresses may result in a lower likelihood of subsidence. However, they did not report stresses in the endplate for an intact scenario. While the current study predicted a slight reduction in strain for a PEEK implant, both the PEEK and and CoCr implants resulted in a substantial increase in peak strain and area of strain maxima compared to the intact state. Additionally, the current study indicated that increasing levels of subsidence result in a reduction of the differences between PEEK and CoCr, further suggesting that there may be limited biomechanical advantage to using PEEK for this application. Furthermore, the reductions in peak strain that resulted from increased subsidence or conformity of the endplate to the device still resulted in peak strain much higher than that documented in the intact condition. The results from the

current study suggest a high subsidence likelihood for either a PEEK or CoCr spherical prosthesis.

Results from the current analysis demonstrate that implantation of a spherical interbody implant maintains segmental RoM. Initial implantation of the device with no subsidence resulted in an increased range of motion for all modes of loading between 10% and 80% depending on the mode of loading. These results are consistent with previous studies that have evaluated RoM after TDR. Two previous FEM studies indicated an increased RoM after implantation of a TDR [20, 22]. Similarly, an *in vitro* cadaveric study also documented increased RoM post TDR during flexion/extension[40].

The current study documented a progressive reduction in the RoM with increased subsidence of the device into the vertebral bodies. Four mm of subsidence resulted in a decreased RoM for all modes of loading when compared with the intact condition. Interestingly, the greatest increases in RoM at 0 mm of subsidence corresponded to the modes of loading that result in contact of the facets, such as axial rotation, extension, and lateral bending. This suggests that changes in relative facet positioning that occur during distraction had an effect on RoM. Increased subsidence progressively reduced RoM by bringing the facets closer to their pre-implantation positioning. This is further corroborated by the fact that flexion, which resulted in no facet contact force, experienced the least sensitivity to subsidence with respect to RoM. These results suggest the need for careful consideration of the amount of surgical distraction required for these types of procedures. A certain

amount is required for disc height restoration and neural foraminal decompression, but too much can prevent or limit facet contact. Future work should investigate the effect of ligament and annulus pre-tensioning as a result of distraction. The lack of pre-tensioning in these structures was a limitation of the current study, but deemed necessary in order to control the applied loading. Similarly, smaller implants should be evaluated to determine the effects when subsidence results in a reduction of disc height compared to the intact state.

The current study demonstrated similar FCF between the intact and implanted models. The FCFs progressively increased with increased subsidence of the device. This resulted in increased FCFs for all modes of loading at 4 mm of subsidence. A previous FE study evaluated the FCF between a fixed and mobile core TDR at varying positions and documented FCFs equivalent to175% of the intact state depending on positioning and TDR type[41]. This study attributed increases in FCF to a fixed center of rotation of a fixed-core TDR. However, this study applied known physiologic rotations to all of the models instead of loads thereby negating the potential for increased mobility that arises post TDR[40], even when using a hybrid loading approach[42]. A finite element study that applied loading consistent with bending over to a model implanted with a TDR documented a doubling of the average facet contact pressure [20]. Similarly, a different finite element study documented the potential for doubling of the FCFs after implantation of a TDR when subjected to rotational loading[22]. The current study documented a maximum increase of FCF of 34%, which occurred during extension and 4 mm of subsidence of

the implant. However, at 2mm of subsidence FCFs were decreased 35% compared to the intact model during extension. Further examination of the model revealed that subsidence of the implant resulted in a reduction in posterior translation of L3 relative to L4 during extension. At 4 mm of subsidence the total translation was less (2.1 mm) than what was experienced for the intact model (2.41 mm). These results suggest that subsidence of the implant prevents relative translation of the vertebrae, which results in increased loading of the facets. It is difficult to compare the changes in FCFs documented in the current study with those reported in previous evaluations of modern TDRs due to the differences in surgical technique. Specifically, implantation of a sphere requires minimal resection of the annulus, which likely helps to maintain pre-implantation kinematics and thereby mitigate changes in the facet contact.

The current study documented the presence of large areas of strain maxima adjacent to the implant for all modes of loading. We have previously performed a similar analysis on a fixed core TDR, and evaluated the von Mises strains of the cancellous bone [22]. The results from that study indicated that strains typically remained under 1% after implantation with the exception of a small area during flexion. This is likely the result of the larger contact surface area for a TDR compared to the Fernström sphere, especially at 0 mm of subsidence. This is further indicated by the decreasing area of strain maxima that was observed for increasing levels of subsidence. As the implant nested further into the cancellous bone, the area of contact increased, which resulted in a more distributed load. Even though

increased subsidence resulted in reduced areas of strain maxima, the fully nested models still depicted strains substantially greater than the intact state. Despite the large areas of strain maxima above 1% documented for all modes of loading, the clinical results depict reasonable levels of subsidence and satisfactory clinical outcomes[1, 13]. This suggests that the initial strains experienced by the bone after implantation may not be relevant when investigating long-term subsidence of spinal arthroplasty devices. Alternatively, the disparity between the clinical outcomes and high peak strain documented in the current study may be explained by increased load bearing in the annulus fibrosus. Specifically, since the fernstrom prosthesis maintains the majority of the annulus, continued subsidence may offset the axial loading from the device to the surrounding annulus. The current model did not take this phenomenon into consideration.

Additionally, the current model did not account for densification of the underlying bone as a result of the subsidence. This could also act to strengthen the underlying bone and prevent subsequent subsidence, which helps to explain the discrepancy with the reported clinical data. Recent implantations of an interbody sphere by one of the authors of this study has provided radiographic follow-up at 9 months (Figure 2-5). This image indicates high signal intensity in the bone adjacent to the implant suggesting bony remodeling, which may help to prevent long-term subsidence. However, implantation of TDRs in elderly patients has resulted in severe subsidence[9], which suggests that good initial bone quality is imperative.

The current study further emphasizes the need for a better understanding of the factors attributing to long-term subsidence of spinal implants.

Figure 2-5. Coronal CT image of a spherical CoCr interbody device implanted at L5-S1. Vertebral bodies demonstrate high signal intensity around the implant at 9 months.

In conclusion, the current study evaluated the biomechanical effects of the implantation of a simple spherical interbody implant at three levels of subsidence. The results suggest that this simple implant design is able to maintain segmental RoM and provide minimal differences in FCFs. Large areas of von Mises strain were generated in the bone adjacent to the implant regardless of whether the implant

was PEEK or CoCr. Despite the large areas of strain documented in the current study, clinical results suggest that severe subsidence is not a common complication, and initial subsidence of the device helps secure the device and prevent intervertebral shear translations. However, the disc height loss associated with subsidence may preclude the efficacy of such a device.

References

1. Fernstrom, U., *Arthroplasty with intercorporal endoprothesis in herniated disc and in painful disc.* Acta Chir Scand Suppl, 1966. **357**: p. 154-9.
2. Wiltberger, B.R., *Surgical Treatment of Degenerative Disease of the Back.* J Bone Joint Surg Am, 1963. **45**: p. 1509-16.
3. Kumar, M.N., A. Baklanov, and D. Chopin, *Correlation between sagittal plane changes and adjacent segment degeneration following lumbar spine fusion.* Eur Spine J, 2001. **10**(4): p. 314-9.
4. Pellise, F., et al., *Radiologic assessment of all unfused lumbar segments 7.5 years after instrumented posterior spinal fusion.* Spine, 2007. **32**(5): p. 574-9.
5. Schulte, T.L., et al., *Disc height reduction in adjacent segments and clinical outcome 10 years after lumbar 360 degrees fusion.* Eur Spine J, 2007.
6. Coric, D. and P.V. Mummaneni, *Nucleus replacement technologies.* J Neurosurg Spine, 2008. **8**(2): p. 115-20.
7. Bono, C.M. and S.R. Garfin, *History and evolution of disc replacement.* Spine J, 2004. **4**(6 Suppl): p. 145S-150S.
8. Punt, I.M., et al., *Complications and reoperations of the SB Charite lumbar disc prosthesis: experience in 75 patients.* Eur Spine J, 2008. **17**(1): p. 36-43.
9. Bertagnoli, R., et al., *Lumbar total disc arthroplasty in patients older than 60 years of age: a prospective study of the ProDisc prosthesis with 2-year minimum follow-up period.* J Neurosurg Spine, 2006. **4**(2): p. 85-90.
10. David, T., *Long-term results of one-level lumbar arthroplasty: minimum 10-year follow-up of the CHARITE artificial disc in 106 patients.* Spine, 2007. **32**(6): p. 661-6.
11. Siepe, C.J., et al., *Total lumbar disc replacement in athletes: clinical results, return to sport and athletic performance.* Eur Spine J, 2007. **16**(7): p. 1001-13.
12. Bertagnoli, R. and R. Schonmayr, *Surgical and clinical results with the PDN prosthetic disc-nucleus device.* Eur Spine J, 2002. **11 Suppl 2**: p. S143-8.
13. McKenzie, A.H., *Ferstrom Intervertebral Disc Arthroplasty: Long-Term Clinical Results.* Orthopaedics International, 1995. **3**: p. 313-324.
14. Shim, C.S., et al., *CHARITE versus ProDisc: a comparative study of a minimum 3-year follow-up.* Spine, 2007. **32**(9): p. 1012-8.

15. van Ooij, A., F.C. Oner, and A.J. Verbout, *Complications of artificial disc replacement: a report of 27 patients with the SB Charite disc.* J Spinal Disord Tech, 2003. **16**(4): p. 369-83.
16. Siepe, C.J., et al., *Analysis of post-operative pain patterns following total lumbar disc replacement: results from fluoroscopically guided spine infiltrations.* Eur Spine J, 2007.
17. Link, H.D., *History, design and biomechanics of the LINK SB Charite artificial disc.* Eur Spine J, 2002. **11 Suppl 2**: p. S98-S105.
18. Huang, R.C., et al., *Long-term flexion-extension range of motion of the prodisc total disc replacement.* J Spinal Disord Tech, 2003. **16**(5): p. 435-40.
19. Liu, J., et al., *Effect of the increase in the height of lumbar disc space on facet joint articulation area in sagittal plane.* Spine, 2006. **31**(7): p. E198-202.
20. Denoziere, G. and D.N. Ku, *Biomechanical comparison between fusion of two vertebrae and implantation of an artificial intervertebral disc.* J Biomech, 2006. **39**(4): p. 766-75.
21. Rousseau, M.A., et al., *Disc arthroplasty design influences intervertebral kinematics and facet forces.* Spine J, 2006. **6**(3): p. 258-66.
22. Rundell, S.A., Auerbach, J.D., Balderston, R.A., Kurtz, S.M., *Total Disc Replacement Positioning Affects Facet Contact Forces and Vertebral Body Strains.* Spine, 2008. **33**(23): p. 2510-2517.
23. Kopperdahl, D.L. and T.M. Keaveny, *Yield strain behavior of trabecular bone.* J Biomech, 1998. **31**(7): p. 601-8.
24. Mosekilde, L. and C.C. Danielsen, *Biomechanical competence of vertebral trabecular bone in relation to ash density and age in normal individuals.* Bone, 1987. **8**(2): p. 79-85.
25. Hansson, T.H., T.S. Keller, and M.M. Panjabi, *A study of the compressive properties of lumbar vertebral trabeculae: effects of tissue characteristics.* Spine, 1987. **12**(1): p. 56-62.
26. White, A.A., Panjabi, M.M.,, *Clinical Biomechanics of the Spine, 2nd ed.*1990, Philadelphia-Toronto: J.B. Lippincott Company.
27. Yosibash, Z., et al., *A CT-based high-order finite element analysis of the human proximal femur compared to in-vitro experiments.* J Biomech Eng, 2007. **129**(3): p. 297-309.
28. Sawatari, T., et al., *Three-dimensional finite element analysis of unicompartmental knee arthroplasty--the influence of tibial component inclination.* J Orthop Res, 2005. **23**(3): p. 549-54.
29. Ulrich, D., et al., *The ability of three-dimensional structural indices to reflect mechanical aspects of trabecular bone.* Bone, 1999. **25**(1): p. 55-60.
30. Morgan, E.F., H.H. Bayraktar, and T.M. Keaveny, *Trabecular bone modulus-density relationships depend on anatomic site.* J Biomech, 2003. **36**(7): p. 897-904.
31. Frei, H., et al., *The effect of nucleotomy on lumbar spine mechanics in compression and shear loading.* Spine, 2001. **26**(19): p. 2080-9.
32. Yamamoto, I., et al., *Three-dimensional movements of the whole lumbar spine and lumbosacral joint.* Spine, 1989. **14**(11): p. 1256-60.

33. Mimura, M., et al., *Disc degeneration affects the multidirectional flexibility of the lumbar spine.* Spine, 1994. **19**(12): p. 1371-80.
34. Panjabi, M.M., et al., *Mechanical behavior of the human lumbar and lumbosacral spine as shown by three-dimensional load-displacement curves.* J Bone Joint Surg Am, 1994. **76**(3): p. 413-24.
35. Fujiwara, A., et al., *The effect of disc degeneration and facet joint osteoarthritis on the segmental flexibility of the lumbar spine.* Spine, 2000. **25**(23): p. 3036-44.
36. Schmoelz, W., et al., *Dynamic stabilization of the lumbar spine and its effects on adjacent segments: an in vitro experiment.* J Spinal Disord Tech, 2003. **16**(4): p. 418-23.
37. Niosi, C.A., et al., *Biomechanical characterization of the three-dimensional kinematic behaviour of the Dynesys dynamic stabilization system: an in vitro study.* Eur Spine J, 2006. **15**(6): p. 913-22.
38. Nagaraja, S., T.L. Couse, and R.E. Guldberg, *Trabecular bone microdamage and microstructural stresses under uniaxial compression.* J Biomech, 2005. **38**(4): p. 707-16.
39. Vadapalli, S., et al., *Biomechanical rationale for using polyetheretherketone (PEEK) spacers for lumbar interbody fusion-A finite element study.* Spine, 2006. **31**(26): p. E992-8.
40. O'Leary, P., et al., *Response of Charite total disc replacement under physiologic loads: prosthesis component motion patterns.* Spine J, 2005. **5**(6): p. 590-9.
41. Moumene, M. and F.H. Geisler, *Comparison of biomechanical function at ideal and varied surgical placement for two lumbar artificial disc implant designs: mobile-core versus fixed-core.* Spine, 2007. **32**(17): p. 1840-51.
42. Goel, V.K., et al., *Effects of charite artificial disc on the implanted and adjacent spinal segments mechanics using a hybrid testing protocol.* Spine, 2005. **30**(24): p. 2755-64.

3. Total Disc Replacement Positioning Affects Facet Contact Forces and Vertebral Body Strains

Abstract

TDR has the potential to replace fusion as the gold standard for treatment of painful degenerative disc disease. However, complications after TDR include index level facet arthrosis and implant subsidence. Alterations in facet and vertebral body loading after TDR and their dependence on implant positioning are not fully understood. The objective of the current study was to evaluate how TDR implantation and positioning affects facet joint forces and vertebral body strains. We hypothesized that facet contact forces would increase with TDR to compensate for the loss of periprosthetic load bearing structures, and that vertebral body strains would increase in the region around the metallic footplates. A FEM of L3-L4 was created and validated using range of motion, disc pressure, and bony strains from previously published data. A TDR was incorporated into the L3-L4 spine model. All models were subjected to a compressive follower load of 500N and moments of 7.5 Nm about the three anatomical axes. Overall RoM and facet contact forces tended to increase with TDR. Facet contact forces increased by an order of magnitude during flexion. Posterior placement of the device resulted in an unloading of the facets during extension. Areas of strain maxima were observed in the anterior portion of the vertebral body during flexion after TDR. The area of initial bone resorption signal under the metal footplate was greater when the device was placed anterior. The current study predicted a decrease in segmental rotational stiffness resulting

from TDR. This resulted from the removal of load bearing soft tissue structures, and caused increased loading in the facets. Additionally, vertebral body strains were generally higher after TDR, and tended to increase with decreased rotational stiffness. Posterior placement of the device provided a more physiologic load transfer to the vertebral body.

Introduction

Symptomatic degenerative disc disease (DDD) of the lumbar spine can result in a substantial reduction in the quality of life. Although the current gold standard treatment continues to be lumbar spinal fusion, the development of adjacent level disease, which may be in part attributed to an altered biomechanical environment, has been shown clinically and in vitro studies [1-5]. Recently, total disc replacement systems (TDR) have been introduced as an alternative to fusion. These devices are intended to restore the disc height, maintain or correct segmental lordosis, and preserve segmental range of motion [6]. Biomechanical studies have documented a reduction in adjacent level effects after TDR when compared with fusion [5, 7]. However, some of the potential complications include subsidence and migration of the metal footplates into the vertebral body [8, 9] and facet arthrosis at the implanted level [10].

TDR in the lumbar spine is currently indicated for patients who report with single level DDD, although research is under way to explore the outcomes following implantation in multiple levels. However, there are many contraindications for lumbar TDRs, including central or lateral recess stenosis, facet arthrosis,

spondylolisthesis or spondylolysis, herniated nucleus pulposus with neural compression, scoliosis, osteoporosis, and postsurgical psuedoarthrosis or deficiency of posterior elements[11],[12]. A recent clinical study compared the outcome of patients implanted with two different types of TDR[10] and documented facet arthrosis at the implanted level in approximately one third of the patients after three years regardless of TDR type. The etiology behind facet arthrosis following TDR surgery is unclear and further complicated by difficulties associated with diagnosing the disease in its early stages. Additionally, the biomechanical effects on the facets after TDR are not fully understood and difficult to elucidate *in vivo* and *in vitro.* It has been hypothesized that TDR may result in increased loading of the facets [13, 14], particularly during axial rotation where there is limited constraint to motion. However, it has also been suggested that an increase in joint space arising from distraction during surgical implantation could cause facet joint subluxation [15]. A finite element (FE) study comparing TDR with fusion observed increases in facet contact pressures, which were associated with increases in rotational range of motion [16]. A recent *in vitro* experiment compared the effects of a three and five degree-of-freedom TDR on facet contact forces, and observed both increases and decreases in facet contact forces, as well as changes to the motion segment's center of rotation, depending on implant design and loading direction [17]. These data suggest that TDR affects vertebral kinematics and facet contact forces. However, the precise mechanisms responsible for these alterations have not been thoroughly investigated. Additionally, the effects of implant positioning, and consequences on other load bearing structures have not been fully addressed.

Requisite removal of the natural, diseased disc and associated anterior and posterior longitudinal ligaments (ALL and PLL) during TDR implantation will inevitably alter the motion segment load bearing characteristics [18, 19]. A recent *in vivo* fluoroscopic evaluation demonstrated increased relative motion at the operative level during extension in TDR compared with controls, with no differences in flexion, most likely attributable to the loss of the ALL [5]. Intervertebral disc pressure also contributes to resistance in extension [19]. While changes in facet loading have been documented [16, 17], loading borne by the vertebral body from the artificial disc has not been investigated. TDR subsidence and migration of the metallic footplates has been documented clinically [8, 20] and may become a more clinically relevant problem as the patient population ages and experiences bone loss and osteoporosis. In a recent study, two reports of vertical split fractures were documented in patients with TDR [21]. In a separate study, a large cavity was observed in the vertebral body of L5 in a patient who received a two-level TDR at L4-L5 and L5-S1 [22]. The author indicated that the cavity was caused by migration of the keel at that level. Sagittal split fractures were also observed in a patient who underwent two level cervical disc arthroplasty [23]. Tropiano et al. reported vertebral body fracture as a complication in a clinical study involving TDR in 53 patients [24]. While a previous FE study has shown that the compressive strength of the vertebral body is sensitive to endplate loading distribution [25], the effects on vertebral body strains during loading from a TDR *in situ* remains unknown. Additionally, the effects of implant positioning across the nonhomogenous vertebral body has not been evaluated.

The objective of the current study was to evaluate how TDR implantation and positioning affects facet joint contact forces and implant subsidence. It was hypothesized that facet contact forces would increase with TDR to compensate for the loss of various load bearing structures, vertebral body strains would be high in the area around the metallic footplates, and initial bone remodeling stimulus in the vertebral body would predict resorption under the footplates from load shielding. We used a validated nonlinear 3-D finite element model of L3-L4 with a TDR implanted at two different positions along the sagittal midline to determine vertebral cancellous bone strains, initial vertebral bone remodeling stimulus, and facet contact forces.

Methods

A three-dimensional finite element model of a ligamentous L3-L4 motion segment was generated from quantitative computed tomography (QCT) data of a cadaveric spine. The donor was a 78 year old male who died from Cardiac Arrythemia. The data set was taken from an Institutional Review Board-approved cadaveric study. The spine was chosen due to its lack of any bony or disc deformities, i.e, osteophytes or herniations. Hounsfield units were used as a surrogate for bone mineral density (BMD).

A combination of automatic and manual image segmentation techniques (Analyze, AnalyzeDirect, Inc., Lenexa, KS) were used to extract detailed surfaces corresponding to the major bony structures of L3-L4. The software package allowed for automatic segmentation based on thresholding of the QCT grayscale values while

still allowing the user the ability to interactively segment sections of the images slice by slice. These surfaces were imported into the commercial finite element mesh generation program, HyperMesh (Altair Inc., Troy, MI), and were discretized into a combination of tetrahedral elements for the bony structures and hexahedral elements for the intervertebral disc (IVD). The central portion of the IVD, approximately 40% of the volume, was designated to be the nucleus pulposus (NP), while the remaining volume was considered the annulus fibrosus (AF). Major spinal ligaments (anterior longitudinal ligament, posterior longitudinal, intraspinatus, supraspinatus, intratransverse, facet capsule, ligamentum flavum) were implemented in the model using tension-only nonlinear springs. Shell elements were used to plate the exterior surface of the vertebral bodies and represented the cortex and bony endplate (Figure 3-1).

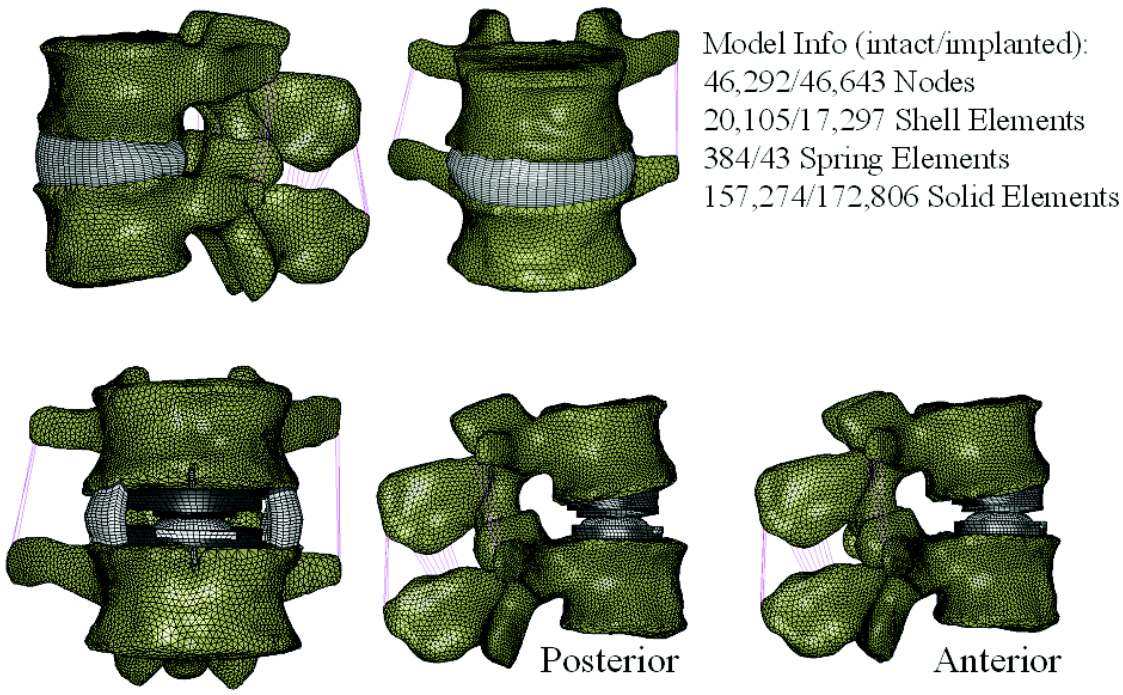

Figure 3-1. 3-D finite element model of a ligamentous L3-L4 motion segment with and without a fixed core TDR implanted at two anterior-posterior positions

Bone mineral density (BMD)-dependent orthotropic material properties were assigned to the cancellous bone of the vertebral bodies. Custom software was written to apply the measured Hounsfield numbers from the QCT data to the nodal points within the finite element mesh. Similar methodology has been used to create models with heterogeneous bone properties of the tibia and femur [26, 27]. The quantitative relationship between bone mineral density and elastic modulus in cancellous vertebral bone, as reported by Morgan et al., and Ulrich et al., was utilized to define a nonlinear relationship between bone mineral density and orthotropic elastic modulus [28, 29]. Elastic moduli within the vertebral body fell within what has been previously reported in the literature [30-32]. The remaining structures were assigned material properties from the literature and are depicted in Table 1-1.

Frictionless contact was defined between the facets using a penalty-based contact algorithm.

Two separate analyses were performed in order to validate the results of the model. The first analysis involved applying a 1000 N compressive force to the intact model in order to simulate a study previously published using cadaveric specimens [33]. The total vertical displacement of L3, intervertebral disc pressure, and cortical and endplate first principal strains were compared between the FEM and the previously published experimental data[33]. A second validation study was performed by applying moments of 7.5 Nm along the three principal anatomic axes and comparing total range of motion (RoM) in flexion-extension, lateral bending, and axial rotation with previously published data [18, 34-38].

Geometric surfaces for an appropriately sized model of the ProDisc-L (Synthes Spine, West Chester, PA) was created by reverse engineering dimensions from a commercially available component with a large footprint size, a six degree lordotic angle, and a 10 mm disc height. These surfaces were used to generate a hexahedral mesh using the commercial mesh generation software Truegrid (XYZ Scientific, Livermore, CA). The model of the ProDisc-L was placed in the intervertebral disc space at two surgically relevant locations along the sagittal midline a distance of 4 mm apart, resulting in a “posterior” and “anterior” placement. The vertebral bodies were augmented to include resections of bone along the path of the implant keels. The interface between the metallic endplates and the vertebral bone was fully fixed to simulate complete bone ongrowth. An equal amount of the lateral annulus was

preserved for both TDR positions. The ALL and PLL were completely resected. Material properties for cobalt chrome alloy (E = 215 GPa, $\nu = 0.3$) was assigned to the metallic footplates. A nonlinear material representation for polyethylene (PE) with an initial Young's modulus of 940 MPa was assigned to the insert [39]. Sliding contact was defined between the superior footplate and the PE insert with a coefficient of friction of 0.083 [40].

The implanted and intact models were exercised in flexion (7.5 Nm), extension (7.5 Nm), axial rotation (7.5 Nm), and lateral bending (7.5 Nm) with a 500 N compressive follower load applied to the superior endplate of L3. The inferior endplate of L4 was fixed in space to provide an appropriate boundary condition. Interface forces at each node in the facets were summed to yield the facet contact force (FCF). Vertebral body cancellous bone effective von Mises (VM) strains were also determined. Strain was chosen over stress due to the heterogeneous nature of the vertebral bone. Strain has been documented to have less dependence on the apparent density when compared with stress [30]. Von Mises strains were chosen in order to depict the distortional strains being experienced in the vertebral bodies after implantation of a TDR, and how this is affected by anterior-posterior placement. Von Mises yield criterion is often used to predict the yield point for bone [41]. The von Mises strain is intended to qualitatively depict areas of the bone that may be most at risk of yielding after TDR. Range of motion was defined as the total angular rotation of L3.

Initial bone remodeling signal for the vertebral bodies was calculated for each node by applying the following equation, which used strain energy density (SED) results from the implanted and intact models [42]:

$$Signal = \frac{SED_{implanted} - SED_{natural}}{SED_{natural}}$$

It has been previously determined that an appropriate threshold for humans is 0.75 [43]. Therefore, signal values greater than 0.75 were indicated as areas of increased bone formation, while areas below –0.75 were indicated as areas of bone resorption.

Results

Results from the validation analysis indicated good agreement between the FEM and previously reported experimental data. The FEM was generally able to predict cortical and endplate strains within the ranges reported in the literature [33]. Typically, the FEM's results matched the trends demonstrated by the experimental median values (Figure 1-2). Additionally, the FEM predicted a disc pressure of 0.75 MPa and a total vertical displacement of 1.1 mm after application of 1000N of compression, which fell within the range of the experimentally reported values. Further validation indicated that the FEM predicted the total range of motion in flexion-extension, lateral bending, and axial rotation (Figure 1-3).

TDR increased the RoM for all modes of loading regardless of implant positioning (Figure 3-2). Posterior placement of the implant resulted in an increased RoM when compared with the anterior placement for all modes of loading with the exception of

flexion (Figure 3-2a). Flexion RoM was the highest when the TDR was implanted anteriorly (10.8 degrees), whereas extension RoM was highest for a posterior placement (11.5 degrees) (Figure 3-2a). Extension RoM increased from 4.4 degrees with posterior placement to 11.5 degrees with anterior placement. Both axial rotation and lateral bending RoM increased from intact to anterior implantation and increased again with posterior shifting of the implant (Figure 3-2a).

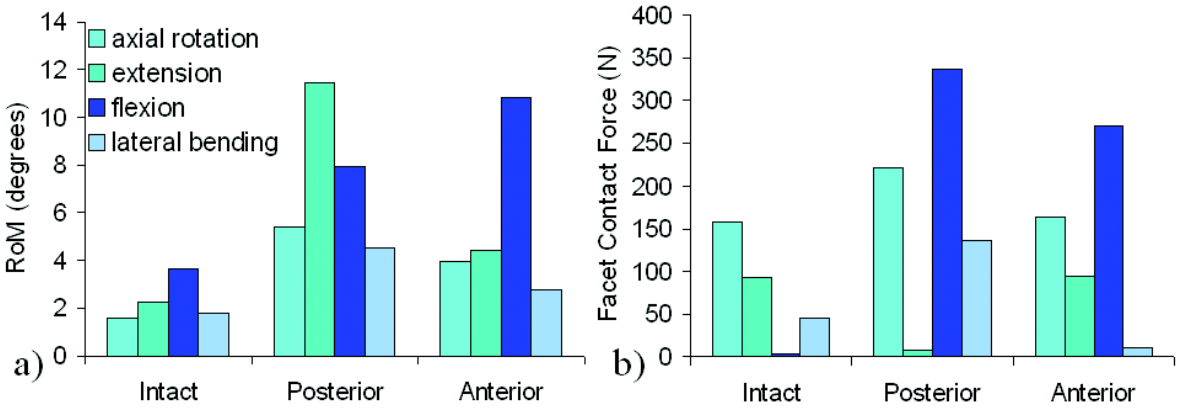

Figure 3-2. Bar graphs demonstrating the RoM (a) and facet contact forces (b) experienced by the intact and implanted FE models

The intact model experienced highest FCFs during axial rotation (Figure 3-2b). The implanted models both experienced the highest FCFs during flexion. Implantation resulted in an increase in FCFs in axial rotation, which further increased with posterior placement of the TDR (Figure 4b). FCFs in extension were reduced with implantation of the TDR posteriorly (7.7 N), but increased with anterior placement (95.3 N). A similar trend was documented in lateral bending, but with posterior placement resulting in an increase in FCFs (Figure 3-2b).

Contour plots of VM strain for the intact model indicated effective (VM) strains typically under 1% in the cancellous bone with the exception of a small area on the superior surface of L4 in lateral bending (Figure 3-3). Contour plots of effective strain contained numerical ranges from zero to one percent. One percent was chosen since it is the approximate yield strain of vertebral cancellous bone [30]. Following TDR, the area of bone directly underneath the metallic footplates and slightly posterior to the keel exhibited an unloading when compared with the intact scenario (Figure 3-3). Areas of bone that were not under the footplate appeared to be unloaded after implantation as well. Generally, the areas of bone around the edges of the footplates in the implanted models experienced higher strains when compared with the intact. An area of high strain was observed anteriorly in the intact model in extension as a result of load transfer from the ALL. Strains in this area were reduced to essentially negligible values (<0.001%) with TDR. Strain maxima were observed around the posterior edge of the metallic footplate in flexion and extension for both implant positions (Figure 3-3). These values generally ranged from 0.8 to 1.5 % strain. Strain maxima were also observed toward the anterior portion of the footplate during flexion. This was also observed underneath the keel (Figure 3-4).

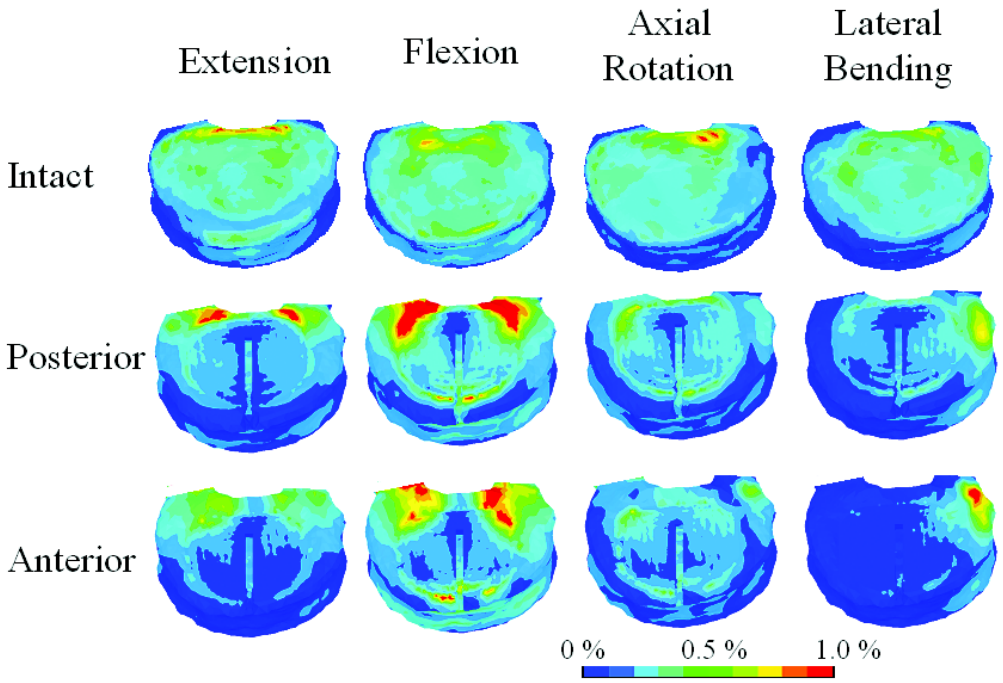

Figure 3-3. Effective (VM) strain contour plots of the L4 vertebral body cancellous bone

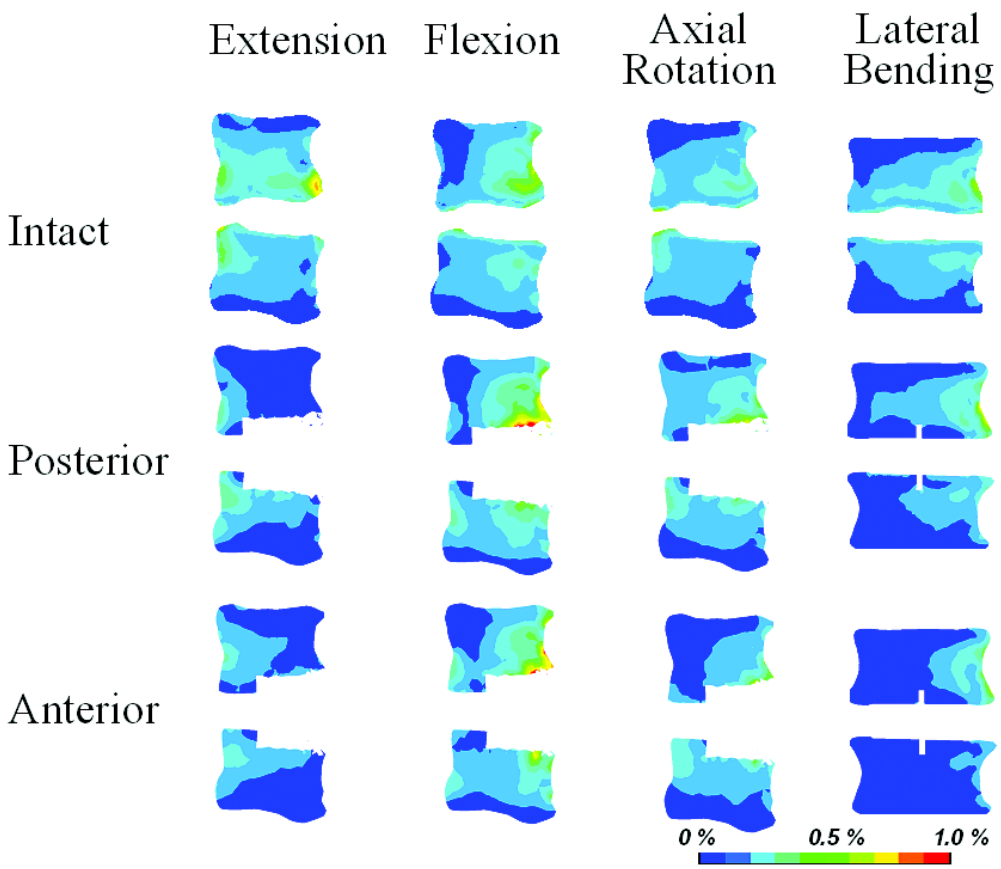

Figure 3-4. Effective (VM) strain contour plots of the L4 vertebral body cancellous bone at a sagittal or coronal cutplane

Initial bone remodeling stimulus in the vertebral body predicted a greater tendency for bone resorption under the inferior footplate when the implant was positioned anteriorly (Figure 3-5). Generally, bone resorption signal was observed anterior of the implant. Bone formation was predicted at the location of the pedicles for all modes of loading, but predominately during flexion.

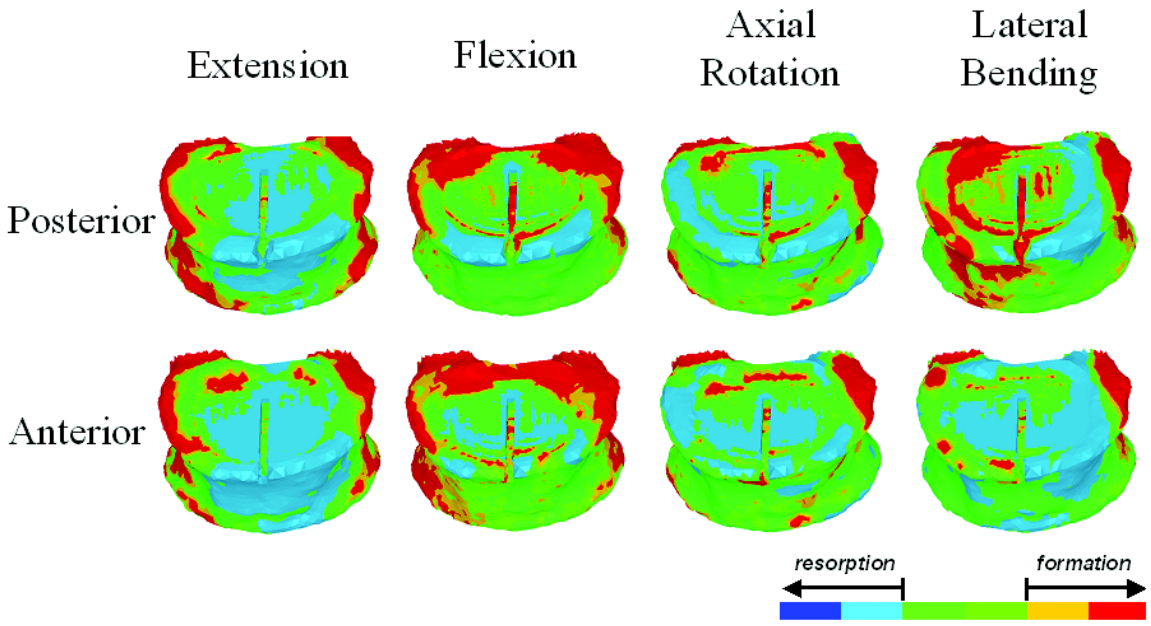

Figure 3-5. Initial remodeling stimulus contour plots for the L4 vertebral body

Discussion

In the current study, we used a nonlinear 3-D FEM of a single lumbar spinal segment to investigate the effect of TDR on facet contact forces and vertebral body cancellous bone strains. A thorough validation of the model, which included comparison of RoM, disc pressure, and bone strains with previously reported experimental data was performed. The intact model was altered to include a fixed core TDR at two locations, and exercised in four loading modes. Results indicated that TDR increases joint mobility, which has an effect on both facet contact forces and vertebral body strains.

TDR increased facet contact forces in flexion by an order of magnitude. The intact model predicted very low FCFs in flexion, which agreed with previously reported experimental data [17]. Unlike the natural disc, which has an axis of rotation that

depends on the applied loading [44], the TDR we evaluated had a fixed center of rotation. The fixed center of rotation was inferior of the intact location, and therefore results in greater relative vertebral anterior and posterior translation in flexion and extension, respectively. The increase in FCFs documented in flexion was the result of increased anterior translation of L3 relative to L4.

Similarly, during extension, L3 experienced increased posterior translation after TDR. The combination of this posterior translation and posterior placement of the device resulted in an unloading of the facets in extension. This effect has been documented in other studies as well [17, 45]. Anterior placement of the implant did not unload the facets, but actually resulted in similar and slightly increased FCFs compared to the intact model. These results suggest that there is the potential to either increase or decrease FCFs after TDR during extension depending on implant placement.

Lateral bending and axial rotation were not as sensitive to implant placement with respect to FCFs. During these modes of loading the FCF tended to increase with posterior placement of the TDR. Posterior placement of the TDR moved the center of rotation closer to the point of facet contact effectively reducing the facet's mechanical advantage in resisting the applied loading. These data suggest that posterior placement of a fixed core TDR has the potential to increase the loading on the facets when compared with a more anterior placement.

Posterior placement is recommended to encourage load transfer to the stiffer posterior cortex. Results from the current study suggest that load is transferred through the anterior portion of the device during flexion causing higher strains in the centrally located less stiff bone. Data from the current study indicate strain maxima in the trabecular bone near the anterior portion of the keel during flexion. This suggests that implant subsidence and anterior migration of the metallic footplate may be the result of activities that place the spine in flexion.

A major limitation of the current study is the model's ability to only consider the initial response of the bone. Subsequent remodeling and the viscoelastic nature of bone may alleviate the areas of high strain over time, a phenomenon that cannot be assessed in the current study. A recent clinical study which evaluated TDRs in athletes documented minor subsidence in 13 patients within the first 3 months after implantation, but did not observe further implant migration thereafter for 12 of the patients [46]. These data combined with results from the current study further enforce the need for careful evaluation of bone quality in prospective TDR candidates.

The current study attempted to better understand the consequences of TDR implantation and placement on future subsidence risk by evaluating the initial bony remodeling signal. The bone remodeling signal was evaluated by comparing strain energy densities between the intact and implanted FEMs. Posterior placement of the TDR resulted in less initial bony resorption signal beneath the metallic footplate. This suggests that posterior placement of the device may result in a more

physiologic load transfer to the underlying bone. Recently, it has been suggested that restoration of physiologic loading of the vertebral bone may increase the success of the clinical outcome [47]. Further examination of the models revealed that the posteriorly placed TDR was better centered with the intact nucleus. These data suggest that optimal placement of the TDR with respect to initial bone remodeling stimulus may depend on the location of the nucleus. Future studies should also consider the effects of TDR sizing with respect to the nucleus. The model predicted bone formation at the location of the pedicles for all modes of loading. This resulted from increased dependence on the facets and ligaments to limit the rotational degrees of freedom in the absence of intradiscal pressure.

The increased range of motion and facet contact forces documented in the current study indicates a general reduction in the spinal segment's stiffness post TDR. A previous clinical study, which examined RoM post TDR implantation, also documented an increase in the RoM at L3-L4 [48]. Additionally, an *in vitro* study using a mobile bearing lumbar TDR documented a reduction in stability after surgery, and indicated a greater tendency towards scoliosis especially with implantation at multiple levels [49]. In the current analysis, there was a general increase in RoM with implantation, which was greater with posterior placement of the implant. This decreased rotational stiffness correlated with increased areas of strain maxima in the vertebral body for all modes of loading. This was most notable during extension, and was further complicated by an unloading of the facets, which was compensated for at the bone-implant interface. These data suggest that the

reduction in rotational stiffness following TDR may be one of the contributing factors to implant subsidence. Furthermore, posterior positioning of the implant decreased rotational stiffness, but both positions tested in the current study resulted in a decrease of rotational stiffness when compared with the intact scenario.

The current study used a validated FE model of the spine, which shares the certain limitations of previously published models [50-52]. The bone geometry and material properties were generated from a specific QCT data set of a single L3-L4 motion segment. While this prevents extrapolations to a wider population it provides the ability to perform a well-controlled comparative study. Therefore, the data depicted in the current study should be interpreted as trends. Future studies should consider the effects of varying bone quality and morphology by performing similar analyses on a wider variety of patient data sets, including the effects of TDR at different lumbar levels, which have different facet orientations and stresses.

In conclusion, the current study predicted a decrease in segmental stiffness resulting from TDR. This reduction in stiffness was evidenced by a general increase in the overall RoM about the three anatomical axes. The decreased stiffness resulted in a dependence on the facets to limit range of motion after TDR for the majority of the tested scenarios, which may in part be responsible for the subsequent development of degenerative changes seen clinically [10]. Additionally, vertebral body strains were generally higher after TDR and tended to increase with decreasing segmental stiffness. The results from initial bone remodeling stimulus

suggested that posterior placement of the implant resulted in a more physiologic load transfer to the vertebral body.

References

1. Kumar, M.N., A. Baklanov, and D. Chopin, *Correlation between sagittal plane changes and adjacent segment degeneration following lumbar spine fusion.* Eur Spine J, 2001. 10(4): p. 314-9.

2. Pellise, F., et al., *Radiologic assessment of all unfused lumbar segments 7.5 years after instrumented posterior spinal fusion.* Spine, 2007. 32(5): p. 574-9.

3. Schulte, T.L., et al., *Disc height reduction in adjacent segments and clinical outcome 10 years after lumbar 360 degrees fusion.* Eur Spine J, 2007.

4. Cunningham, B.W., et al., *Biomechanical evaluation of total disc replacement arthroplasty: an in vitro human cadaveric model.* Spine, 2003. 28(20): p. S110-7.

5. Auerbach, J.D., et al., *Evaluation of spinal kinematics following lumbar total disc replacement and circumferential fusion using in vivo fluoroscopy.* Spine, 2007. 32(5): p. 527-36.

6. Mayer, H.M. and A. Korge, *Non-fusion technology in degenerative lumbar spinal disorders: facts, questions, challenges.* Eur Spine J, 2002. 11 Suppl 2: p. S85-91.

7. Panjabi, M., et al., *Multidirectional testing of one- and two-level ProDisc-L versus simulated fusions.* Spine, 2007. 32(12): p. 1311-9.

8. Bertagnoli, R., et al., *Lumbar total disc arthroplasty in patients older than 60 years of age: a prospective study of the ProDisc prosthesis with 2-year minimum follow-up period.* J Neurosurg Spine, 2006. 4(2): p. 85-90.

9. David, T., *Long-term results of one-level lumbar arthroplasty: minimum 10-year follow-up of the CHARITE artificial disc in 106 patients.* Spine, 2007. 32(6): p. 661-6.

10. Shim, C.S., et al., *CHARITE versus ProDisc: a comparative study of a minimum 3-year follow-up.* Spine, 2007. 32(9): p. 1012-8.

11. Huang, R.C., et al., *The prevalence of contraindications to total disc replacement in a cohort of lumbar surgical patients.* Spine, 2004. 29(22): p. 2538-41.

12. Bertagnoli, R. and S. Kumar, *Indications for full prosthetic disc arthroplasty: a correlation of clinical outcome against a variety of indications.* Eur Spine J, 2002. 11 Suppl 2: p. S131-6.

13. Link, H.D., *History, design and biomechanics of the LINK SB Charite artificial disc.* Eur Spine J, 2002. 11 Suppl 2: p. S98-S105.

14. Huang, R.C., et al., *Long-term flexion-extension range of motion of the prodisc total disc replacement.* J Spinal Disord Tech, 2003. 16(5): p. 435-40.

15. Liu, J., et al., *Effect of the increase in the height of lumbar disc space on facet joint articulation area in sagittal plane.* Spine, 2006. 31(7): p. E198-202.

16. Denoziere, G. and D.N. Ku, *Biomechanical comparison between fusion of two vertebrae and implantation of an artificial intervertebral disc.* J Biomech, 2006. 39(4): p. 766-75.

17. Rousseau, M.A., et al., *Disc arthroplasty design influences intervertebral kinematics and facet forces.* Spine J, 2006. 6(3): p. 258-66.

18. Niosi, C.A., et al., *Biomechanical characterization of the three-dimensional kinematic behaviour of the Dynesys dynamic stabilization system: an in vitro study.* Eur Spine J, 2006. 15(6): p. 913-22.

19. Heuer, F., et al., *Stepwise reduction of functional spinal structures increase range of motion and change lordosis angle.* J Biomech, 2007. 40(2): p. 271-80.

20. van Ooij, A., F.C. Oner, and A.J. Verbout, *Complications of artificial disc replacement: a report of 27 patients with the SB Charite disc.* J Spinal Disord Tech, 2003. 16(4): p. 369-83.

21. Shim, C.S., et al., *Vertical split fracture of the vertebral body following total disc replacement using ProDisc: report of two cases.* J Spinal Disord Tech, 2005. 18(5): p. 465-9.

22. Stieber, J.R. and G.D. Donald, 3rd, *Early failure of lumbar disc replacement: case report and review of the literature.* J Spinal Disord Tech, 2006. 19(1): p. 55-60.

23. Datta, J.C., et al., *Sagittal split fractures in multilevel cervical arthroplasty using a keeled prosthesis.* J Spinal Disord Tech, 2007. 20(1): p. 89-92.

24. Tropiano, P., et al., *Lumbar disc replacement: preliminary results with ProDisc II after a minimum follow-up period of 1 year.* J Spinal Disord Tech, 2003. 16(4): p. 362-8.

25. Buckley, J.M., D.C. Leang, and T.M. Keaveny, *Sensitivity of vertebral compressive strength to endplate loading distribution.* J Biomech Eng, 2006. 128(5): p. 641-6.

26. Yosibash, Z., et al., *A CT-based high-order finite element analysis of the human proximal femur compared to in-vitro experiments.* J Biomech Eng, 2007. 129(3): p. 297-309.

27. Sawatari, T., et al., *Three-dimensional finite element analysis of unicompartmental knee arthroplasty--the influence of tibial component inclination.* J Orthop Res, 2005. 23(3): p. 549-54.

28. Ulrich, D., et al., *The ability of three-dimensional structural indices to reflect mechanical aspects of trabecular bone.* Bone, 1999. 25(1): p. 55-60.

29. Morgan, E.F., H.H. Bayraktar, and T.M. Keaveny, *Trabecular bone modulus-density relationships depend on anatomic site.* J Biomech, 2003. 36(7): p. 897-904.

30. Kopperdahl, D.L. and T.M. Keaveny, *Yield strain behavior of trabecular bone.* J Biomech, 1998. 31(7): p. 601-8.

31. Mosekilde, L. and C.C. Danielsen, *Biomechanical competence of vertebral trabecular bone in relation to ash density and age in normal individuals.* Bone, 1987. 8(2): p. 79-85.

32. Hansson, T.H., T.S. Keller, and M.M. Panjabi, *A study of the compressive properties of lumbar vertebral trabeculae: effects of tissue characteristics.* Spine, 1987. 12(1): p. 56-62.

33. Frei, H., et al., *The effect of nucleotomy on lumbar spine mechanics in compression and shear loading.* Spine, 2001. 26(19): p. 2080-9.

34. Yamamoto, I., et al., *Three-dimensional movements of the whole lumbar spine and lumbosacral joint.* Spine, 1989. 14(11): p. 1256-60.

35. Mimura, M., et al., *Disc degeneration affects the multidirectional flexibility of the lumbar spine.* Spine, 1994. 19(12): p. 1371-80.

36. Panjabi, M.M., et al., *Mechanical behavior of the human lumbar and lumbosacral spine as shown by three-dimensional load-displacement curves.* J Bone Joint Surg Am, 1994. 76(3): p. 413-24.

37. Fujiwara, A., et al., *The effect of disc degeneration and facet joint osteoarthritis on the segmental flexibility of the lumbar spine.* Spine, 2000. 25(23): p. 3036-44.

38. Schmoelz, W., et al., *Dynamic stabilization of the lumbar spine and its effects on adjacent segments: an in vitro experiment.* J Spinal Disord Tech, 2003. 16(4): p. 418-23.

39. Bergström JS, R.C., Kurtz SM., *Prediction of multiaxial mechanical behavior for conventional and highly crosslinked UHMWPE using a hybrid constitutive model.* Biomaterials, 2003. 24(8): p. 1365-80.

40. Kurtz, S.M., A.A. Edidin, and D.L. Bartel, *The role of backside polishing, cup angle, and polyethylene thickness on the contact stresses in metal-backed acetabular components.* J Biomech, 1997. 30(6): p. 639-42.

41. Nagaraja, S., T.L. Couse, and R.E. Guldberg, *Trabecular bone microdamage and microstructural stresses under uniaxial compression.* J Biomech, 2005. 38(4): p. 707-16.

42. Weinans, H., et al., *Sensitivity of periprosthetic stress-shielding to load and the bone density-modulus relationship in subject-specific finite element models.* J Biomech, 2000. 33(7): p. 809-17.

43. Kerner, J., et al., *Correlation between pre-operative periprosthetic bone density and post-operative bone loss in THA can be explained by strain-adaptive remodelling.* J Biomech, 1999. 32(7): p. 695-703.

44. White, A.A., Panjabi, M.M.,, *Clinical Biomechanics of the Spine, 2nd ed.*1990, Philadelphia-Toronto: J.B. Lippincott Company.

45. Dooris, A.P., et al., *Load-sharing between anterior and posterior elements in a lumbar motion segment implanted with an artificial disc.* Spine, 2001. 26(6): p. E122-9.

46. Siepe, C.J., et al., *Total lumbar disc replacement in athletes: clinical results, return to sport and athletic performance.* Eur Spine J, 2007. 16(7): p. 1001-13.

47. Mulholland, R.C., *The myth of lumbar instability: the importance of abnormal loading as a cause of low back pain.* Eur Spine J, 2008.

48. Kim, D.H., et al., *Factors influencing segmental range of motion after lumbar total disc replacement using the ProDisc II prosthesis.* J Neurosurg Spine, 2007. 7(2): p. 131-8.

49. McAfee, P.C., et al., *Biomechanical analysis of rotational motions after disc arthroplasty: implications for patients with adult deformities.* Spine, 2006. 31(19 Suppl): p. S152-60.

50. Schmidt, H., et al., *Application of a calibration method provides more realistic results for a finite element model of a lumbar spinal segment.* Clin Biomech (Bristol, Avon), 2007. 22(4): p. 377-84.

51. Rohlmann, A., et al., *Analysis of the influence of disc degeneration on the mechanical behaviour of a lumbar motion segment using the finite element method.* J Biomech, 2006. 39(13): p. 2484-90.

52. Noailly, J., et al., *How does the geometry affect the internal biomechanics of a lumbar spine bi-segment finite element model? Consequences on the validation process.* J Biomech, 2007. 40(11): p. 2414-25.

4. Evaluation of lumbar total disc replacement after disc height distraction during sagittally balanced postures

Abstract

Disc height distraction during total disc replacement (TDR) is essential for relieving compressed nerve roots, but will also alter the relative facet orientation. Excessive distraction will cause facet separation, and limit the segment's ability to resist anterior translation and extension. This increased laxity may allow implant impingement, which has been associated with unintended device wear. The objective of the current study was to evaluate both a fixed and mobile bearing TDR with disc height distractions of 0 mm and 3 mm during simulated standing and bending in the sagittal plane. We hypothesized that disc height distraction would increase RoM and the risk of impingement. A previously validated finite element model of L4-L5 was used. The intact model was altered to create a degenerative disc disease (DDD) model and implanted models with either a mobile (MTDR) or fixed bearing (FTDR) TDR. DDD was simulated by decreasing the disc height 3 mm and reducing the nucleus bulk modulus. Implanted models were created by implementing either a MTDR or FTDR into the disc space. Disc height distraction was set to 0 or 3 mm with 0 being equal to the intact healthy height. All models were subjected to compression and anterior shear characteristic of upper body weight during standing. Bending was simulated by progressively increasing the erector spinae force from 0 to 125 N. This force was applied between the spinous processes approximately 5.5 cm posterior of the joint center and normal to the disc's shear

plane. Facet contact forces, RoM, and endplate impingement were evaluated. Distraction resulted in impingement scenarios for both the MTDR and FTDR during maximum extension. Impingement consisted of two-sided contact between the metallic foot plates and polyethylene core for the MTDR and anterior lift off with posterior focal contact for the FTDR. Total flexion-extension RoM was 4.8o for the intact, 4.2o for DDD, 5.7o for the MTDR-0mm, 5.4o for the FTDR-0mm, 9o for the MTDR-3mm, and 12.9o for the FTDR-3mm. Distraction resulted in a general decrease in resultant facet reaction forces, but anterior-posterior forces increased during extension for the MTDR. The results from the study supported the hypothesis that distraction results in increased RoM and impingement risk. Specifically, distracting the disc height prevented facet contact during extension which allows for excessive rotation and subsequent implant impingement. Interestingly, while the resultant facet contact force was reduced during extension for the MTDR, the anterior-posterior force component increased resulting in posterior shear of L4 relative to L5. This posterior shear resulted in a characteristic downward bending of the posterior polyethylene rim during impingement which has been observed in our retrieval collection. The results from the current study suggests that excessive disc height distraction may be partly responsible for cases of implant impingement documented clinically. Clinicians should consider this data when deciding how much distraction to use during TDR procedures. Additionally, designers should consider the effects of distraction and facet contact contribution when performing pre-clinical testing of new TDR designs.

Introduction

Recently, lumbar total disc replacement systems (TDRs) have been introduced as an alternative to spinal fusion in the treatment of degenerative disc disease. Currently, there are two lumbar TDRs approved for implantation in the United States, and several more undergoing pre-clinical testing. These devices are intended to restore the disc height, maintain or correct segmental lordosis, and preserve segmental range of motion. The approved implants include a mobile (Charite, Depuy Spine) or fixed (Prodisc, Synthes Spine) polyethylene (PE) bearing surface between two cobalt chrome alloy endplates. Biomechanical studies have documented a reduction in adjacent level deformation after TDR when compared with fusion [1, 2], which has been attributed to their ability to maintain motion. Due to their motion preserving capabilities, they pose new challenges in the development of appropriate *in vitro* testing protocols. Specifically, articulating components provide the potential for device impingement and associated accelerated wear of the bearing surfaces. Despite the relatively recent introduction of lumbar TDRs, device impingement [3, 4] and osteolysis[5-7] has been documented clinically. These data indicate the importance of understanding the biomechanical environment and developing testing methodologies that exploit worst-case scenarios.

During normal standing, compressive and anterior shear forces are applied to the lower lumbar spine due to upper body weight[8]. When these forces are applied to an osteoligamentous spinal segment it will translate and flex forward, lose sagittal

balance, tense the posterior ligaments and disc, and engage the facets[9]. Muscle forces must be generated in order to restore sagittal balance. The primary group of deep muscles in the lumbar spine is the erector spinae (ES), which attaches along the spinous processes, posterior of the facets. Force generated in this muscle group has the ability to restore sagittal balance, and encourages greater facet engagement[10]. Generally, the muscle forces and upper body compressive forces are simulated via a follower load applied at the joint centers. However, this neglects the contribution of anterior shear, and has been shown to result in no facet engagement[11]. While this phenomenological method of applying muscle forces enables the ability to apply physiological levels of compression in vitro, it is unclear how anterior shear forces are balanced in the sagittal plane without contribution of the facets. Consequently, use of this loading method to evaluate implantable devices may not adequately capture the biomechanical environment, and ignore important effects from facet loading or the loss thereof. Previous studies have indicated that simulation of the erector spinae force in concert with vertical upper body loading will result in facet engagement and balance anterior shear forces [10, 12]

Disc height distraction during total disc replacement (TDR) is essential for relieving compressed nerve roots, but will also alter the relative facet orientation. Recent anatomical studies have documented alterations in facet overlap and spacing in the sagittal plane following simulated and actual TDR in both the cervical and lumbar spine, respectively[13, 14]. These data indicate that excessive distraction results in facet separation, which will alter the segment's ability to resist anterior translation

and extension rotation. Clinical results have indicated increases in the index level lordotic angle[15] and posterior component impingement after TDR[16]. Similarly, An in vitro study also documented an increase in the implanted segments lordotic angle after TDR implantation[17]. This increased propensity towards extension rotation may be, in part, the result of a loss of facet contact, which has been shown to contribute to sagittal balance during erect posture[10]. However, it remains unclear if the loss of facet contact from increased disc distraction contributes to device impingement. Therefore, the objective of the current study was to evaluate both a fixed and mobile bearing TDR with disc height distractions of 0 mm and 3 mm through a range of sagitally balanced postures, which incorporate the erector spinae muscle force, anterior shear, and compression. We hypothesized that disc height distraction would result in a greater risk of posterior component impingement during erect posture.

Methods

A three-dimensional finite element model of a ligamentous L4-L5 motion segment was generated from quantitative computed tomography (QCT) data of a cadaveric spine. The data set was taken from an Institutional Review Board-approved cadaveric study. The spine was chosen due to its lack of any bony or disc deformities, i.e, osteophytes or herniations. Hounsfield units were used as a surrogate for bone mineral density (BMD).

The methodology used to develop and validate the model has been previously described [18, 19], but will be outlined below. A combination of automatic and

manual image segmentation techniques (Analyze, AnalyzeDirect, Inc., Overland Park, KS) were used to extract detailed surfaces corresponding to the major bony structures of L4-L5. The software package allowed for automatic segmentation based on thresholding of the QCT grayscale values. These surfaces were imported into the commercial finite element mesh generation program, HyperMesh (Altair Inc., Troy, MI), and were discretized into a combination of tetrahedral elements for the bony structures and hexahedral elements for the intervertebral discs (IVDs). The central portion of the IVDs, approximately 40% of the volume [20], were designated to be the nucleus pulposus (NP), while the remaining volume was considered the annulus fibrosus. Major spinal ligaments (anterior longitudinal ligament, posterior longitudinal, intraspinatus, supraspinatus, intratransverse, facet capsule, ligamentum flavum) were implemented in the model using tension-only nonlinear springs. Shell elements were used to plate the exterior surface of the vertebral bodies and represented the cortex and bony endplate.

Bone mineral density (BMD)-dependent orthotropic material properties were assigned to the cancellous bone of the vertebral bodies. Custom software was written to apply the Young's moduls at each of the nodal points based on the density of the bone. Similar methodology has been used to create models with heterogeneous bone properties of the tibia and femur [21, 22]. The quantitative relationship between bone mineral density and elastic modulus in cancellous vertebral bone, as reported by Morgan et al. and Ulrich et al., was utilized to define a nonlinear relationship between bone mineral density and orthotropic elastic

modulus [23, 24]. Elastic moduli within the vertebral body fell within what has been previously reported in the literature [25-27]. The remaining structures were assigned material properties from the literature and are described in Table 1-1. Summary of Element Type and Material Properties Used in the FE model. Frictionless contact was defined between the facets using a penalty-based contact algorithm.

A total of five models were utilized for the current study (Figure 4-1). Geometric surfaces for appropriately sized models of both a mobile and fixed core TDR were created by reverse engineering dimensions from commercially available components of a Charite III (Depuy Spine, Raynham, MA) and Prodisc-L (Synthes, Paoli, PA), respectively. The interface between the implant's metallic footplates and the bony endplates were ideally fixed and rigid. The disc material, anterior longitudinal ligament, and posterior longitudinal ligament were completely removed for all implanted models. Material properties for cobalt chrome alloy (E = 215 GPa, n = 0.3) were assigned to the metallic footplates. A nonlinear material representation for polyethylene (PE) with an initial Young's modulus of 940 MPa was assigned to the mobile core[28]. Frictionless sliding contact was defined between the metallic footplates and the core. The models were placed into the intervertebral disc space at L4-L5 without increasing the disc space from the pre-implanted, intact level. Additional models were created in which the disc space was distracted by 3 mm beyond the intact, pre-implanted state. The distraction was performed by translating L4 superiorly without applying any superimposed

rotations. The superior direction was considered the vector normal to the plane that bisected the disc space.

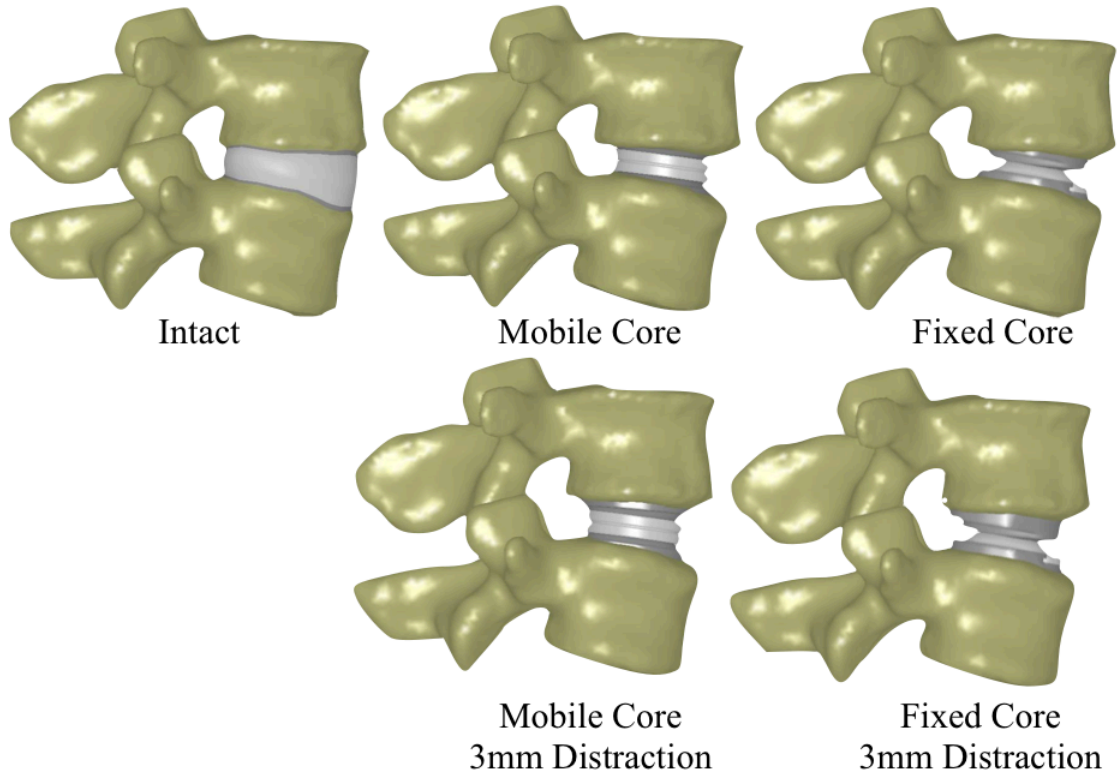

Figure 4-1. Images depicting the five finite element models used for the current study (ligaments not pictured)

Vertical upper body weight was simulated by applying combined compression and anterior shear directly to L4. A total vertical upper body weight of 425 N (approximately 100 lb) was simulated by applying a compressive and anterior shear follower loads of 400 and 140 N, respectively (Figure 4-2). This assumed an angle of L4 of 20° with respect to the horizon. The erector spinae force was simulated by applying a single degree of freedom force element between the spinous processes at

5 cm posterior of the approximate joint center. The erector spinae force ranged from 0 N to 125 N in increments of 25 N. The amount of sagittal rotation (negative = extension) relative to the nominal, undeformed position was recorded. Additionally, facet contact force, annulus fibrosus maximum shear stress (intact model only), and effective stress (von Mises) in the polyethylene cores was recorded for each analysis.

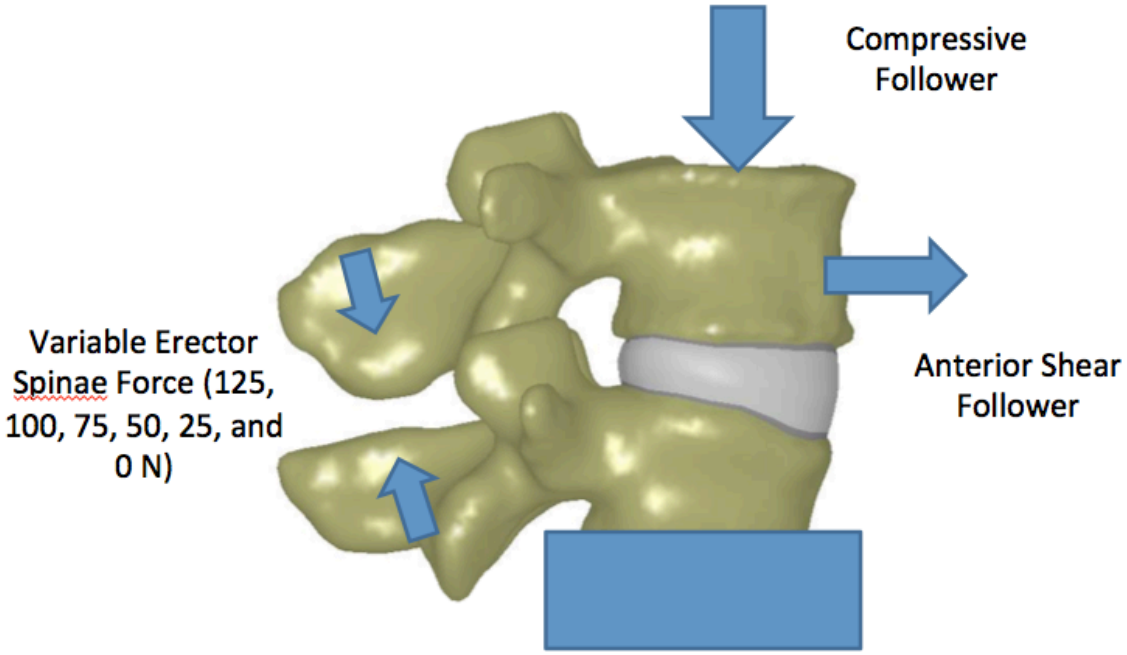

Figure 4-2. Schematic depicting the loading paradigmed used to generate multiple sagittaly balanced postures

Results

For the intact model, erector spinae forces of 100 and 125 N resulted in sagittal rotations of 0.2° and -0.6°, respectively (Figure 4-3). Progressive decrease of the erector spinae force tended to result in flexion rotation of L4. Zero erector spinae

force resulted in a maximum flexion rotation of 3.7°. Qualitatively, shear stress maxima were minimized in the annulus fibrosus at these levels of erector spinae force (Figure 4-4). At lower levels of erector spinae force, shear stress maxima occurred in the anterior portion of the annulus. Progressive increase of the erector spinae force resulted in a more even distribution of shear stress. An erector spinae force of 125 N, which resulted in slight sagittal rotation towards extension resulted in shear stress maxima at the posterior annulus, but with lesser magnitude than corresponding anterior annulus shear stress with no erector spinae force. All levels of erector spinae force resulted in some level of facet contact force for the intact model. Peak resultant, anterior-posterior, and inferior-superior facet contact forces occurred during an erector spinae force of 100 N.

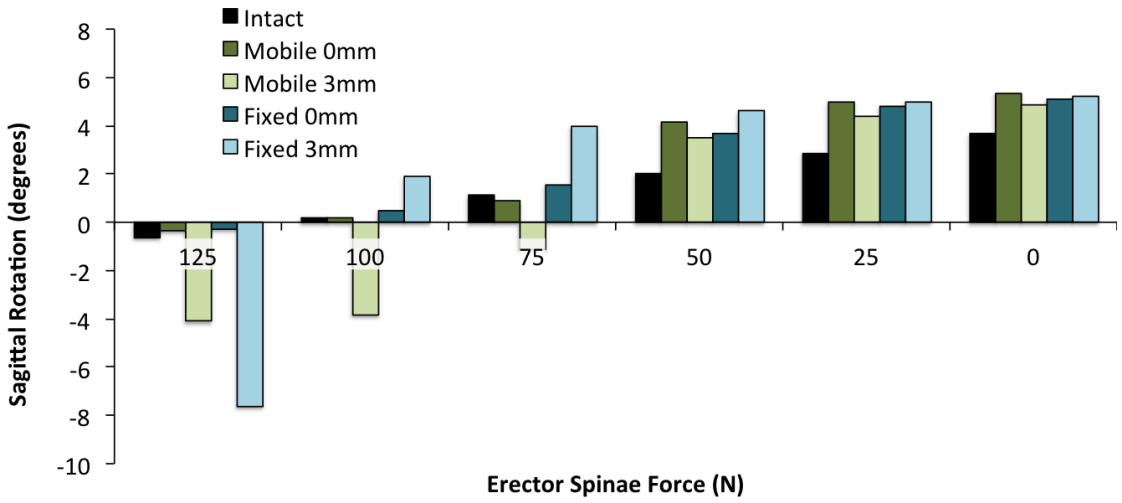

Figure 4-3. Bar graph depicting the sagittal rotation of L4 with respect to the nominal, undeformed state as a function of erector spinae force. Negative values denote extension rotation.

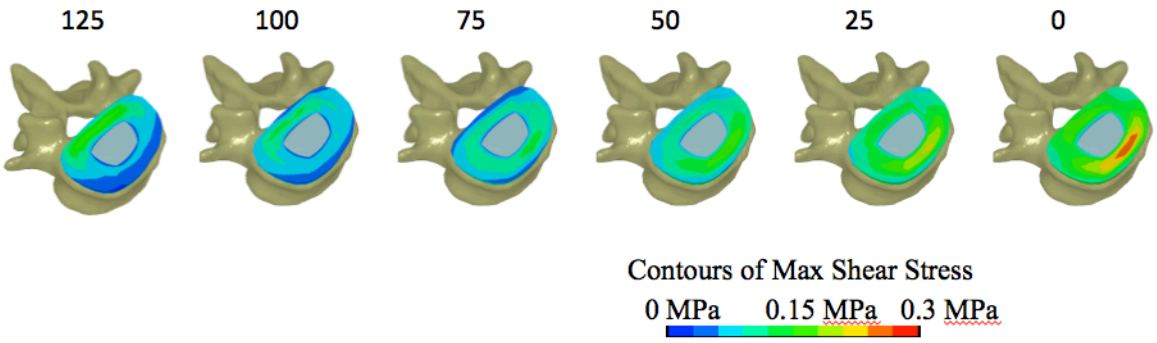

Figure 4-4. Contour plots of maximum shear stress at an axial mid-section of the annulus fibrosus. Numbers above images indicate the associated erector spinae force in Newtons.

Generally, implantation of both a mobile and fixed core TDR with 0 mm of disc distraction resulted in similar levels of sagittal rotation when compared to the intact model (Figure 4-3). Specifically, implantation of a mobile core TDR resulted in sagittal rotations of 0.2° and -0.3° at erector spinae forces of 100 and 125 N, respectively. Implantation of a fixed core TDR with no disc height distraction resulted in sagittal rotations of 0.5° and -0.3° at erector spinae forces of 100 and 125 N, respectively. Disc height distraction of 3 mm resulted in an increase in extension rotation of 11 and 27 fold for the mobile and fixed core TDRs at 125 N of erector spinae force, respectively. Generally, implantation of a TDR resulted in a slight increase in allowed flexion rotation irrespective of disc height distraction or TDR type when compared with the intact condition. Disc height distraction tended to result in a slight reduction of allowed flexion rotation for the mobile core implant. Conversely, disc height distraction increased the potential for flexion rotation for a fixed core TDR.

Peak resultant, anterior-posterior, and inferior-superior facet contact forces occurred during an erector spinae force of 100 N. All levels of erector spinae force resulted in some level of facet contact force for the intact and all implanted models. For the intact model, facet contact forces generally tended to decrease with progressive decrease of the erector spinae force (Figure 4-5). A similar trend was observed for the mobile core prosthesis irrespective of disc height distraction. Conversely, the fixed core TDR tended to result in increased facet contact force during decreased erector spinae forces. For both the mobile and fixed core TDR, disc height distraction tended to result in a decrease of inferior-superior directed facet contact forces relative to no distraction. Conversely, at higher levels of erector spinae force, disc height distraction resulted in an increased anterior-posterior facet contact force for the mobile TDR only. Generally, facet contact forces tended to be greater than intact values. However, disc height distraction resulted in a reduction of the facet contact forces relative to the intact for the mobile core TDR at erector spinae forces of 50 N, 25 N, and 0 N. Similarly, disc height distraction of the fixed core device resulted in reduced facet contact forces relative to the intact condition for erector spinae forces of 125 N and 100 N.

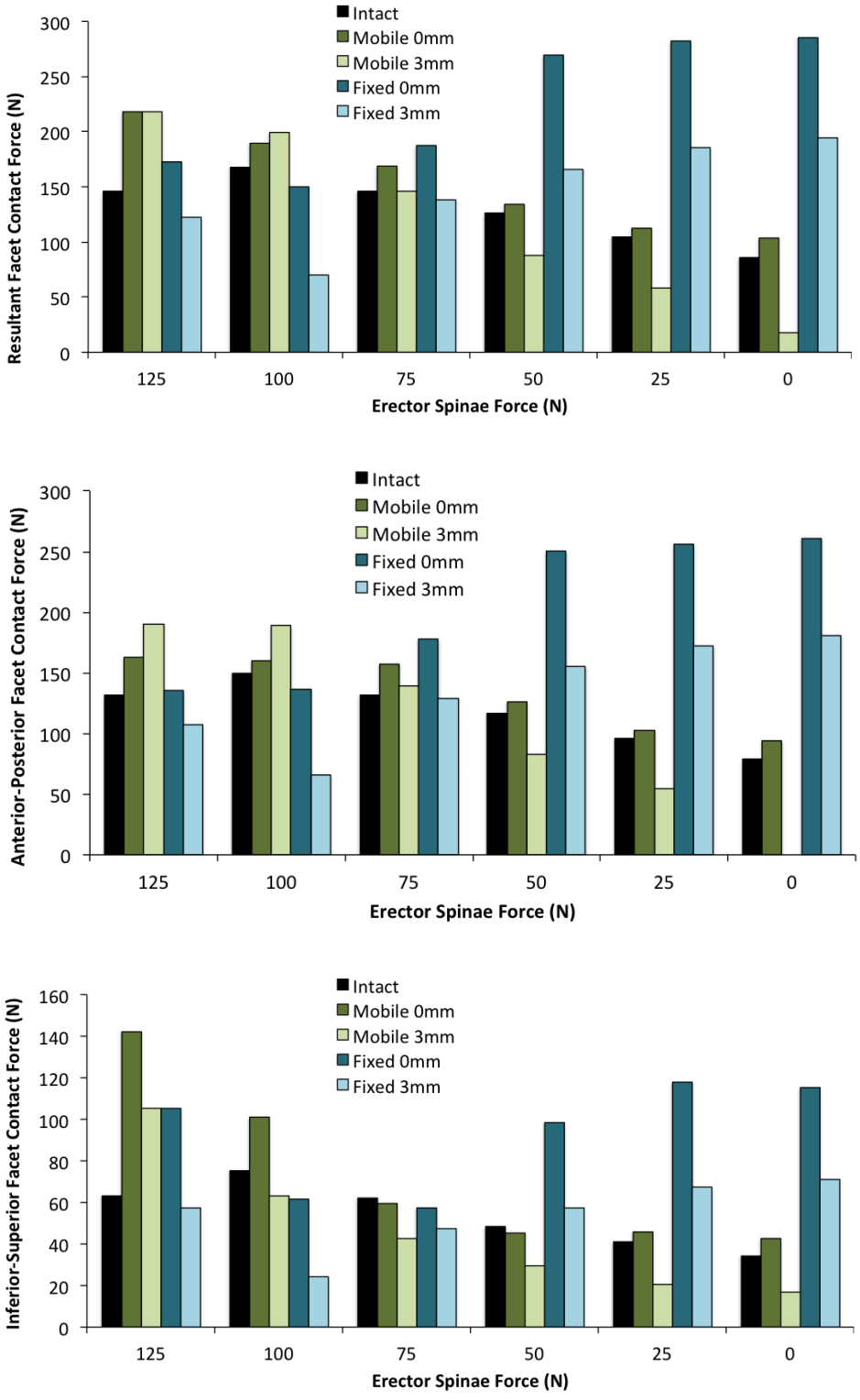

Figure 4-5. Bar graphs depicting the resultant, anterior-posterior, and inferior-superior facet contact forces for all models and simulations

At the maximum erector spinae force (125 N) the mobile core TDR experienced posterior impingement of the polyethylene rim (Figure 4-6). Similarly, the fixed core TDR experienced anterior lift-off of the articulating surfaces and associated focal contact between the superior metallic footplate and polyethylene insert. At the minimum erector spinae force (0N), 0 mm of distraction resulted in posterior lift-off and focal anterior contact for the fixed core TDR. The mobile core TDR experienced one-sided anterior contact between the metallic footplate and polyethylene core's rim irrespective of disc height distraction.

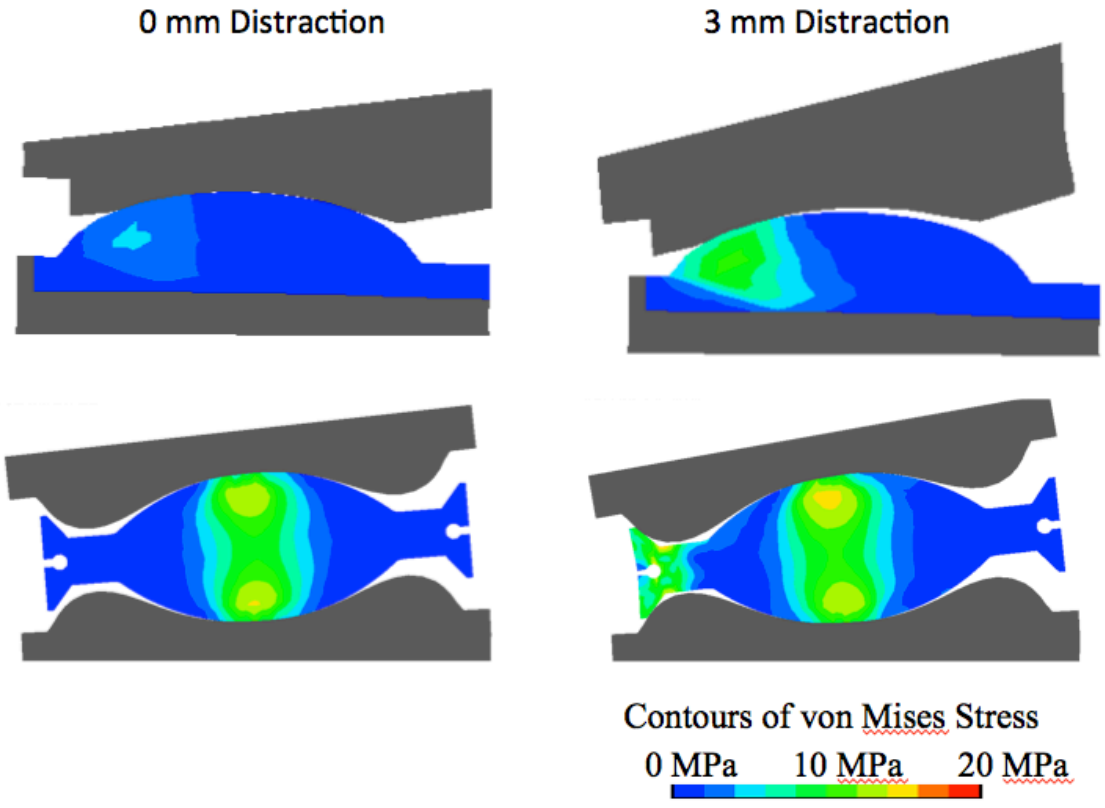

Figure 4-6. Contour plots of effective (von Mises) stress at a sagittal mid-section of both the fixed (top) and mobile (bottom) TDRs at 0 mm (left) and 3 mm (right) of distraction at 125 N of erector spinae force. 3 mm of distraction resulted in anterior lift-off and focal posterior contact for the fixed core TDR. 3mm of distraction resulted in posterior component impingement of the mobile core device.

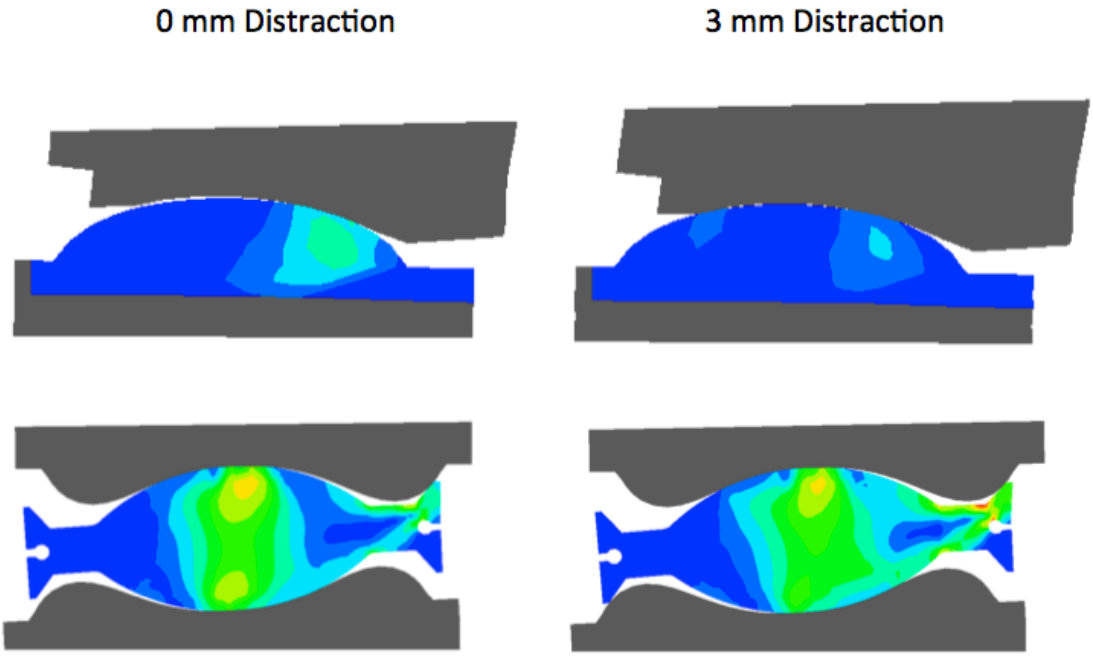

Figure 4-7. Contour plots of effective (von Mises) stress at a sagittal mid-section of both the fixed (top) and mobile (bottom) TDRs at 0 mm (left) and 3 mm (right) of distraction at 0 N of erector spinae force. 0 mm of distraction resulted in posterior lift-off and focal anterior contact for the fixed core TDR. The mobile core TDR experienced one-sided anterior contact between the metallic footplate and polyethylene core's rim.

Discussion

The results from the study supported the hypothesis that distraction results in increased extension rotation and impingement risk. Specifically, distracting the disc height reduced inferior-superior facet contact during extension rotation, which allowed for increased rotation and subsequent posterior component implant impingement or anterior lift-off of the bearing surface. The results from the current study suggest that excessive disc height distraction may be partly responsible for cases of implant posterior component impingement documented clinically. Clinicians should consider this data when deciding how much distraction to use during TDR procedures. Additionally, designers should consider the effects of

distraction and facet contact contribution when performing pre-clinical testing of new TDR designs.

Results from the current study indicated that forces generated in the erector spinae resulted in a reduction in the distortional stress maxima experienced by the disc and an increase in facet contact force. These data demonstrate that a combination of active erector spinae muscle force and passive facet contact force can restore sagittal balance and minimize shear forces acting on the disc. These findings are consistent with a previous *in vitro* study[10]. It also indicates that the facets may be in constant contact during normal standing. This is consistent with a recent in vivo study that observed no change in the distance between the spinous processes during normal standing and extension [29]. Interestingly, upon closer review of the data, application of erector spinae force did not have a substantial effect on the disc normal force (data not included) indicating that active muscle force is replacing the passive ligament reaction force. Active force generated in the erector spinae was required to enable the benefit of increased facet contact, suggesting that maintenance of erector spinae muscle strength and relative facet orientation is paramount to a healthy biomechanical environment for the disc.

Previously, it has been suggested that shearing forces applied to the lumbar spine are balanced by the generation of various muscle forces[30], and hence the development of the compressive follower load. However, the lordosis of the lumbar spine combined with the facet geometry is consistent with a scenario where the facets are responsible for balancing shear forces. Specifically, the angle of the facets

in the transverse plane increases at the lower levels of the lumbar spine [20], which corresponds with the natural increasing lordosis at these levels. As the lordosis increases so does the amount of relative anterior shear applied from the upper body mass, suggesting that lower lumbar facet morphology is an adaptation to the applied loading from body weight. Furthermore, this angulation of the facets in the axial plane has been associated with the development of spondylolisthesis [31-33].

The current study indicated that both a mobile and fixed-bearing TDR have the ability to maintain sagittal balance. These results are consistent with the vast majority of clinical data which indicates positive clinical findings following TDR[34]. However, the data from the current study indicates that the ability to maintain sagittal balance following TDR is sensitive to disc height distraction. The current study did not, however, evaluate other potentially sensitive parameters such as device placement, device sizing, and variations in patient morphology. Future studies should consider these parameters and how they may affect impingement risk since they may confound or compound the effects of disc height distraction.

Erector spinae forces of 100 N and 125 N resulted in approximate sagittal balance for the intact and non-distracted TDR models. However, the TDR models with 3 mm of distraction experienced high levels of extension under these levels of loading, and caused impingement in the mobile core device. These results indicate that application of pre-implantation standing forces has the potential to produce device impingement. This is consistent with results from a previous *in vivo* study in which TDR impingement was documented during standing[16]. Furthermore, after disc

height distraction, sagittal balance consistent with the intact model was not achieved at the tested load levels. This suggests a fundamental loss of stability as a result of disc distraction. A major limitation to the current study was the lack of pre-tension developed in the surrounding soft tissues. The presence of this tension will likely result in increased stiffness of the segment after TDR. However, it is likely that tension developed in the surrounding tissues will generate a combined intervertebral compression and moment. Since most of the ligamentous tissues are posterior of the disc space, tissue tension will likely provide an additional extension moment. Under this scenario, the likelihood of posterior component impingement would be even greater.

The results from the current study did not necessarily indicate device impingement for the fixed bearing TDR. However, the fixed bearing TDR did experience non-conforming articulation between the bearing surfaces during both extension and flexion rotation. The fixed center of rotation of the fixed bearing TDR resulted in an overly constrained system during facet contact. As a result, the articulating surfaces became non-conforming, and focal contact occurred between the footplate and the polyethylene core. This type of loading would result in increased wear of the bearing surfaces. A similar phenomenon was observed during flexion rotation with the mobile bearing TDR. The mobile bearing TDR is intended to provide a variable center of rotation in order to accommodate facet loading [35]. However, the current study documented one-sided contact between the superior metallic footplate and the implant's rim. Stress maxima in the area of contact indicate that the implant was

locked in place and unable to articulate away from the contacting footplate. Similar locking of a mobile bearing TDR has been observed *in vitro*[36]. Additionally, analysis of retrieved implants frou our laboratories retrieval collection has indicated grossly visible bending and one-sided wear of mobile bearing TDR rims[37].

The current study only considered sagittal plane movement. While this is a limitation it was deemed necessary in order to accept or reject the hypothesis. As a result, the erector spinae muscle attachments were limited to the spinous processes. Future studies should consider out of plane rotations and additional muscle atttachment sites. This study also shared the limitations inherent in all finite element modeling studies. Particularly, the geometry of the model was based on a single QCT data set. However, the facet geometry was analyzed in the context of previously published morphological data. Specifically, the angle of the facet joints in the transverse plane was found to be approximately 45°, which is consistent with previously reported values [20].

In conclusion, the current study demonstrated a series of sagittaly balanced postures for an intact L4-L5 segment, which resulted in a qualitative reduction in distortional stress maxima in the annulus during a combination of erector spinae muscle tension and facet contact. Evaluation of the same sagittaly balanced posutures after implantation of both a mobile and fixed core TDR with no disc distraction resulted in a reasonable agreement with the intact model. Distraction of the disc space prevented sagittal balance at the tested levels of loading and resulted

in device impingement for the mobile bearing TDR and non-conformance of the articulating surfaces for the fixed bearing TDR.

References

1. Panjabi, M., et al., *Multidirectional testing of one- and two-level ProDisc-L versus simulated fusions.* Spine, 2007. **32**(12): p. 1311-9.
2. Auerbach, J.D., et al., *Evaluation of spinal kinematics following lumbar total disc replacement and circumferential fusion using in vivo fluoroscopy.* Spine, 2007. **32**(5): p. 527-36.
3. van Ooij, A., et al., *Polyethylene wear debris and long-term clinical failure of the Charite disc prosthesis: a study of 4 patients.* Spine, 2007. **32**(2): p. 223-9.
4. Choma, T.J., et al., *Retrieval analysis of a ProDisc-L total disc replacement.* J Spinal Disord Tech, 2009. **22**(4): p. 290-6.
5. Hallab, N.J., B.W. Cunningham, and J.J. Jacobs, *Spinal implant debris-induced osteolysis.* Spine (Phila Pa 1976), 2003. **28**(20): p. S125-38.
6. Punt, I.M., et al., *Periprosthetic tissue reactions observed at revision of total intervertebral disc arthroplasty.* Biomaterials, 2009. **30**(11): p. 2079-84.
7. Devin, C.J., T.G. Myers, and J.D. Kang, *Chronic failure of a lumbar total disc replacement with osteolysis. Report of a case with nineteen-year follow-up.* J Bone Joint Surg Am, 2008. **90**(10): p. 2230-4.
8. Farfan, H.F., V. Osteria, and C. Lamy, *The mechanical etiology of spondylolysis and spondylolisthesis.* Clin Orthop Relat Res, 1976(117): p. 40-55.
9. Cyron, B.M. and W.C. Hutton, *Articular tropism and stability of the lumbar spine.* Spine (Phila Pa 1976), 1980. **5**(2): p. 168-72.
10. el-Bohy, A.A., K.H. Yang, and A.I. King, *Experimental verification of facet load transmission by direct measurement of facet lamina contact pressure.* J Biomech, 1989. **22**(8-9): p. 931-41.
11. Rohlmann, A., et al., *Applying a follower load delivers realistic results for simulating standing.* J Biomech, 2009. **42**(10): p. 1520-6.
12. Rundell, S., Isaza, J., Guillory, S., Day, J., Kurtz, S., *Posterior Muscle Activation in the Lumbar Spine Engages Facet Contact and Reduces Shear Forces in the Intervertebral Disc durin g Simulated Standing.* Transactions of the Orthopaedic Research Society, 2010. **35**(New Orleans, LA).
13. Kafchitsas, K., et al., *Effect of lumbar disc replacement on the height of the disc space and the geometry of the facet joints: a cadaver study.* J Bone Joint Surg Br, 2010. **92**(4): p. 595-601.
14. Liu, J., et al., *How the increase of the cervical disc space height affects the facet joint: an anatomy study.* Spine (Phila Pa 1976), 2006. **31**(12): p. E350-4.
15. Cakir, B., et al., *The impact of total lumbar disc replacement on segmental and total lumbar lordosis.* Clin Biomech (Bristol, Avon), 2005. **20**(4): p. 357-64.

16. Kafer, W., et al., *Posterior component impingement after lumbar total disc replacement: a radiographic analysis of 66 ProDisc-L prostheses in 56 patients.* Spine, 2008. **33**(22): p. 2444-9.
17. Gaffey, J.L., et al., *Effect of Increasing Implant Height on Lumbar Spine Kinematics and Foraminal Size Using the ProDisc-L Prosthesis.* Spine (Phila Pa 1976), 2010.
18. Rundell, S.A., et al., *Total disc replacement positioning affects facet contact forces and vertebral body strains.* Spine, 2008. **33**(23): p. 2510-7.
19. Rundell, S.A., et al., *Effect of nucleus replacement device properties on lumbar spine mechanics.* Spine (Phila Pa 1976), 2009. **34**(19): p. 2022-32.
20. White, A.A., Panjabi, M.M.,, *Clinical Biomechanics of the Spine, 2nd ed.*1990, Philadelphia-Toronto: J.B. Lippincott Company.
21. Yosibash, Z., et al., *A CT-based high-order finite element analysis of the human proximal femur compared to in-vitro experiments.* J Biomech Eng, 2007. **129**(3): p. 297-309.
22. Sawatari, T., et al., *Three-dimensional finite element analysis of unicompartmental knee arthroplasty--the influence of tibial component inclination.* J Orthop Res, 2005. **23**(3): p. 549-54.
23. Ulrich, D., et al., *The ability of three-dimensional structural indices to reflect mechanical aspects of trabecular bone.* Bone, 1999. **25**(1): p. 55-60.
24. Morgan, E.F., H.H. Bayraktar, and T.M. Keaveny, *Trabecular bone modulus-density relationships depend on anatomic site.* J Biomech, 2003. **36**(7): p. 897-904.
25. Kopperdahl, D.L. and T.M. Keaveny, *Yield strain behavior of trabecular bone.* J Biomech, 1998. **31**(7): p. 601-8.
26. Mosekilde, L. and C.C. Danielsen, *Biomechanical competence of vertebral trabecular bone in relation to ash density and age in normal individuals.* Bone, 1987. **8**(2): p. 79-85.
27. Hansson, T.H., T.S. Keller, and M.M. Panjabi, *A study of the compressive properties of lumbar vertebral trabeculae: effects of tissue characteristics.* Spine, 1987. **12**(1): p. 56-62.
28. Bergstrom, J.S., C.M. Rimnac, and S.M. Kurtz, *Prediction of multiaxial mechanical behavior for conventional and highly crosslinked UHMWPE using a hybrid constitutive model.* Biomaterials, 2003. **24**(8): p. 1365-80.
29. Xia, Q., et al., *In vivo range of motion of the lumbar spinous processes.* Eur Spine J, 2009. **18**(9): p. 1355-62.
30. Potvin, J.R., R.W. Norman, and S.M. Mcgill, *Reduction in Anterior Shear Forces on the L4/L5 Disk by the Lumbar Musculature.* Clinical Biomechanics, 1991. **6**(2): p. 88-96.
31. Toyone, T., et al., *Facet joint orientation difference between cephalad and caudad portions: a possible cause of degenerative spondylolisthesis.* Spine (Phila Pa 1976), 2009. **34**(21): p. 2259-62.
32. Berlemann, U., et al., *Facet joint remodeling in degenerative spondylolisthesis: an investigation of joint orientation and tropism.* Eur Spine J, 1998. **7**(5): p. 376-80.

33. Grobler, L.J., et al., *Etiology of spondylolisthesis. Assessment of the role played by lumbar facet joint morphology.* Spine (Phila Pa 1976), 1993. **18**(1): p. 80-91.
34. Freeman, B.J. and J. Davenport, *Total disc replacement in the lumbar spine: a systematic review of the literature.* Eur Spine J, 2006. **15 Suppl 3**: p. S439-47.
35. Link, H.D., *History, design and biomechanics of the LINK SB Charite artificial disc.* Eur Spine J, 2002. **11 Suppl 2**: p. S98-S105.
36. O'Leary, P., et al., *Response of Charite total disc replacement under physiologic loads: prosthesis component motion patterns.* Spine J, 2005. **5**(6): p. 590-9.
37. Kurtz, S.M., et al., *What is the correlation of in vivo wear and damage patterns with in vitro TDR motion response?* Spine (Phila Pa 1976), 2008. **33**(5): p. 481-9.

5. Derivation of clinically relevant boundary conditions suitable for evaluation of chronic impingement of lumbar total disc replacement: Application to standard development

Abstract

Current available standardized methods for evaluating the long-term wear of total disc replacements do not incorporate the effects of potential device impingement. Creation of a standard that incorporates device impingement is difficult without a thorough understanding of the associated biomechanical environment. Arbitrary modification of the currently available wear-test protocols to account for device impingement may add unnecessary cost, and potentially inaccurate, unrealistic results. Finite element models provide the ability to control variation and test for a wide range of parameters without the excessive time and monetary costs associated with cadaveric testing or wear simulations. However, careful validation of these models is required in order to ensure predictability. Retrieved implants can be used to validate the clinical predictability of finite element models. The objective of the current study was to quantify the ability of a previously developed finite element model (FEM) of the lumbar spine to predict polyethylene damage modes and impingement in actual clinical scenarios, and extract the loading and boundary conditions for implementation into a new lumbar TDR wear simulation standard. In order to achieve this objective, actual clinical scenarios, associated with retrieved implants, were modeled and simulated. We hypothesized that clinical damage modes, including both impingement and non-impingement scenarios, can be

predicted using a finite element model that incorporates case-specific clinical factors, anterior-posterior shear forces, coupled translations, and facet contact.

Introduction

Recently, total disc replacement systems (TDRs) have been introduced as an alternative to spinal fusion in the treatment of degenerative disc disease. Currently, there are two lumbar TDRs approved for implantation in the United States, and several more undergoing pre-clinical testing. The approved implants include a mobile (Charite, Depuy Spine) or fixed (Prodisc, Synthes Spine) polyethylene (PE) bearing surface between two cobalt chrome alloy endplates. These devices are intended to restore the disc height, maintain or correct segmental lordosis, and preserve segmental range of motion [1]. Biomechanical studies have documented a reduction in adjacent level effects after TDR when compared with fusion [2, 3]. Despite generally positive clinical results, complications have been reported. Specifically, impingement of the devices has been observed clinically[4-6], and excessive wear of the polyethylene and associated osteolysis has been reported in a small number of cases [4, 7-10]. These data indicate the importance of understanding the long-term clinical wear performance of lumbar TDRs, especially since they are often indicated for young, active patients[11].

Determining the clinical wear performance of lumbar TDRs utilizing pre-clinical protocols can be extremely difficult due to the spine's complex loading environment, large variations in patient morphology and tissue properties, and variation in surgical placement. Currently, two different testing protocols exist for spinal wear

simulation (ISO/FDIS 18192-1 and ASTM F2423-05), which consist of different loading and boundary conditions. While these protocols may provide reasonable approximation of wear for the majority of implanted devices, they do not account for potential impingement of the device. Serhan et al. (2006) utilized the ASTM standard to evaluate long-term wear characteristics of the Charite III mobile bearing total disc replacement. The authors concluded that, under these loading conditions, wear debris was minimal, and made no reference to implant impingement. A similar computational study[12] evaluated wear of the Charite using the ISO standard. This study indicated preferential articulation at the superior surface of the mobile core, but did not indicate rim loading or device impingement. These studies indicate that current test protocols do not necessarily evaluate worst-case scenarios, such as device impingement, which has been documented clinically for both mobile and fixed core TDRs [6, 9].

While several studies have been performed in order to evaluate the biomechanical effects of lumbar disc replacement technologies using a range of different loading modes[2, 3, 13-20], none have specifically attempted to model device impingement. Device impingement in total hip arthroplasty (THA) has been extensively studied[21, 22]. Impingement in THA has been associated with poor clinical outcomes, and can lead to instability, accelerated wear, and unexplained pain. As a result, hip simulator loading and boundary conditions have been developed in order to account for impingement[23]. Currently, there is no such similar standard available for total disc replacements. In order to generate such a standard, a better

understanding of the biomechanical environment associated with TDR impingement is required.

Both TDR wear simulation standards incorporate applied rotational displacements in concert with axial compression. This set of loading conditions is based on various assumptions that prevent the ability to evaluate device impingement. First, the magnitudes of these rotations are based on physiologic levels of rotation documented in unimplanted, intact spines. Several biomechanical studies have indicated that implantation of a TDR alters the spine's kinematics [13, 14, 24, 25]. Second, these inputs neglect the contribution of intervertebral shearing forces, which have been indicated in activities of daily living, bending, and lifting[26-29], and have been shown to affect wear patterns in TDR[30]. Third, the standards do not indicate applied translational displacements, which are coupled with rotational motions[31]. Finally, the standards do not include a contribution of the facets, which has been shown to effect intervertebral kinematics[32], and are affected by TDR[24].

It is unclear what the effect of altering applied rotations, including shear forces, dictating fixed translations, and adding facet constraint would have on device wear if implemented into the current standards. However, altering the loading and boundary conditions of the currently available wear-test protocols to account for worst-case scenarios, such as impingement, may be necessary to fully understand potential clinical consequences and assess design robustness. Arbitrary modification of the currently available wear-test protocols may add unnecessary

cost, and potentially inaccurate, unrealistic results. Finite element models provide the ability to control variation and test for a wide range of parameters without the excessive time and monetary costs associated with cadaveric testing or wear simulations [24, 33]. However, careful validation of these models is required to ensure that the results can be interpreted as predictive and indicative of what is happening clinically. Specifically, the outcome measures provided by these analyses must be associated with known physical outcomes to ensure and quantify the level of predictability.

Component retrieval studies can provide a valuable source of validation data for finite element studies. To date, these studies have identified changes in TDR shape due to mechanical deformation (creep), evidence of adhesive-abrasive wear, chronic inflammation in the peri-prosthetic tissue, and even reported cases of osteolysis[4, 8, 9, 34-38]. These studies, however, cannot quantitatively determine the mechanical environment or *in situ* component level stresses and strain. Combining computational analyses with retrieval data provides a means for validating preclinical test procedures, and can be used to optimize future device and experimental protocol designs[39].

The objective of the current study was to quantify the ability of a previously developed finite element model (FEM) of the lumbar spine to predict polyethylene damage modes and impingement in actual clinical scenarios, and extract the loading and boundary conditions for implementation into a new lumbar TDR wear simulation standard. In order to achieve this objective, actual clinical scenarios,

associated with retrieved implants, were modeled and simulated. We hypothesized that clinical damage modes, including both impingement and non-impingement scenarios, can be predicted using a finite element model that incorporates case-specific clinical factors, anterior-posterior shear forces, coupled translations, and facet contact. Contact pressure acting on the polyethylene cores was output from the FEM and compared with wear maps of the retrievals. Resultant forces experienced by the device and facets as well as the resulting sagittal rotation were determined. Additionally, 1st principal and von Mises strain in the core and forces acting on the core were compared to rim penetration, rim penetration rate, and maximum oxidation index.

Methods

The following sections outline the methods utilized to simulate clinical scenarios using a previously developed finite element model of a lumbar spine[24, 33]. The clinical scenarios were taken from retrieved implants from Drexel University's Implant Retrieval Center. Exclusion criteria (explained below) were applied to the entire collection of retrieved TDRs, which resulted in a total of 10 scenarios appropriate for simulation. Geometric parameters were derived from the available pre-revision radiology and measurements taken directly from the implants. These parameters were used to alter the existing finite element model such that it approximated the implanted, pre-revision state. Loading and boundary conditions, consistent with standing were applied in order to achieve a resultant lordotic angle consistent with the available radiology on a case-by-case basis. Various outcomes

from the finite element model were compared with data for each of the retrieved implants.

Finite Element Model

A three-dimensional finite element model (FEM) of a ligamentous L3-S1 lumbar spine was generated from quantitative computed tomography (QCT) data of a cadaveric spine. The data set was taken from the publicly available Visible Human data set (Visible Human Project®, National Library of Medicine, National Institute of Health). The spinal geometry was reviewed and found to be free of any bony or disc deformities, i.e., osteophytes or herniations. Hounsfield units were used as a surrogate for bone mineral density (BMD).

The methodology used to develop and validated the model has been previously described [24, 33], but will be outlined below. A combination of automatic and manual image segmentation techniques (Analyze, AnalyzeDirect, Inc., Overland Park, KS) were used to extract detailed surfaces corresponding to the major bony structures of L3-S1. The software package allowed for automatic segmentation based on thresholding of the QCT grayscale values. These surfaces were imported into the commercial finite element mesh generation program, HyperMesh (Altair Inc., Troy, MI), and were discretized into a combination of tetrahedral elements for the bony structures and hexahedral elements for the intervertebral discs (IVDs). The central portion of the IVDs, approximately 40% of the volume [40], were designated to be the nucleus pulposus (NP), while the remaining volume was considered the annulus fibrosus. Major spinal ligaments (anterior longitudinal

ligament, posterior longitudinal, intraspinatus, supraspinatus, intratransverse, facet capsule, ligamentum flavum) were implemented in the model using tension-only nonlinear springs. Shell elements were used to plate the exterior surface of the vertebral bodies and represented the cortex and bony endplate.

Bone mineral density (BMD)-dependent orthotropic material properties were assigned to the cancellous bone of the vertebral bodies. Custom software was written to apply the Young's modulus at each of the nodal points based on the density of the bone. Similar methodology has been used to create models with heterogeneous bone properties of the tibia and femur [41, 42]. The quantitative relationship between bone mineral density and elastic modulus in cancellous vertebral bone, as reported by Morgan et al. and Ulrich et al., was utilized to define a nonlinear relationship between bone mineral density and orthotropic elastic modulus [43, 44]. Elastic moduli within the vertebral body fell within what has been previously reported in the literature [45-47]. The remaining structures were assigned material properties from the literature and are described in Table 1-1. Frictionless contact was defined between the facets using a penalty-based contact algorithm.

Retrieval Selection

Retrieved total disc replacements from the Drexel Universiy Implant Retrieval Center were utilized for the current study. The current retrieval collection consists of a total of 55 mobile bearing implants. In order to determine which retrievals were candidates for modeling and simulating, a variety of exclusion criteria were applied.

Primarily, the selected subset of implants would have pre-revision radiology in order to create an implanted finite element model that is geometrically consistent. This limited the available pool of implants to a total of 22. Additionally, there were some implant complications that were determined to be confounding variables when attempting to evaluate impingement. Specifically, implants that were revised due to subsidence, anterior migration, and osteolysis/endplate loosing were not considered candidates for this analysis. This left a total of 10 available implants for modeling.

In order to determine how representative the subset of 10 implants was to the entire collection, patient (Table 5-1) and implant (Table 5-2) data were compared. The subset of implants was generally a fair representation of the entire collection. All of the implants in the subset were from L3-L4 (n=1), L4-L5 (n=4) or L5-S1 (n=5). The average implantation time for the entire collection was 7.6 years, and 7.5 years for the subset. Seven of the 10 implants from the subset exhibited signs of chronic impingement compared to 43 of 55 for the entire collection. The average rim penetration was approximately three times higher for the entire collection compared to the subset indicating that the subset did not incorporate the more severe cases of rim penetration. However, the subset did encompass implants with essentially zero rim penetration as well as those exhibiting rim penetration, allowing for simulation of both scenarios.

Table 5-1. Patient data comparison of the subset of implants chosen for modeling with respect to the total retrieval collection.

	Total Collection		Modeling Subset	
Total Number of Implants	55		10	
Level				
L2/L3	1		0	
L3/L4	2		1	
L4/L5	26		4	
L5/S1	25		5	
Unknown	1		0	
Surgeon Totals				
Dr. VO	35		9	
Dr. R	8		0	
Dr. I	6		1	
Dr. vWdM	1		0	
Dr. P	1		0	
Dr. K	1		0	
Total Number of Patients	48		10	
Gender				
Female	32	66.67%	9	90%
Male	12	25.00%	1	10%
Unknown	4	8.33%	0	
Implant Fixation Method				
Non Coated	38		4	
Coated	14		3	
Unknown	3		3	
Implantation Time (y)				
Average	7.6		7.5	
Min	1.7		2.2	
Max	16.3		13.6	

Table 5-2. Implant data comparison of the subset of implants chosen for modeling with respect to the total retrieval collection.

	Total Collection	Modeling Subset
Dome Wear (mm)		
Average	0.31	0.31
Min	0.06	0.16
Median	0.25	0.28
Max	0.92	0.61
Wear Rate (mm/yr)		
Average	0.06	0.05
Min	0.02	0.02
Median	0.04	0.04
Max	0.25	0.18

Radial Rim Cracks		
Yes	28	7
No	26	3
Transverse Cracks		
Yes	24	4
No	30	6
Not Applicable	1	0
Fractured Wire		
Yes	17	2
No	37	8
Unknown	1	0
Intact Rim		
Yes	49	10
No	5	0
Not Applicable	1	0
Chronic Impingement		
Yes	43	7
No	12	3
Rim Penetration (mm)		
Average	0.38	0.13
Min	0.00	0.02
Median	0.23	0.06
Max	2.77	0.18
Rim Penetration Rate (mm/yr)		
Average	0.08	0.05
Min	0.00	0.00
Median	0.02	0.01
Max	1.10	0.36

Geometric Case-Specific Model Development

Single level models of L4-L5 and L5-S1 were constructed from the L3-S1 model. Mobile core disc replacements were virtually implanted in each model. A combination of pre-revision radiology measurements, retrieval implant size data, and visual approximation were used to generate geometric case-specific models. Specifically, disc height, intervertebral lordotic angle, implant position, implant size, implant orientation, and sagittal orientation relative to vertical were modeled for each scenario.

The retrieved implant size data was used to determine the appropriate geometric attributes of the finite element model. Specifically, dome height, footplate size, and footplate angles measured from the retrievals were used. Corresponding CAD geometry was discretized into finite element models for virtual implantation into either L4-L5 or L5-S1. The footplate angles, however, did not always fully account for the pre-implantation lordosis (Figure 5-1). In order to compensate for this the finite element models of the implants were biased towards extension. The amount of bias was determined by subtracting the pre-implantation lordotic angle from the implant lordotic angle. For example, if two non-angled footplates were used for L4-L5, which had a pre-implantation lordosis of 7.2 degrees, then the implants were biased 7.2 degrees towards extension such that they would fit in the disc space, and no alteration to the intact lordotic angle would be required.

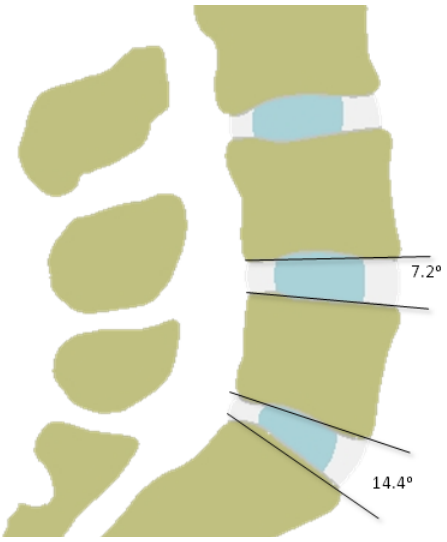

Figure 5-1. Sagittal cutplane of the finite element model depicting the lordotic angles of L4-L5 and L5-S1.

Implant size data was used to determine the maximum total inferior-superior dimension of the implanted disc height. The total dome height plus two times the thickness of the metallic footplates at the center of the dome (2.3 mm) equaled the total average post-implantation disc height. Dome heights varied between 8.5 mm and 11.5 mm. Therefore, total post-implantation disc height ranged from 13.1 mm to 16.1 mm. The average pre-implantation disc heights were 10.4 mm for L4-L5 and 10.1 mm for L5-S1. Total implantation disc height distraction ranged from 2.7 mm to 6 mm.

X-rays for the subset of implants were imported into the publicly available open source software (OsiriX, v3.6, 32 bit). The angle of the superior endplate of the superior vertebral body at the index level relative to the horizon was measured for each radiograph. The implanted finite element models were then rotated about the medial-lateral axis in order to match these angles. This was done in order to ensure

that the shear contribution from vertical upper body weight loading would be case-specific.

Loading and Boundary Conditions

The loading paradigm consisted of application of a vertical force simulating upper body weight, which was offset anteriorly 30 mm to be at the approximate location of the human upper body center of mass [48]. Additionally, a one dimensional force element was placed between the spinous processes in order to simulate the erector spinae force and restore sagittal balance.

Patient weights were not available for each of the implants within the subset. Therefore, upper body weight for a 50th percentile male was chosen. This provided the ability to verify that the loading paradigm resulted in disc pressures consistent with those reported in the literature [49]. Orientation of the spinal segment relative to the vertical upper body weight force was determined from the endplate angle radiographic measurements. The force was applied to the upper endplate of the superior-most vertebrae. The erector spinae force was increased from 0 to 300 N for the intact models to determine the point at which the resultant flexion-extension rotation was minimized, i.e., sagittaly balanced in the neutral zone. This loading was then applied to the implanted models. Previous work performed by this laboratory has demonstrated that this loading protocol can produce both impingement and non-impingement for both a mobile and fixed-core device, which suggests that this loading does not bias results towards either outcome. distraction (Rundell et al., 2010, Trans of the Spinal Arthroplasty Society).

Application of erector spinae loading was performed on a closed-loop. The resulting lordosis from the deformed FEM was compared to the radiographic data to verify that the models were reasonably predicting the final geometric state. The erector spinae force was then increased or decreased in order to result in a more accurate lordosis. Several iterations were performed until the resulting lordotic angle from the finite element model closely approximated the angle observed in the pre-revision x-rays. In one of the cases spinous process contact prevented the implant from reaching the necessary lordosis. Initial bias of the implant was implemented in this case.

Contour plots of contact stress on the polyethylene core were output for each analysis and compared with the retrieval wear maps. A thorough description of the methods utilized to develop detailed wear maps has been previously described[50]. In order to determine a correlation between the level of impingement exhibited by the retrievals and that predicted by the finite element models, the amount of rim penetration per year was plotted against peak contact stress at the interfaces of the superior and inferior footplate and core versus peak 1st principal strain. Strain was selected over stress since the polyethylene was modeled using an elastic-plastic model, which results in very small increases in stress after reaching yield. Rim penetration, which reflects the combined effects of creep and wear, was determined by calculating the difference in the measured rim thickness in worn and unworn regions, as previously described[51]. Pearson correlation tests were performed and statistical significance was considered for $p<0.05$.

Results

All of the models, with the exception of one, resulted in extension rotation as a result of the applied loading (Figure 5-2). The average extension rotation was 4.8 degrees with a standard deviation of 3.7 degrees. The average erector spinae force required to reach a lordotic angle consistent with the retrieved radiographs was 284.5 N with a standard deviation of 26.6 N. The intact models experienced extension rotation of 1.5 and 0.4 degrees at 300 N of erector spinae force for L4-L5 and L5-S1, respectively. The resultant anterior-posterior shear force between the superior footplate and polyethylene core was negative for all cases (Table 5-3). This indicates that the superior vertebra was applying a posterior force relative to the inferior vertebra (posterior shear). All of the finite element models resulted in facet contact forces, which had anterior-posterior and superior-inferior components. The anterior-posterior translation of the superior vertebrae was significantly correlated with rotation in the sagittal plane (Figure 5-3a). Extension rotation was coupled with posterior translation. The resultant facet forces were significantly correlated with anterior-posterior translation of the superior vertebrae (Figure 5-3b).

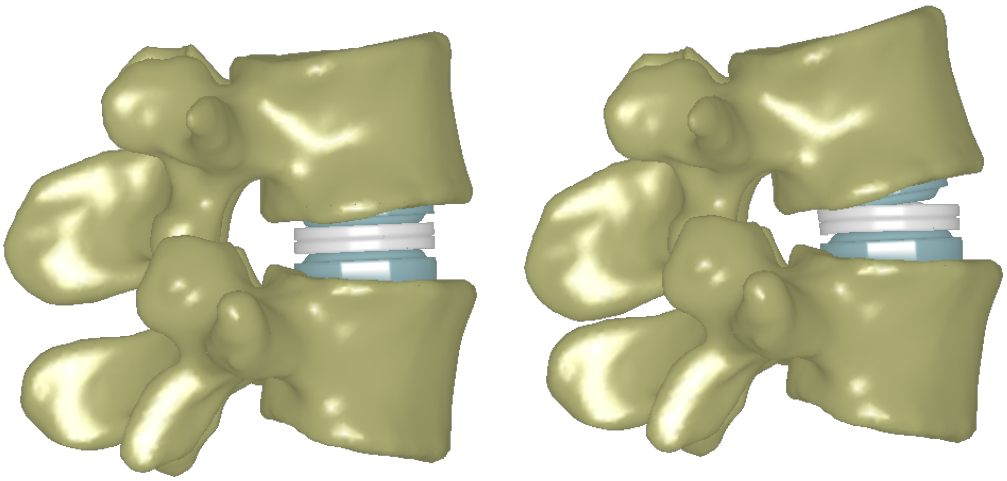

Figure 5-2. Images of the finite element model depicting the undeformed state (left) compared to the final, deformed state (right)

Table 5-3. Values of reaction forces generated in the finite element models (negative values for A-P shear indicate posterior force at the superior component; positive values for facet A-P force indicate an anterior directed force applied by the superior vertebra)

	Average	Standard Deviation
Facet A-P Force (N)	53.0	31.8
Facet Inf-Sup (N)	56.8	33.5
Facet Resultant (N)	84.9	44.0
Disc A-P (N)	-129.6	69.5
Disc Inf-Sup (N)	467.6	31.4
Disc Resultant (N)	490.3	28.1

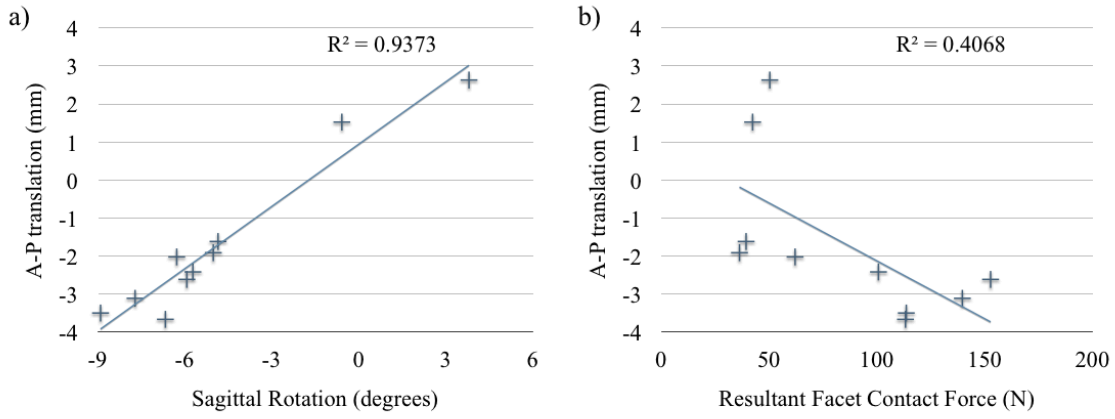

Figure 5-3. Graphs depicting the relationships between anterior-posterior translation and sagittal rotation (negative values correspond to extension) (a) as well as resultant translation and resultant facet contact force (b).

The average percent difference in the lordotic angle measured from the retrieval x-rays compared to the final state of the corresponding finite element model was 18.0% with a standard deviation of 19.4 %. In one case, the FEM substantially underestimated the lordotic angle measured in the retrieval x-ray (71.0%). Detailed review of this scenario indicated two-sided rim impingement for both the retrieval and FEM. The two-sided rim impingement present in the FEM prevented it from being able to fully reach a lordotic angle consistent with the retrieval despite increases in erector spinae force. The greater lordotic angle measured in the retrieval x-ray likely resulted from either subsidence or anterior lift-off of the imlant, which the model was unable to predict. Removal of this case results in an average percent difference between the x-ray measurement and FEM of 12.1% with a standard deviation of 5.8%. Lordotic angles ranged from 9.8 to 23.1 degrees for the retrieved implants, and 10.6 to 23.3 degrees for the FEMs.

Qualitatively, contour plots of contact stress appeared similar to the wear maps (Figure 5-4). Specifically, areas of contact stress maxima indicated areas of increased inward deformation or wear of the retrieved implants. These areas tended to occur offset from the center of the dome, and in the cases of impingement, somewhere near the rim. Impingement occurred either as one (6/10) or both (2/10) of the metallic footplates contacting the core's rim. Wear maps of the implants indicated wear patterns consistent with both one-sided and two-sided impingement. The model was able to simulate both scenarios.

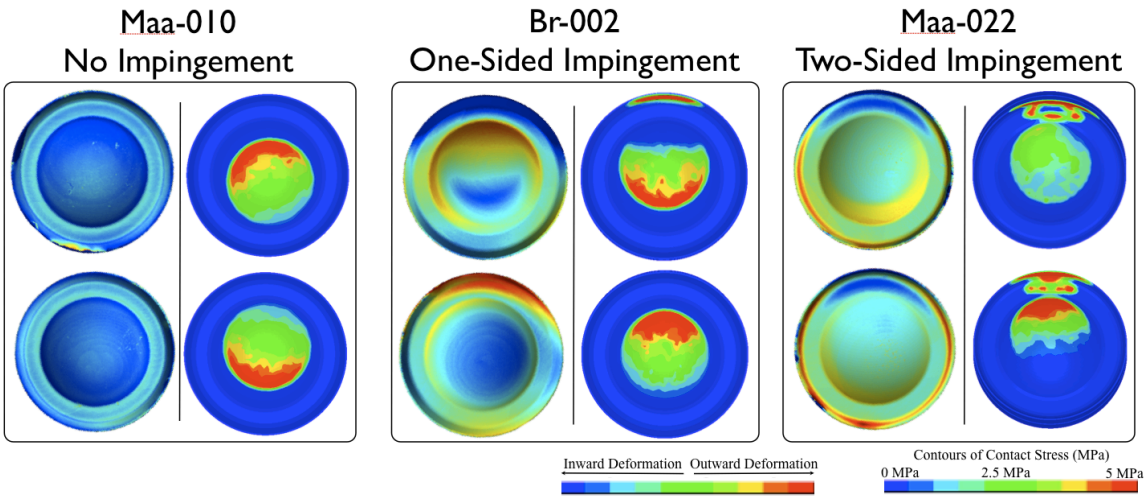

Figure 5-4. Three exemplar side-by-side comparisons of retrieval wear maps (left) with FEM contact stress contour plots (right). The FEM was able to simulate no impingement, one-sided impingement, and two-sided impingement.

One-sided rim impingement resulted in bending of the implant core's rim. This was observed by inward deformation on one surface of the rim with outward deformation on the corresponding opposite side (see Br-002 in Figure 5-4). This bending was grossly visible in micro computed tomography three-dimensional reconstructions of the retrieved cores. This indicates that the bending experienced *in vivo* was of a great enough magnitude to result in plastic deformation of the core's rim. Evaluation of the finite element model indicated similar bending in the form of tensile stress generated on the side of the rim being contacted by the metallic footplate (Figure 5-5).

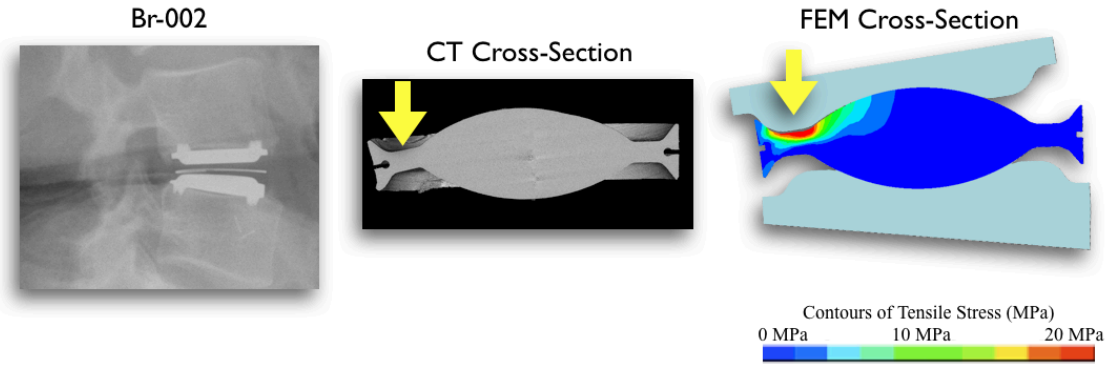

Figure 5-5. Images depicting a sagittal x-ray (left), sagittal cross-section of a retrieved implant from a 3-D Ct reconstruction, and sagittal cross-section of the finite element model with contours of 1st principal stress in the core depicted.

Significant correlations were observed between rim penetration rate and loading of the core from the FEM (Table 5-4). Specifically, the rim penetration rate (mm/year) significantly correlated with peak contact stress at the superior core-footplate interface and peak 1st principal strain. The rim penetration rate did not significantly correlate with inferior peak contact stress at the core-footplate interface.

Table 5-4. Summary of Pearson correlation test results.

Correlations	R^2	r	p (1-sided)	p (2-sided)
Peak superior contact stress (MPa) vs. rim penetration (mm/year)	0.53	0.72	0.008	0.017
Peak inferior contact stress (MPa) vs. rim penetration (mm/year)	0.16	0.40	0.125	0.24
Peak 1st principal strain (mm/mm) vs. rim penetration (mm/year)	0.43	0.66	0.019	0.038

Discussion

In the current study, we used nonlinear 3-D FEMs of lumbar spinal segments (L4-L5 and L5-S1) to simulate clinical TDR scenarios based on explanted retrieval data. The results indicate that the FEM was able to predict both impingement and non-

impingement scenarios. Contact stresses on the polyethylene cores were consistent with the wear patterns depicted for the retrieved implants. Peak superior contact stress and peak 1st principal strain in the core from the FEM were significantly correlated with damage of the retrieved implants. These results indicate that the FEM is capable of simulating post-implantation *in situ* TDR, and predicting polyethylene performance. The model also provided valuable insight into the biomechanical environment associated with both impingement and non-impingement scenarios. The loading and boundary conditions generated in the current study are being utilized to generate a new standard for lumbar TDR wear simulation.

In nine out of the ten simulated cases, loading application resulted in an increase in lordotic angle when compared with the pre-implantation state. These results are consistent with previously reported findings of TDR, which have indicated increased potential for extension rotation post implantation [14, 24, 52]. A previous *in vivo* study indicated a significant increase in lumbar lordosis following TDR[53]. The authors of this study suggested a combination of anterior longitudinal ligament transection, an anterior center of rotation, and an increase in disc height with concomitant distraction of the facets as being responsible for the increased lordosis post-TDR. Specifically, they indicated that these factors contributed to an altered biomechanical environment such that static equilibrium of forces and moments occured at a greater lordotic angle post-TDR. Data from the current study provides a basis for this theoretical suggestion, and indicates that TDR has the ability to alter

sagittal balance such that application of standing loads results in initial extension rotation. Data from the current study demonstrates that this initial bias towards extension contributes to posterior device impingement. Inclusion of a simple extension bias in current wear testing standards may provide a cost-effective, initial step towards evaluating device impingement *in vitro*.

Results from the current study indicated that extension rotation was coupled with posterior translation of the superior vertebra. The posterior translation increased with increasing facet contact force. Loading conditions used in the current study incorporated a vertical load consistent with upper body weight. Due to the spine's relative orientation to vertical this resulted in a baseline intervertebral anterior shear force, which acted to engage the facets. Subsequently, extension rotation generated by activation of the erector spinae caused the facets to articulate and guide the superior vertebra posteriorly. This posterior translation, imparted by facet contact during extension rotation, resulted in intervertebral posterior shear experienced by the TDR. This posterior shear essentially locked the core in place, which allowed for one-sided impingement to cause bending of the rim (Figure 5-6). Evidence from the retrieval collection verified the presence of posterior shear *in vivo* post TDR via downward bending of the posterior rim. A similar phenomenon was observed in several of the other simulations and corresponding retrievals. Moreover, the finite element model predicted asymmetric loading of the mobile core's inferior and superior faces that was consistent with the retrieval wear maps. Currently, the available wear test standards do not prescribe a relationship between

rotational and translational displacements. Results from the current study suggest that inclusion of the geometrical constraint provided by the facets in addition with a baseline anterior shear consistent with vertical upper body loading can provide the necessary rotation-translation relationship to predict polyethylene deformation patterns *in vivo*.

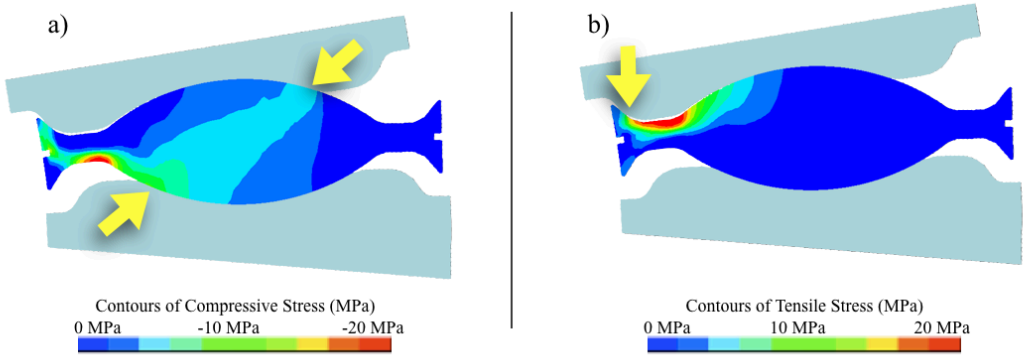

Figure 5-6. Images depicting the core becoming locked (left) resulting in downward bending of the posterior rim as a result of contact between the superior footplate and superior surface of the core (right)

Generally, during laboratory testing, the lumbar muscle forces and upper body compressive forces are simulated via a follower load applied at the joint centers, which neglects intervertebral shear. A recent study introduced anterior-posterior shear into the current ISO standard, and observed differences in surface wear patterns for a Prodisc-L, but no significant difference in the overall wear volume[30]. This study applied shearing forces based on previously reported values from the literature, but did not incorporate the geometrical boundary conditions imposed by the facets. As demonstrated in the current study, anterior shear force will engage the facet joints and guide motion during sagittal plane rotation. This will

result in a semi-constrained motion pattern, which is necessary to simulate in order to accurately and thoroughly evaluate wear.

A significant correlation was observed between the rim penetration rate and peak superior contact stress. Contact stress is often utilized when evaluating wear performance of polyethylene using computational analyses[54, 55]. There was no significant correlation, however, between inferior peak contact stress and rim penetration rate. Closer review of the data indicated that intervertebral shear loading acted to lock the core in place. The superior footplate articulated relative to the locked core, and in many cases contacted the rim. The majority of the simulations that resulted in one-sided impingement (6/10) consisted of contact at the superior footplate-core interface (4/10). These results are consistent with a previous computational and laboratory analyses that have indicated preferential superior relative motion for the Charite device along with evidence of one-sided wear in retrieved implants[12, 51].

In conclusion, this is the first study to validate a methodology for evaluating TDR using a finite element model with inputs derived from clinical retrieval data. The significant correlations determined in the current study provide the ability to perform future studies that target specific parameters that may influence device wear and impingement. Moreover, the current study provides valuable insight into the biomechanical environment associated with device impingement such that it can be employed in wear simulation. Currently, a work item (WK25942) is focused on taking the results of these analyses and creating a testing guide to simulate

impingement in lumbar total disc replacements. This new standard will incorporate the effects of anterior shear from upper body weight and translational motions imposed by the geometrical constraint of the facets. The guidelines provided in this new standard will describe an approach for evaluating new designs and design changes to help manufacturers and regulatory agencies make more informed decisions on design choices.

Acknowledgements

This study was funded in part by NIH R01 AR47904, R01 AR056264, and the Food and Drug Administration's Critical Path Initiative. We would also like to thank Jonathan Peck and Genevieve Hill from the FDA for their assistance and support.

References

1. Mayer, H.M. and A. Korge, *Non-fusion technology in degenerative lumbar spinal disorders: facts, questions, challenges.* Eur Spine J, 2002. **11 Suppl 2**: p. S85-91.
2. Panjabi, M., et al., *Multidirectional testing of one- and two-level ProDisc-L versus simulated fusions.* Spine, 2007. **32**(12): p. 1311-9.
3. Auerbach, J.D., et al., *Evaluation of spinal kinematics following lumbar total disc replacement and circumferential fusion using in vivo fluoroscopy.* Spine, 2007. **32**(5): p. 527-36.
4. Kurtz, S.M., et al., *Polyethylene wear and rim fracture in total disc arthroplasty.* Spine J, 2007. **7**(1): p. 12-21.
5. Choma, T.J., et al., *Retrieval analysis of a ProDisc-L total disc replacement.* J Spinal Disord Tech, 2009. **22**(4): p. 290-6.
6. Kafer, W., et al., *Posterior component impingement after lumbar total disc replacement: a radiographic analysis of 66 ProDisc-L prostheses in 56 patients.* Spine, 2008. **33**(22): p. 2444-9.
7. Kurtz, S.M., et al., *Analysis of a retrieved polyethylene total disc replacement component.* Spine J, 2005. **5**(3): p. 344-50.
8. Punt, I.M., et al., *Complications and reoperations of the SB Charite lumbar disc prosthesis: experience in 75 patients.* Eur Spine J, 2008. **17**(1): p. 36-43.

9. van Ooij, A., et al., *Polyethylene wear debris and long-term clinical failure of the Charite disc prosthesis: a study of 4 patients.* Spine, 2007. **32**(2): p. 223-9.
10. van Ooij, A., F.C. Oner, and A.J. Verbout, *Complications of artificial disc replacement: a report of 27 patients with the SB Charite disc.* J Spinal Disord Tech, 2003. **16**(4): p. 369-83.
11. Siepe, C.J., et al., *Total lumbar disc replacement in athletes: clinical results, return to sport and athletic performance.* Eur Spine J, 2007. **16**(7): p. 1001-13.
12. Goreham-Voss, C.M., et al., *Preferential superior surface motion in wear simulations of the Charite total disc replacement.* Eur Spine J, 2010.
13. Cunningham, B.W., et al., *Biomechanical evaluation of total disc replacement arthroplasty: an in vitro human cadaveric model.* Spine, 2003. **28**(20): p. S110-7.
14. Denoziere, G. and D.N. Ku, *Biomechanical comparison between fusion of two vertebrae and implantation of an artificial intervertebral disc.* J Biomech, 2006. **39**(4): p. 766-75.
15. Huang, R.C., et al., *The implications of constraint in lumbar total disc replacement.* J Spinal Disord Tech, 2003. **16**(4): p. 412-7.
16. Kim, D.H., et al., *Factors influencing segmental range of motion after lumbar total disc replacement using the ProDisc II prosthesis.* J Neurosurg Spine, 2007. **7**(2): p. 131-8.
17. Le Huec, J.C., et al., *Influence of facet and posterior muscle degeneration on clinical results of lumbar total disc replacement: two-year follow-up.* J Spinal Disord Tech, 2005. **18**(3): p. 219-23.
18. Moumene, M. and F.H. Geisler, *Comparison of biomechanical function at ideal and varied surgical placement for two lumbar artificial disc implant designs: mobile-core versus fixed-core.* Spine, 2007. **32**(17): p. 1840-51.
19. Noailly, J., D. Lacroix, and J.A. Planell, *Finite element study of a novel intervertebral disc substitute.* Spine, 2005. **30**(20): p. 2257-64.
20. Rousseau, M.A., et al., *Disc arthroplasty design influences intervertebral kinematics and facet forces.* Spine J, 2006. **6**(3): p. 258-66.
21. Brown, T.D. and J.J. Callaghan, *Impingement in Total Hip Replacement: Mechanisms and Consequences.* Curr Orthop, 2008. **22**(6): p. 376-391.
22. Malik, A., A. Maheshwari, and L.D. Dorr, *Impingement with total hip replacement.* J Bone Joint Surg Am, 2007. **89**(8): p. 1832-42.
23. Holley, K.G., et al., *Impingement of acetabular cups in a hip simulator: comparison of highly cross-linked and conventional polyethylene.* J Arthroplasty, 2005. **20**(7 Suppl 3): p. 77-86.
24. Rundell, S.A., et al., *Total disc replacement positioning affects facet contact forces and vertebral body strains.* Spine, 2008. **33**(23): p. 2510-7.
25. O'Leary, P., et al., *Response of Charite total disc replacement under physiologic loads: prosthesis component motion patterns.* Spine J, 2005. **5**(6): p. 590-9.
26. Schultz, A.B., et al., *Analysis and measurement of lumbar trunk loads in tasks involving bends and twists.* J Biomech, 1982. **15**(9): p. 669-75.

27. Potvin, J.R., R.W. Norman, and S.M. Mcgill, *Reduction in Anterior Shear Forces on the L4/L5 Disk by the Lumbar Musculature.* Clinical Biomechanics, 1991. **6**(2): p. 88-96.
28. Callaghan, J.P., A.E. Patla, and S.M. McGill, *Low back three-dimensional joint forces, kinematics, and kinetics during walking.* Clin Biomech (Bristol, Avon), 1999. **14**(3): p. 203-16.
29. Kingma, I., D. Staudenmann, and J.H. van Dieen, *Trunk muscle activation and associated lumbar spine joint shear forces under different levels of external forward force applied to the trunk.* J Electromyogr Kinesiol, 2007. **17**(1): p. 14-24.
30. Vicars, R., et al., *The effect of anterior-posterior shear load on the wear of ProDisc-L TDR.* Eur Spine J, 2010.
31. Li, G., et al., *Segmental in vivo vertebral motion during functional human lumbar spine activities.* Eur Spine J, 2009. **18**(7): p. 1013-21.
32. Schmidt, H., et al., *The relation between the instantaneous center of rotation and facet joint forces - A finite element analysis.* Clin Biomech (Bristol, Avon), 2008. **23**(3): p. 270-8.
33. Rundell, S.A., et al., *Effect of nucleus replacement device properties on lumbar spine mechanics.* Spine (Phila Pa 1976), 2009. **34**(19): p. 2022-32.
34. McAfee, P.C., et al., *Revisability of the CHARITE artificial disc replacement: analysis of 688 patients enrolled in the U.S. IDE study of the CHARITE Artificial Disc.* Spine (Phila Pa 1976), 2006. **31**(11): p. 1217-26.
35. Pitzen, T., et al., *Cervical spine disc prosthesis: radiographic, biomechanical and morphological post mortal findings 12 weeks after implantation. A retrieval example.* Eur Spine J, 2007. **16**(7): p. 1015-20.
36. Fraser, R.D., et al., *AcroFlex design and results.* Spine J, 2004. **4**(6 Suppl): p. 245S-251S.
37. Hallab, N., H.D. Link, and P.C. McAfee, *Biomaterial optimization in total disc arthroplasty.* Spine (Phila Pa 1976), 2003. **28**(20): p. S139-52.
38. Pimenta, L., R.C. Diaz, and L.G. Guerrero, *Charite lumbar artificial disc retrieval: use of a lateral minimally invasive technique. Technical note.* J Neurosurg Spine, 2006. **5**(6): p. 556-61.
39. Rawlinson, J.J., et al., *Retrieval, experimental, and computational assessment of the performance of total knee replacements.* J Orthop Res, 2006. **24**(7): p. 1384-94.
40. White, A.A., Panjabi, M.M.,, *Clinical Biomechanics of the Spine, 2nd ed.*1990, Philadelphia-Toronto: J.B. Lippincott Company.
41. Yosibash, Z., et al., *A CT-based high-order finite element analysis of the human proximal femur compared to in-vitro experiments.* J Biomech Eng, 2007. **129**(3): p. 297-309.
42. Sawatari, T., et al., *Three-dimensional finite element analysis of unicompartmental knee arthroplasty--the influence of tibial component inclination.* J Orthop Res, 2005. **23**(3): p. 549-54.
43. Ulrich, D., et al., *The ability of three-dimensional structural indices to reflect mechanical aspects of trabecular bone.* Bone, 1999. **25**(1): p. 55-60.

44. Morgan, E.F., H.H. Bayraktar, and T.M. Keaveny, *Trabecular bone modulus-density relationships depend on anatomic site.* J Biomech, 2003. **36**(7): p. 897-904.
45. Kopperdahl, D.L. and T.M. Keaveny, *Yield strain behavior of trabecular bone.* J Biomech, 1998. **31**(7): p. 601-8.
46. Mosekilde, L. and C.C. Danielsen, *Biomechanical competence of vertebral trabecular bone in relation to ash density and age in normal individuals.* Bone, 1987. **8**(2): p. 79-85.
47. Hansson, T.H., T.S. Keller, and M.M. Panjabi, *A study of the compressive properties of lumbar vertebral trabeculae: effects of tissue characteristics.* Spine, 1987. **12**(1): p. 56-62.
48. Rohlmann, A., et al., *Applying a follower load delivers realistic results for simulating standing.* J Biomech, 2009. **42**(10): p. 1520-6.
49. Wilke, H.J., et al., *New in vivo measurements of pressures in the intervertebral disc in daily life.* Spine (Phila Pa 1976), 1999. **24**(8): p. 755-62.
50. Shkolnikov, Y.P., et al., *Wear pattern observations from TDR retrievals using autoregistration of voxel data.* J Biomed Mater Res B Appl Biomater, 2010. **94**(2): p. 312-7.
51. Kurtz, S.M., et al., *What is the correlation of in vivo wear and damage patterns with in vitro TDR motion response?* Spine (Phila Pa 1976), 2008. **33**(5): p. 481-9.
52. Dooris, A.P., et al., *Load-sharing between anterior and posterior elements in a lumbar motion segment implanted with an artificial disc.* Spine, 2001. **26**(6): p. E122-9.
53. Cakir, B., et al., *The impact of total lumbar disc replacement on segmental and total lumbar lordosis.* Clin Biomech (Bristol, Avon), 2005. **20**(4): p. 357-64.
54. Brown, T.D. and D.L. Bartel, *What design factors influence wear behavior at the bearing surfaces in total joint replacements?* J Am Acad Orthop Surg, 2008. **16 Suppl 1**: p. S101-6.
55. Ong, K.L., et al., *Biomechanical modeling of acetabular component polyethylene stresses, fracture risk, and wear rate following press-fit implantation.* J Orthop Res, 2009. **27**(11): p. 1467-72.

6. Lumbar TDR impingement sensitivity to disc height distraction, spinal sagittal orientation, implant position, and implant lordosis

Abstract

TDR has the potential to replace fusion as the gold standard for treatment of painful degenerative disc disease. However, complications after TDR have been associated with device impingement and accelerated polyethylene wear. The effect of disc height distraction, implant lordotic angle, implant anterior-posterior position, and spinal orientation relative to the horizon on impingement risk remains unclear.The objective of the current study was to determine the sensitivity of TDR impingement to disc height distraction, implant lordotic angle, implant anterior-posterior position, and spinal orientation relative to the horizon using a validated finite element model based on actual clinical scenarios. A previously developed finite element model of the lumbar spine was altered to include implantation of a mobile bearing total disc replacement. A series of sensitivity analyses were performed to determine which parameters resulted in the highest impingement risk. Specifically, spinal orientation, disc height distraction, footplate lordotic angle, and anterior-posterior position were evaluated. Based on a previous study, peak superior contact stress and peak 1st principal strain of the polyethylene core were used to determine impingement risk. Generally, TDR tended to result in an increase in extension rotation and facet contact force during simulated erect posture when compared with the intact models. Impingement risk was sensitive to all of the tested parameters. Underestimating the spine's lordotic angle with the use of flat

footplates resulted in the greatest peak 1st principal strain and peak contact stress. The data from the current study indicates that lumbar mobile-bearing TDR impingement is sensitive to disc height distraction, anterior-posterior position, implant lordosis, and spinal sagittal orientation. TDR impingement risk can be minimized by choosing an implant with an appropriate amount of lordosis, not over distracting the disc space, and taking care to not place the implant too far anterior or posterior.

Introduction

Recently, total disc replacement systems (TDRs) have been introduced as an alternative to spinal fusion in the treatment of degenerative disc disease. Currently, there are two lumbar TDRs approved for implantation in the United States, and several more undergoing pre-clinical testing. The approved implants include either a mobile (Charite, Depuy Spine) or fixed (Prodisc, Synthes Spine) polyethylene (PE) bearing surface between two cobalt chrome alloy endplates. Biomechanical studies have documented a reduction in adjacent level deformation after TDR when compared with fusion [1, 2]. Despite generally positive clinical results, complications have been reported. Specifically, impingement of the devices has been observed clinically[3-5], and associated with excessive wear of the polyethylene. For a small number of cases, polyethylene wear after TDR has resulted in osteolysis [3, 6-9]. These data indicate the importance of understanding the parameters associated with impingement risk, which may include disc height distraction, patient morphology, implant lordotic angle, and device placement[5, 10-12].

One of the goals of TDR is to restore disc height to an optimal level. However, there is a paucity of available guidance regarding the appropriate amount of distraction. Delamarter et al.[13] suggested choosing a disc height based on observation during surgery or utilizing templates under fluoroscopy. David et al. [14] suggested choosing the prosthesis with the highest possible disc height. The biomechanical or clinical rationale underlying these suggestions remains unclear. A clinical study of TDR reported an average increase in disc height after implantation of 1.8 times the original height[15]. Recent anatomical studies have demonstrated that increases in disc height after cervical and lumbar TDR affect facet articulation[16, 17], which the authors suggest could accelerate failure of the artificial disc. Clinically, facet arthrosis following TDR has been documented in approximately a third of patients for both mobile and fixed core prostheses[18]. Although these data indicate potential ramifications for both the device and facets as a result of disc height distraction, the effect of disc height distraction on impingement risk is poorly understood.

In addition to disc height restoration, TDRs are also intended to restore or maintain segmental lordosis. Currently available TDR designs are provided with a variety of footplate lordotic angles intended to approximate a physiological degree of post-implantation lordosis. Under- or over-estimation of the necessary implant lordotic angle may result in an initial bias of the implant, and increase impingement risk. A clinical study documented an increase in lordotic angle at the index level after mono-segmental TDR[10]. A similar clinical study indicated that the increase in the

implanted level lordotic angle resulted in posterior impingement of the device in 9 to 15% of patients[5]. The prior study proposed a theoretical basis for the increased lordosis based on the loss of the anterior longitudinal ligament, increased disc height, and shifting of the center of rotation. Neither study, however, documented the initial lordotic angle of the implants' footplates and whether this played a significant role in impingement likelihood.

Several studies have been performed in order to determine the optimum placement of a TDR within the intervertebral space[12, 19, 20]. Generally, these studies have focused on the effects to spinal parameters, such as kinematics, facet contact forces, and endplate loading rather than device wear performance parameters such as impingement risk. These studies consistently demonstrate that placement of the implant affects both facet contact forces and spinal range of motion, which will in turn affect loading and motions of the TDR itself. These studies generally suggest that posterior placement of the implant is optimal since it allows for close approximation of the intact spine's center of rotation and provides the most physiologic load transfer to the bony endplate and cancellous bone. However, it remains unknown if this position is also optimal for reducing impingement risk.

In addition to TDR placement, appropriate endplate lordosis selection, and disc height distraction, the clinician must also select the optimal patient. TDR in the lumbar spine is currently indicated for patients who report with single level DDD. There are many contraindications for lumbar TDRs, including central or lateral recess stenosis, facet arthrosis, spondylolisthesis or spondylolysis, herniated

nucleus pulposus with neural compression, scoliosis, osteoporosis, and postsurgical psuedoarthrosis or deficiency of posterior elements[21, 22]. Non-pathological patient-specific variations in lumbar spine morphology are generally not included amongst the contra-indications. However, variations in sacral slope[23, 24] will alter the lumbar spine's orientation with respect to the horizon and therefore affect the component of anterior-posterior intervertebral shear from vertical upper body weight[25]. Intervertebral shear forces have been associated with activities of daily living, bending, and lifting[26-29], and have been shown to affect wear patterns in TDR[11]. This suggests that variations in sagittal spinal orientation, specifically the sacral slope, may have an affect on long term TDR wear performance via an increase or decrease in impingement risk. However, there are no current guidelines for clinicians to determine what, if any amount, of sacral slope is appropriate for TDR implantation.

Several studies have evaluated various spinal kinematic and implant performance parameters after TDR implantation[12, 19, 20, 30]. While these studies provide valuable insight into the biomechanics associated with TDR, they do not provide a link to clinical outcomes, and are therefore limited in their ability to provide guidance for clinicians and device designers. Recently, our laboratory has developed a finite element model of the lumbar spine after TDR[19] and validated its outcomes based on clinical retrieval data[31]. The objective of the current study was to determine the sensitivity of TDR impingement to disc height distraction, implant lordotic angle, implant anterior-posterior position, and spinal orientation relative to

the horizon using a finite element model validated based on actual clinical scenarios. We hypothesized that horizontal spinal orientation, underestimation of footplate angle, increased disc height distraction, and implant anterior-posterior position would have an effect on the likelihood of impingement.

Methods

A three-dimensional finite element model (FEM) of a ligamentous L3-S1 lumbar spine was generated from quantitative computed tomography (QCT) data of a cadaveric spine. The data set was taken from the publicly available Visible Human data set (Visible Human Project®, National Library of Medicine, National Institute of Health). The spinal geometry was reviewed and found to be free of any bony or disc deformities, i.e., osteophytes or herniations. Hounsfield units were used as a surrogate for bone mineral density (BMD).

The methodology used to develop and validate the model has been previously described [19, 32], but will be outlined below. A combination of automatic and manual image segmentation techniques (Analyze, AnalyzeDirect, Inc., Overland Park, KS) were used to extract detailed surfaces corresponding to the major bony structures of L3-S1. The software package allowed for automatic segmentation based on thresholding of the QCT grayscale values. These surfaces were imported into the commercial finite element mesh generation program, HyperMesh (Altair Inc., Troy, MI), and were discretized into a combination of tetrahedral elements for the bony structures and hexahedral elements for the intervertebral discs (IVDs). The central portion of the IVDs, approximately 40% of the volume [33], were

designated to be the nucleus pulposus (NP), while the remaining volume was designated as annulus fibrosus. Major spinal ligaments (anterior longitudinal ligament, posterior longitudinal, intraspinatus, supraspinatus, intratransverse, facet capsule, ligamentum flavum) were implemented in the model using tension-only nonlinear springs. Shell elements were used to plate the exterior surface of the vertebral bodies and represented the cortex and bony endplate.

Bone mineral density (BMD)-dependent orthotropic material properties were assigned to the cancellous bone of the vertebral bodies. Custom software was written to apply the Young's modulus to each individual element based on the density of the bone. Similar methodology has been used to create models with heterogeneous bone properties of the tibia and femur [34, 35]. The quantitative relationship between bone mineral density and elastic modulus in cancellous vertebral bone, as reported by Morgan et al. and Ulrich et al., was utilized to define a nonlinear relationship between bone mineral density and orthotropic elastic modulus [36, 37]. Elastic moduli within the vertebral body fell within what has been previously reported in the literature [38-40]. The remaining structures were assigned material properties from the literature and are described in Table 1-1. Frictionless contact was defined between the facets using a penalty-based contact algorithm.

Single level models of L4-L5 and L5-S1 were constructed from the L3-S1 model and subjected to loading consistent with upright standing. The loading paradigm consisted of application of a vertical force simulating upper body weight, which was

offset anteriorly 30 mm to be located at the approximate location of the human upper body center of mass [41]. Additionally, a one dimensional force element was placed between the spinous processes in order to simulate the erector spinae force and restore sagittal balance. Upper body weight for a 50th percentile male was chosen (260 N) (Figure 6-1). This provided the ability to verify that the loading paradigm resulted in disc pressures consistent with those reported in the literature [42]. The erector spinae force was increased from 0 to 300 N for the intact models to determine the point at which the resultant flexion-extension rotation was minimized, i.e., sagittaly balanced in the neutral zone. This resulted in an erector spinae force of 250 N for L4-L5 and 300 N for L5-S1. This loading was then applied to the implanted models.

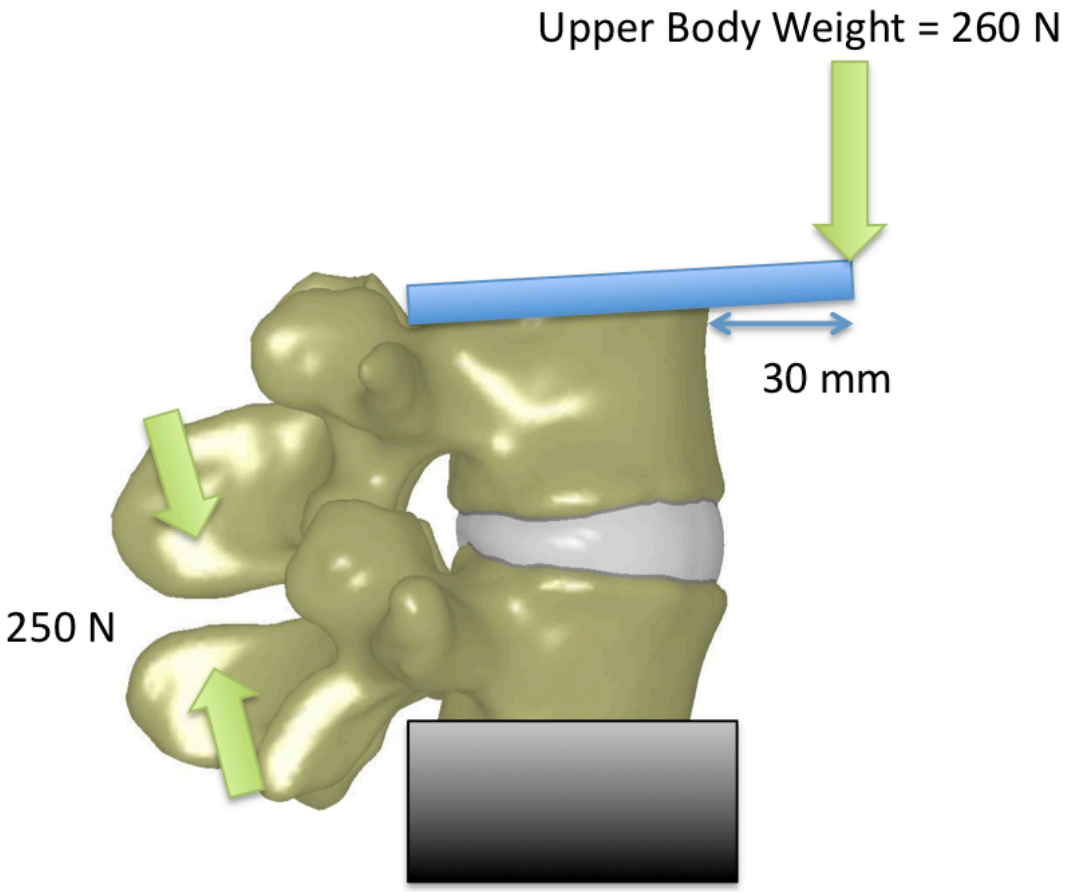

Figure 6-1. Diagram depicting the loading paradigm utilized for the L4-L5 motion segment

Mobile core disc replacements were virtually implanted in each model. Geometric surfaces for the mobile core disc replacements were generated based on CAD drawings of a Charite III implant (Depuy Spine, Raynham, MA). The interface between the implant's metallic footplates and the bony endplates were ideally fixed and rigid. The disc material, anterior longitudinal ligament, and posterior longitudinal ligament were completely removed for all implanted models. Material properties for cobalt chrome alloy (E = 215 GPa, n = 0.3) was assigned to the metallic footplates. A nonlinear material representation for polyethylene (PE) with

an initial Young's modulus of 940 MPa was assigned to the mobile core[43]. Frictionless sliding contact was defined between the metallic footplates and the core.

Ideal implanted models were generated for both the L4-L5 and L5-S1 models (Figure 6-2). These models consisted of no disc height distraction, implant positions slightly posterior of center, a device lordosis equal to the intact lordosis, and no alteration to the spinal orientation. These models were altered in order to perform sensitivity analyses for disc height distraction, device lordosis, implant anterior-posterior position, and spinal orientation (Table 6-1). For disc height distraction sensitivity, only the L4-L5 model was utilized. A total of three models were created, which included 0, 1.5, and 3 mm of distraction from the intact, pre-implanted state. The original intact disc height was 10 mm at the location of the central endplate. A sensitivity analysis for device lordosis was performed using the L5-S1 model. The intact model consisted of a lordotic angle of 14.4°. Therefore, models were created with a total implant lordosis of 14.4°(ideal), 10°, 5°, and 0° where the 0° degree model used two non-angled footplates essentially accounting for none of the natural lumbar lordosis. Sensitivity to anterior-posterior implant position was performed using both the L4-L5 and L5-S1 models. In both models, the implant was positioned such that the posterior edge rested near the posterior cortex. The implant was shifted anteriorly 4 mm and 8 mm for the central and anterior positions, respectively. Finally, the sensitivity to overall spinal orientation in the sagittal plane was evaluated for both L4-L5 and L5-S1. Based on radiographic measurements

taken from retrieved implants[3, 44], the superior endplate angle of L4 relative to the horizon ranged from -10° to 10° (clockwise = positive) and 10° to 30° for L5. Therefore, for the L4-L5 model, L4's superior endplate was oriented -10° (negative values considered counter clockwise relative to the horizon), 0°, and 10° to the horizon while L5's superior endplate, for the L5-S1 model, was oriented 10°, 20°, and 30°.

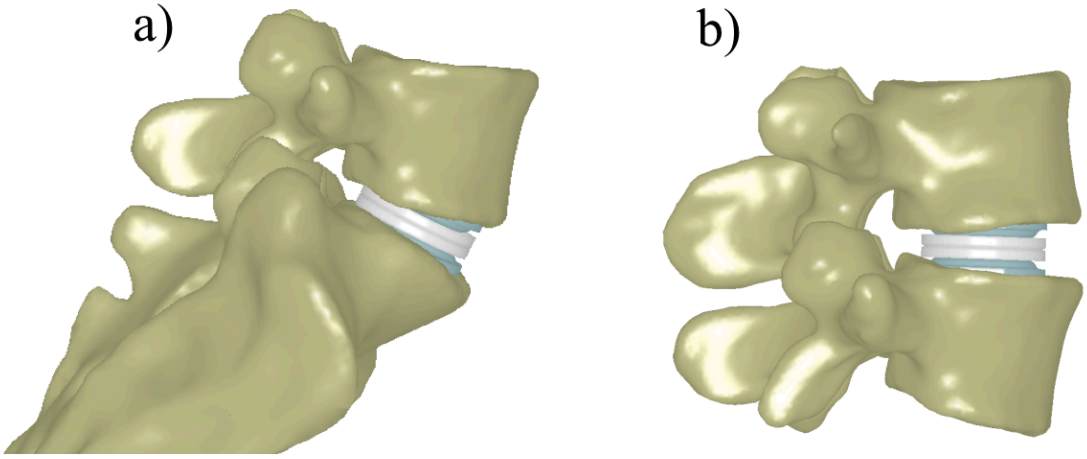

Figure 6-2. Images depicting the implanted L5-S1 (a) and L4-L5 (b) models for an ideally implanted condition (ligaments not pictured)

Table 6-1. Table describing the series of four sensitivity analyses for disc distraction, device lordosis, anterior-posterior positioning, and spinal orientation.

Sensitive Parameter	**Level**				
Disc Distraction	L4-L5	No Distraction	1.5 mm	3 mm	
Device Lordosis	L5-S1	14.4° (ideal)	10°	5°	0°
Anterior-Posterior Position	L4-L5	Posterior	Central	Anterior	
	L5-S1				

Spinal Orientation	L4-L5	-10°	0°	10°	
	L5-S1	10°	20°	30°	

A previous study by this laboratory demonstrated statistically significant correlations between both the peak contact stress on the implant's mobile core and the peak 1st principal strain in the core with rim penetration rate (mm/year) measured from retrieved implants[31]. Therefore, both peak 1st principal strain in the implant's core as well as the peak contact stress on the implant's core were determined. Additionally, the total sagittal rotation generated from application of loading, resultant facet contact force, resultant force on the TDR, as well as the presence of impingement (mobile core rim contact with metallic footplates) was also determined and documented.

Results

The intact models resulted in disc pressures of 0.34 MPa at 250 N of erector spinae force for L4-L5, and 0.52 MPa at 300 N of erector spinae force for L5-S1. The resultant facet contact forces were 7 N and 82.1 N for L4-L5 and L5-S1, respectively. The resultant force for the intervertebral disc was 524.3 N and 568.9 N for L4-L5 and L5-S1, respectively.

Disc Distraction

Generally, implantation of the TDR, with associated disc height distraction, resulted in an increased extension rotation, which corresponded to an increase in the facet

resultant force (Table 6-2). Disc height distractions of 1.5 and 3 mm resulted in contact between the metallic footplate and the polyethylene rim. Specifically, contact occurred between the posterior aspect of the superior footplate and the mobile core's rim (Figure 6-3). The peak 1st principal strain experienced by the core increased by 450% with 1.5 mm of distraction, and by 900% with 3 mm of distraction relative to the pre-implanted disc height (Figure 6-4). The peak contact stress experienced by the core increased from 4.54 MPa to 6.14 MPa and 6.2 MPa after 1.5 and 3 mm of distraction, respectively. The resultant facet contact force for no distraction was 41 N, and increased to 72.3 and 77.5 N for 1.5 and 3 mm of distraction, respectively.

Table 6-2. Results from the disc distraction sensitivity analysis (negative sagittal rotation values indicate extension)

Disc Height Distraction	Peak 1st Principal Strain	Peak Contact Stress (MPa)	Rim Contact	Sagittal Rotation (degs)	Facet Resultant (N)	Disc Resultant (N)
0	0.2%	4.54	No	-2.5	41.0	478.5
1.5	0.9%	6.14	Yes	-5.8	72.3	466.7
3	1.8%	6.2	Yes	-7.5	77.5	456.2

Implant Lordotic Angle

Implants with a lordosis equal to 14.4° (equal to the pre-implantation lordosis) and 10° resulted in no contact between the metallic footplates that mobile core's rim. Implant lordosis angles of 5° and 0° resulted in contact between the posterior rim of the core and the inferior footplate (Figure 6-3). All of the simulated implant lordotic angles resulted in an approximate extension rotation of 2° with the exception of an

implant lordosis of 0°, which resulted in 1.9° of flexion rotation (Table 6-3). The implant with a lordosis of 0° resulted in a peak 1st principal strain of 5.3% (Figure 6-4).

Table 6-3. Results from the implant lordosis sensitivity analysis (negative sagittal rotation values indicate extension)

Implant Lordosis	Peak 1st Principal Strain	Peak Contact Stress (MPa)	Rim Contact	Sagittal Rotation (degs)	Facet Resultant (N)	Disc Resultant (N)
14.4	0.3%	4.84	No	-2.0	107.8	505.0
10	0.4%	6.31	No	-1.9	107.9	504.8
5	1.1%	7.42	Yes	-1.8	95.4	508.1
0	5.3%	8.67	Yes	1.9	50.7	533.5

Implant Anterior-Posterior Position

At the L4-L5 level, anterior placement of the device resulted in contact between the posterior aspect of the core's rim and the superior footplate (Figure 6-3). Posterior placement of the device resulted in flexion while both the central and anterior positions resulted in extension for both the L4-L5 and L5-S1 levels (**Error! Reference source not found.**). Posterior placement of the device at the L4-L5 level resulted in no facet contact force while central and anterior placement resulted in a facet contact force of 64 N and 123.5N, respectively. Peak contact stress was greatest when the implant was placed posteriorly irrespective of level (Figure 6-3).

Table 6-4. Results from the implant positioning analysis (negative sagittal rotation values indicate extension)

	Implant Position	Peak 1st Princ Strain	Peak Contact Stress (Mpa)	Rim Contact	Sagittal Rotation (degs)	Facet Resultant (N)	Disc Resultant (N)
L4/5	**Posterior**	0.4%	7.96	No	5.7	0.0	576.7

	Central	0.3%	5.47	No	-3.5	64.0	461.1
	Anterior	1.5%	6.30	Yes	-4.2	123.5	420.6
	Posterior	0.7%	7.35	Yes	5.1	105.8	557.7
L5/S1	**Central**	0.4%	4.35	No	-2.0	107.8	505.0
	Anterior	0.3%	4.96	No	-4.3	134.5	463.8

Spinal Orientation

At the L4-L5 level, the only spinal orientation that didn't result in the rim contacting the metal footplate was 0°. Spinal orientation of the spine such that the superior endplate was rotated counter-clockwise relative to the horizon or maintained horizontal resulted in extension rotation (Table 6-5). Increased clockwise rotation of the spine relative to horizontal resulted in rim contact of the anterior portion of the rim with the superior footplate (Figure 6-3). Increased clockwise rotation also resulted in progressive increases in facet contact force and peak contact stress experienced by the core.

Table 6-5. Results from the spinal sagittal orientation analysis (negative sagittal rotation values indicate extension)

	Orientation Angle	Peak 1st Princ Strain	Peak Contact Stress (MPa)	Rim Contact	Sagittal Rotation (degs)	Facet Resultant (N)	Disc Resultant (N)
	-15	1.3%	6.15	Yes	-4.5	48.0	466.2
L4/5	**0**	0.2%	4.13	No	-1.1	33.0	488.7
	15	0.9%	7.03	Yes	3.4	44.6	495.4
	10	0.4%	6.41	No	2.9	124.0	520.0
L5/S1	**20**	1.0%	6.62	Yes	4.7	152.1	509.4
	30	1.2%	6.82	Yes	5.0	180.6	489.7

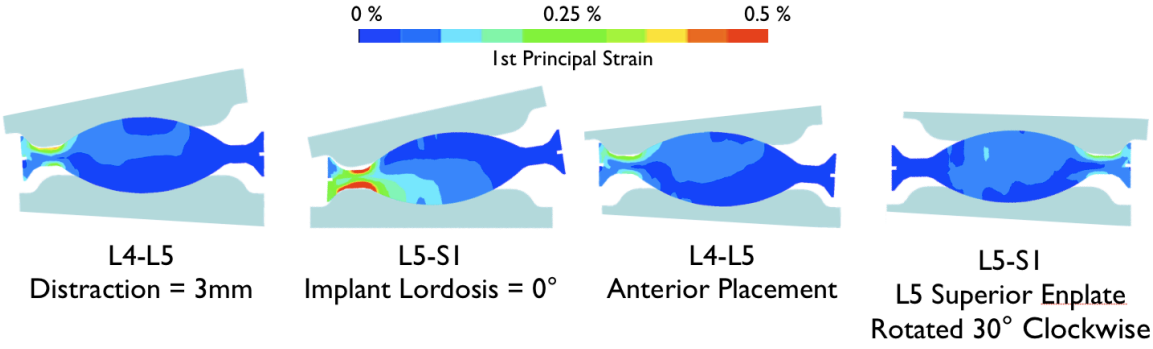

Figure 6-3. Contour plots of 1st principal strain for cross-sections of the polyethylene cores at the sagittal midline for the scenarios that resulted in the greatest peak 1st principal strain.

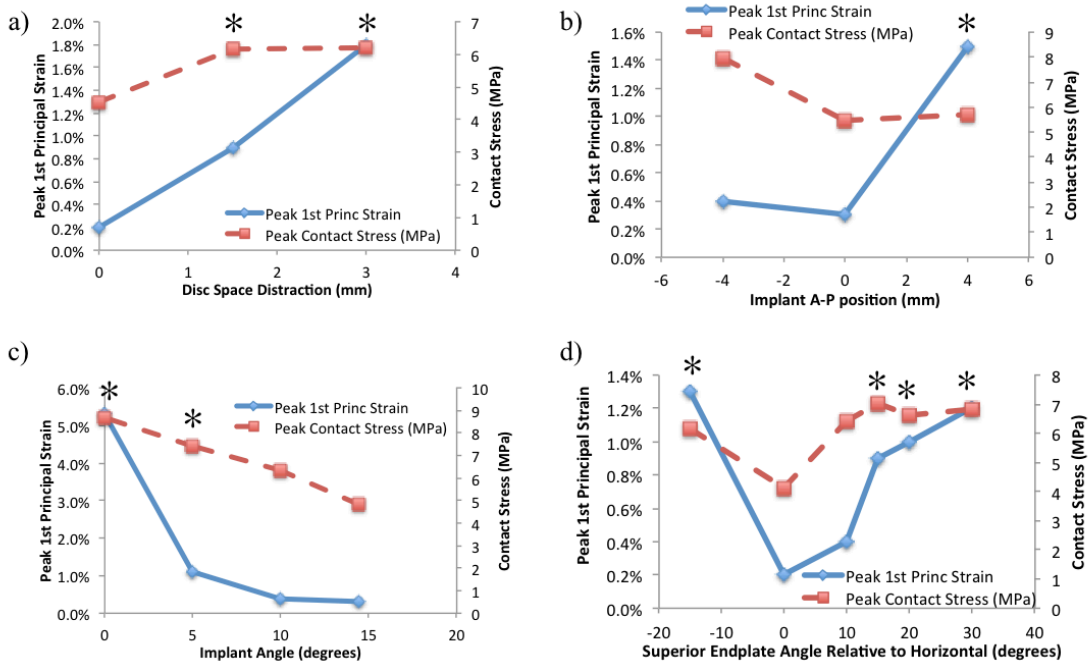

Figure 6-4. Scatter plots depicting the polyethylene peak 1st principal strain and peak contact pressure for the four sensitivity analyses. Implant position data is for L4-L5 only. Asterisks indicate data points that resulted in contact between the metallic footplate and the mobile core's rim.

Discussion

In the current study, we used a nonlinear 3-D finite element model of the lumbar spine to determine a mobile bearing TDR's impingement sensitivity to disc height distraction, implant lordosis, implant anterior-posterior placement, and spinal

orientation. The results indicate that all of these parameters contribute to impingement risk to varying degrees. Additionally, the data generated in the current study provides guidance for clinicians considering implantation of a mobile bearing TDR. Specifically, careful consideration should be given to the selection of the implant's lordotic angle as to fully account for a reasonable approximation of the pre-implantation lordosis. Additionally, increased disc height distraction, placement of the device either too far anterior or posterior, and a large amount of sacral slope can contribute to impingement risk and associated increased polyethylene wear.

Data from the current study indicated that increases in disc height distraction increased the risk for implant impingement. Specifically, increased disc height resulted in increased sagittal plane extension rotation and contact between the posterior metallic footplate and the mobile core's rim. Disc height distraction during TDR implantation is essential for the relief of compressed nerve roots. The current study utilized a model with a pre-implantation disc height of approximately 10 mm at the central endplate, which is not necessarily indicative of degenerative disc disease. Previous research has indicated that severe degenerative disc disease can result in a reduction in the disc space of approximately 3 mm at L5-S1[45]. Therefore, what the current study considered to be a disc height distraction of 0 mm was essentially an ideal restoration of the healthy disc height. Determining the amount of disc height distraction that sufficiently decompresses nerve roots without over-distracting and causing increased risk of posterior impingement of the implant remains a difficult challenge for the clinician. Adjacent level disc heights can be used

as a reference point to guide surgeons, and prevent over distraction of the disc space. Future clinical studies should record disc height distraction and its relationship to both patient and device outcomes.

Results from the current study indicated that an increased disc height resulted in greater extension rotation after application of standing loads. This does not necessarily indicate that an over-distracted segment would tend to be hyper-mobile. Decreased post-operative ranges of motion have been documented clinically, and attributed to overstuffing of the disc space, which can overstretch the surrounding ligaments and muscles[46, 47]. While the current study documented an increase in extension rotation, it did not evaluate overall range of motion nor did it consider the effect of tension developed in the surrounding tissues during distraction. However, the increased extension, which resulted in an increased lordotic angle at the index level, is consistent with a clinical study, which documented an acute increase in index level lordosis after TDR[10]. Future studies should consider the effects of tension developed in the surrounding tissues as well as evaluate overall range of motion as a function of disc height distraction.

The greatest magnitude of 1st principal strain (measure of tensile deformation) and contact stress for the polyethylene core occurred when the implant lordosis was set to 0°, which essentially accounted for none of the pre-implantation lumbar lordosis. A recent study indicated lordotic angles for the intact spine ranging from 14.3° to 20.1° at L4-L5 and from 20.6° to 51° at L5-S1 depending on measurement technique[48]. While these data suggest the presence of a substantial lordotic angle

at these levels of the lumbar spine, they also demonstrate the difficulty of accurately determining this angle from plain radiographs. Review of clinical scenarios from our laboratories' total disc replacement retrieval collection[3, 6, 44] revealed that several implantations involved implants that utilized flat footplates, i.e., no lordotic angle. Currently, there are few tools available for surgeons when determining the appropriate footplate selection as to best approximate the patient's lordosis. As demonstrated by the previously mentioned study[48], methods of determining this angle from plain x-rays are inconsistent, and tools or templates used during surgery will not take into consideration what may happen to the lumbar lordosis when the patient stands. Data from the current study suggests that clinicians should utilize some level of implant lordosis, and that even a close approximation results in a non-impingement scenario. On the contrary, use of non-angled footplates, which account for none of the pre-implantation lordosis, will leave the device at greatest risk for impingement and increased contact stress.

Data from the current study indicated that anterior placement of the device at L4-L5 and posterior placement of the device at L5-S1 resulted in the greatest increase of impingement risk. Results indicated that both the direction and magnitude of the sagittal rotation experienced during standing were sensitive to device placement. Specifically, posterior placement tended to result in flexion rotation while central and anterior placement resulted in extension. A previous finite element study evaluated the effect of anterior-posterior position for a fixed bearing TDR on intersegmental rotation and found that, during standing, the more anterior the

placement of the device, the more extension rotation that level experienced[20]. The loading paradigm utilized in the current study involved an anterior offset vertical force consistent with upper body weight. Posterior placement of the device essentially increased the moment arm for this force and resulted in a greater flexion moment. Conversely, anterior placement of the device effectively reduced the applied flexion moment and increased the effective extension moment from the erector spinae force. As a result, anterior placement tended to result in an increase in facet contact force from the increased extension. This finding is consistent with a previous finite element study of a mobile core TDR, which documented increased facet contact forces with anterior placement of the device[12].

Interestingly, anterior placement of the device at L5-S1 did not result in the same impingement likelihood as that of L4-L5. Closer examination of the L4-L5 model indicated that, during anterior placement of the device, increased extension rotation coupled with facet contact forces resulted in posterior translation of L4. This posterior translation resulted in locking of the mobile core and subsequent one-sided contact with the core's rim. Similar preferential superior articulation and locking of the core from shear loading has been documented *in vitro*[49]. A similar phenomenon was not observed at the L5-S1 level due to the increased sacral slope, which results in a greater component of anterior shear from vertical upper body weight. Essentially, the posterior translation imparted by the facets was offset by the anterior shear force from upper body weight at L5-S1.

The current study documented large variations in facet contact forces as a function of the parameters evaluated. Generally, facet contact forces increased as a result of implantation of a TDR, which typically corresponded to increased extension rotation. However, there were scenarios that yielded a reduction in facet contact forces when compared to the intact, pre-implanted condition. Specifically, the use of two non-angled footplates reduced the facet contact force. However, this scenario also resulted in the largest amount of strain and contact stress experienced by the device, suggesting that the off loading of the facets occurred at the expense of the device. Additionally, posterior placement of the device prevented facet contact force by offsetting the overall force balance towards a flexion moment. Results from a recent clinical study indicated a reduction in facet sub-chondral bone mineral density 6-months post lumbar mobile-bearing TDR implantation suggesting that TDR is responsible for unloading the facet joints[15]. On the contrary, longer-term clinical results have documented facet arthrosis at the implanted level in approximately a third of patients for both a mobile and fixed bearing TDR[18]. Results from the current study suggest the TDR implantation does not necessarily result in the maintenance of sagittal balance, and therefore alters facet loading. However, a key assumption made in the current study was that applied loading remains constant between pre and post TDR implantation. It is possible that proprioception results in altered muscle loading in order to help maintain sagittal balance after TDR implantation, and therefore maintains or reduces facet contact force. Unfortunately, direct measurement of facet contact forces *in vivo* after TDR is

not possible. Despite this, results from the current study, as well as clinical results, suggest that TDR affects facet contact and *vice versa*.

Very few studies have evaluated the effect of intervertebral shearing forces on total disc replacements. The majority of studies have applied pure rotational moments or displacements[1, 12, 19, 49]. The component of intervertebral shear generated from vertical upper body weight is a function of the spinal segment's orientation with respect to the horizon. Data from the current study suggested that rotating the spinal segment with respect to the horizon, and thereby increasing the shear component from vertical upper body weight, resulted in increased impingement likelihood. Specifically, clockwise sagittal (anterior = right) rotation of the entire segment resulted in increased flexion rotation, and consequent contact between the anterior metallic footplate and core (Figure 6-3). Shear loading resulted in locking of the mobile core thereby preventing its ability to articulate with the footplates. Locking of the core due to intervertebral shear occurred during all of the sensitivity analyses. As a result, contact between the metallic footplate and the polyethylene core resulted in bending of the rim, as characterized by an asymmetric distribution of tensile strain throughout the rim (Figure 6-3). Bending of the rim has also been observed in retrieved implants (Table 6-5). It is unclear if this phenomenon has a negative effect on patient outcomes. However, a recent study by our lab has indicated a significant correlation between peak 1st principal strain in the core and rim penetration rate (mm/year) measured from retrieved implants [31]. These data suggest a need to include intervertebral shear during bench-top implant testing.

Additionally, surgeons may wish to consider a patient's sacral slope when deciding if they are a candidate for TDR.

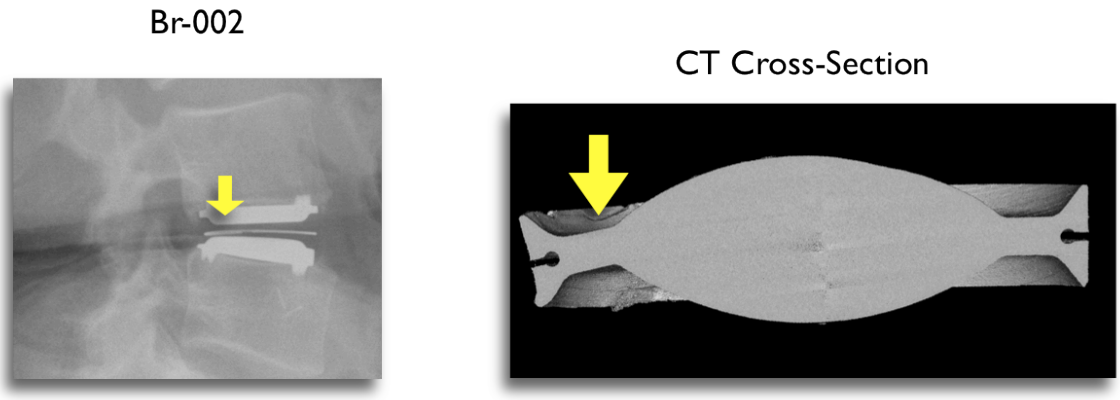

Figure 6-5. Pre-revision sagittal radiograph (left) and micro CT cross-section (right) from a retrieved implant displaying downward bending of the posterior rim.

In conclusion, the data from the current study indicates that lumbar mobile-bearing TDR impingement is sensitive to disc height distraction, anterior-posterior position, implant lordosis, and spinal sagittal orientation. While these parameters had varying effects on implant impingemen, but maintained certain consistencies of the biomechanical environemnt. Specifically, intervertebral shear contributed to locking of the mobile core. This shear occurred as a result of either vertical upper body loading or facet engagement due to an increased lordotic angle. Once locked, rotation of the superior vertebrae resulted in contact between the metallic footplate and the rim. Importantly, the data also indicates that when a device is ideally implanted in a patient with a modest sacral slope, it does not impinge. The results from the current study indicate that TDR impingement risk can be minimized by

choosing an implant with an appropriate amount of lordosis, not over distracting the disc space, and taking care to not place the implant too far anterior or posterior.

References

1. Panjabi, M., et al., *Multidirectional testing of one- and two-level ProDisc-L versus simulated fusions.* Spine, 2007. **32**(12): p. 1311-9.
2. Auerbach, J.D., et al., *Evaluation of spinal kinematics following lumbar total disc replacement and circumferential fusion using in vivo fluoroscopy.* Spine, 2007. **32**(5): p. 527-36.
3. Kurtz, S.M., et al., *Polyethylene wear and rim fracture in total disc arthroplasty.* Spine J, 2007. **7**(1): p. 12-21.
4. Choma, T.J., et al., *Retrieval analysis of a ProDisc-L total disc replacement.* J Spinal Disord Tech, 2009. **22**(4): p. 290-6.
5. Kafer, W., et al., *Posterior component impingement after lumbar total disc replacement: a radiographic analysis of 66 ProDisc-L prostheses in 56 patients.* Spine, 2008. **33**(22): p. 2444-9.
6. Kurtz, S.M., et al., *Analysis of a retrieved polyethylene total disc replacement component.* Spine J, 2005. **5**(3): p. 344-50.
7. Punt, I.M., et al., *Complications and reoperations of the SB Charite lumbar disc prosthesis: experience in 75 patients.* Eur Spine J, 2008. **17**(1): p. 36-43.
8. van Ooij, A., et al., *Polyethylene wear debris and long-term clinical failure of the Charite disc prosthesis: a study of 4 patients.* Spine, 2007. **32**(2): p. 223-9.
9. van Ooij, A., F.C. Oner, and A.J. Verbout, *Complications of artificial disc replacement: a report of 27 patients with the SB Charite disc.* J Spinal Disord Tech, 2003. **16**(4): p. 369-83.
10. Cakir, B., et al., *The impact of total lumbar disc replacement on segmental and total lumbar lordosis.* Clin Biomech (Bristol, Avon), 2005. **20**(4): p. 357-64.
11. Vicars, R., et al., *The effect of anterior-posterior shear load on the wear of ProDisc-L TDR.* Eur Spine J, 2010.
12. Moumene, M. and F.H. Geisler, *Comparison of biomechanical function at ideal and varied surgical placement for two lumbar artificial disc implant designs: mobile-core versus fixed-core.* Spine, 2007. **32**(17): p. 1840-51.
13. Delamarter, R.B., et al., *ProDisc artificial total lumbar disc replacement: introduction and early results from the United States clinical trial.* Spine (Phila Pa 1976), 2003. **28**(20): p. S167-75.
14. David, T., *Lumbar disc prosthesis. Surgical technique, indications and clinical results in 22 patients with a minimum of 12 months follow-up.* Eur Spine J, 1993. **1**(4): p. 254-9.
15. Trouillier, H., et al., *A prospective morphological study of facet joint integrity following intervertebral disc replacement with the CHARITE Artificial Disc.* Eur Spine J, 2006. **15**(2): p. 174-82.

16. Liu, J., et al., *How the increase of the cervical disc space height affects the facet joint: an anatomy study.* Spine (Phila Pa 1976), 2006. **31**(12): p. E350-4.
17. Liu, J., et al., *Effect of the increase in the height of lumbar disc space on facet joint articulation area in sagittal plane.* Spine (Phila Pa 1976), 2006. **31**(7): p. E198-202.
18. Shim, C.S., et al., *CHARITE versus ProDisc: a comparative study of a minimum 3-year follow-up.* Spine, 2007. **32**(9): p. 1012-8.
19. Rundell, S.A., et al., *Total disc replacement positioning affects facet contact forces and vertebral body strains.* Spine, 2008. **33**(23): p. 2510-7.
20. Rohlmann, A., T. Zander, and G. Bergmann, *Effect of total disc replacement with ProDisc on intersegmental rotation of the lumbar spine.* Spine (Phila Pa 1976), 2005. **30**(7): p. 738-43.
21. Bertagnoli, R. and S. Kumar, *Indications for full prosthetic disc arthroplasty: a correlation of clinical outcome against a variety of indications.* Eur Spine J, 2002. **11 Suppl 2**: p. S131-6.
22. Huang, R.C., et al., *The prevalence of contraindications to total disc replacement in a cohort of lumbar surgical patients.* Spine (Phila Pa 1976), 2004. **29**(22): p. 2538-41.
23. Roussouly, P., et al., *Classification of the normal variation in the sagittal alignment of the human lumbar spine and pelvis in the standing position.* Spine (Phila Pa 1976), 2005. **30**(3): p. 346-53.
24. Chanplakorn, P., et al., *Lumbopelvic alignment on standing lateral radiograph of adult volunteers and the classification in the sagittal alignment of lumbar spine.* Eur Spine J, 2010.
25. Farfan, H.F., V. Osteria, and C. Lamy, *The mechanical etiology of spondylolysis and spondylolisthesis.* Clin Orthop Relat Res, 1976(117): p. 40-55.
26. Schultz, A.B., et al., *Analysis and measurement of lumbar trunk loads in tasks involving bends and twists.* J Biomech, 1982. **15**(9): p. 669-75.
27. Potvin, J.R., R.W. Norman, and S.M. Mcgill, *Reduction in Anterior Shear Forces on the L4/L5 Disk by the Lumbar Musculature.* Clinical Biomechanics, 1991. **6**(2): p. 88-96.
28. Callaghan, J.P., A.E. Patla, and S.M. McGill, *Low back three-dimensional joint forces, kinematics, and kinetics during walking.* Clin Biomech (Bristol, Avon), 1999. **14**(3): p. 203-16.
29. Kingma, I., D. Staudenmann, and J.H. van Dieen, *Trunk muscle activation and associated lumbar spine joint shear forces under different levels of external forward force applied to the trunk.* J Electromyogr Kinesiol, 2007. **17**(1): p. 14-24.
30. Rousseau, M.A., et al., *Disc arthroplasty design influences intervertebral kinematics and facet forces.* Spine J, 2006. **6**(3): p. 258-66.
31. Rundell, S.A., Day, J.S., Isaza, J., Siskey, R., MacDonald, D., Kurtz, S.M., *Derivation of clinically relevant boundary conditions suitable for evaluation of chronic impingement of lumbar total disc replacement: Application to standard development.* Journal of ASTM International, 2010. **In Review**.

32. Rundell, S.A., et al., *Effect of nucleus replacement device properties on lumbar spine mechanics.* Spine (Phila Pa 1976), 2009. **34**(19): p. 2022-32.
33. White, A.A., Panjabi, M.M.,, *Clinical Biomechanics of the Spine, 2nd ed.*1990, Philadelphia-Toronto: J.B. Lippincott Company.
34. Yosibash, Z., et al., *A CT-based high-order finite element analysis of the human proximal femur compared to in-vitro experiments.* J Biomech Eng, 2007. **129**(3): p. 297-309.
35. Sawatari, T., et al., *Three-dimensional finite element analysis of unicompartmental knee arthroplasty--the influence of tibial component inclination.* J Orthop Res, 2005. **23**(3): p. 549-54.
36. Ulrich, D., et al., *The ability of three-dimensional structural indices to reflect mechanical aspects of trabecular bone.* Bone, 1999. **25**(1): p. 55-60.
37. Morgan, E.F., H.H. Bayraktar, and T.M. Keaveny, *Trabecular bone modulus-density relationships depend on anatomic site.* J Biomech, 2003. **36**(7): p. 897-904.
38. Kopperdahl, D.L. and T.M. Keaveny, *Yield strain behavior of trabecular bone.* J Biomech, 1998. **31**(7): p. 601-8.
39. Mosekilde, L. and C.C. Danielsen, *Biomechanical competence of vertebral trabecular bone in relation to ash density and age in normal individuals.* Bone, 1987. **8**(2): p. 79-85.
40. Hansson, T.H., T.S. Keller, and M.M. Panjabi, *A study of the compressive properties of lumbar vertebral trabeculae: effects of tissue characteristics.* Spine, 1987. **12**(1): p. 56-62.
41. Rohlmann, A., et al., *Applying a follower load delivers realistic results for simulating standing.* J Biomech, 2009. **42**(10): p. 1520-6.
42. Wilke, H.J., et al., *New in vivo measurements of pressures in the intervertebral disc in daily life.* Spine (Phila Pa 1976), 1999. **24**(8): p. 755-62.
43. Bergstrom, J.S., C.M. Rimnac, and S.M. Kurtz, *Prediction of multiaxial mechanical behavior for conventional and highly crosslinked UHMWPE using a hybrid constitutive model.* Biomaterials, 2003. **24**(8): p. 1365-80.
44. Kurtz, S.M., et al., *What is the correlation of in vivo wear and damage patterns with in vitro TDR motion response?* Spine (Phila Pa 1976), 2008. **33**(5): p. 481-9.
45. Cohn, E.L., et al., *Plain film evaluation of degenerative disk disease at the lumbosacral junction.* Skeletal Radiol, 1997. **26**(3): p. 161-6.
46. Park, J.J., et al., *Analysis of segmental cervical spine vertebral motion after prodisc-C cervical disc replacement.* Spine (Phila Pa 1976), 2010. **35**(8): p. E285-9.
47. Siepe, C.J., et al., *Interdependence between disc space height, range of motion and clinical outcome in total lumbar disc replacement.* Spine (Phila Pa 1976), 2009. **34**(9): p. 904-16.
48. Schuler, T.C., et al., *Segmental lumbar lordosis: manual versus computer-assisted measurement using seven different techniques.* J Spinal Disord Tech, 2004. **17**(5): p. 372-9.

49. O'Leary, P., et al., *Response of Charite total disc replacement under physiologic loads: prosthesis component motion patterns.* Spine J, 2005. **5**(6): p. 590-9.

Conclusion

The previous chapters describe the development of a lumbar spine finite element model and its use in several *in situ* biomechanical investigations of lumbar total disc replacement. Specifically, the outcomes from the model were significantly correlated with measurements taken directly from retrieved implants. The sensitivity of various parameters to device impingement was determined.

In chapter 1, the development of a finite element model of a single lumbar motion segment was described. The sensitivity of the model to variations of nucleus material properties based on nucleus replacement technologies was evaluated. Results from this chapter indicate an optimal modulus between 1 and 4 MPa for a nearly incompressible material for use in a conforming and displacement compatible nucleus replacement (i.e. no gaps between the nucleus and annulus, with the boundary of the two regions tied together). Moduli in this range resulted in physiologic loading in both the annulus and vertebral bodies. A modulus of 0.1 MPa indicated the risk for bony resorption in the adjacent bone and increased strains in the annulus, which could result in implant subsidence or extrusion, respectively. An implant with a modulus of 100 MPa resulted in high strain fields in the adjacent bone indicating an increased risk of subsidence similar to what is experienced clinically by interbody cages. The current study evaluated a variety of nucleus replacement moduli without adjusting the implant geometry, which varies substantially for the current designs. Future studies should evaluate the effects of a

variety of implant geometries in order to determine an ideal size and shape for a nucleus replacement.

In chapter 2, the finite element model was used to evaluate the very first disc replacement technology, the Fernstrom sphere, at varying levels of implant subsidence. Both PEEK and cobalt chrome spheres were evaluated. The results suggested that this simple implant design is able to maintain segmental range of motion and provide minimal differences in facet contact forces. Large areas of von Mises strain were generated in the bone adjacent to the implant regardless of whether the implant was PEEK or CoCr. Despite the large areas of strain documented in the current study, clinical results suggest that severe subsidence is not a common complication, and initial subsidence of the device helps secure the device and prevent intervertebral shear translations. However, the disc height loss associated with subsidence may preclude the efficacy of such a device.

In chapter 3, a modern total disc replacement fixed bearing technology was evaluated with specific attention to loading of the bony endplates and facet contact forces. The results from this chapter predicted a decrease in segmental stiffness resulting from total disc replacement. This reduction in stiffness was evidenced by a general increase in the overall range of motion about the three anatomical axes. The decreased stiffness resulted in a dependence on the facets to limit range of motion after total disc replacement for the majority of the tested scenarios, which may in part be responsible for the subsequent development of degenerative changes, which have been reported clinically. Additionally, vertebral body strains were generally

higher after total disc replacement and tended to increase with decreasing segmental stiffness. The results from initial bone remodeling stimulus suggested that posterior placement of the implant resulted in a more physiologic load transfer to the vertebral body.

In chapter 4, a simple sagittal balance loading paradigm and evaluates the impingement risk associated with disc height distraction for both a mobile and fixed bearing total disc replacement was described. Results demonstrated that a series of sagittaly balanced postures for an intact L4-L5 segment resulted in a qualitative reduction in distortional stress maxima in the annulus during a combination of erector spinae muscle tension and facet contact. Evaluation of the same sagittaly balanced posutures after implantation of both a mobile and fixed core total disc replacement with no disc distraction resulted in a reasonable agreement with the intact model. Distraction of the disc space prevented sagittal balance at the tested load levels and resulted in device impingement for the mobile bearing total disc replacement and non-conformance of the articulating surfaces for the fixed bearing TDR.

Chapter 5 detailed the development of case-specific models based on the clinical scenarios from retrieved implants. Outputs from these analyses were compared with the retrieved implants. Significant correlations were found between the retrieved implant's rim penetration rate and peak contact stress from the finite element model. This was the first study to validate a methodology for evaluating total disc replacement using a finite element model with inputs derived from clinical

retrieval data. The significant correlations determined in this chapter provide the ability to perform future studies that target specific parameters that may influence device wear and impingement. Moreover, the data from the current chapter provides valuable insight into the biomechanical environment associated with device impingement such that it can be employed in wear simulation. Currently, a work item (WK25942) is focused on taking the results of these analyses and creating a testing guide to simulate impingement in lumbar total disc replacements. This new standard will incorporate the effects of anterior shear from upper body weight and translational motions imposed by the geometrical constraint of the facets. The guidelines provided in this new standard will describe an approach for evaluating new designs and design changes to help manufacturers and regulatory agencies make more informed decisions on design choices.

In chapter 6, the validated model generated in chapter 5 was used to determine the impingement risk associated with several parameters. The data from this chapter indicates that lumbar mobile-bearing TDR impingement is sensitive to disc height distraction, anterior-posterior position, implant lordosis, and spinal sagittal orientation. While these parameters had varying effects on implant impingement, certain consistencies of the biomechanical environment were maintained. Specifically, intervertebral shear contributed to locking of the mobile core. This shear occurred as a result of either vertical upper body loading or facet engagement due to an increased lordotic angle. Once locked, rotation of the superior vertebrae resulted in contact between the metallic footplate and the rim. Importantly, the data

also indicates that when a device is ideally implanted in a patient with a modest sacral slope, it does not impinge. The results from the current study indicate that TDR impingement risk can be minimized by choosing an implant with an appropriate amount of lordosis, not over distracting the disc space, and taking care to not place the implant too far anterior or posterior.

The current dissertation focused primarily on lumbar total disc replacements at a single level. Several cervical spine disc replacements currently have FDA approval. These devices also consist of bearing surfaces and the potential for impingement. Therefore, future studies should focus on the development of a validated model of the cervical spine that will be appropriate for evaluation of these devices. Additionally, although considered off-label use, these devices are often implanted at several levels in both the cervical and lumbar spines. The biomechanical environment for multiple level total disc replacement is not fully understood. Future studies should consider the impingement risk associated with multiple level disc replacement

Vita

Steven Anthony Rundell, M.S., P.E.

Ph.D (in process)., Biomedical Engineering, Drexel University, 2011
M.S., Engineering Mechanics, Michigan State University, 2005
B.S., Mechanical Engineering, Michigan State University, 2003

Michigan State University Companion Animal Fund Grant, 2004; TRW Foundation Grant Recipient, 2003; Design News Magazine Award Recipient, 2003; Graduate Fellowship, 2003

Registered Professional Engineer, Michigan, PE# 6201057108

Publications

Rundell, SA, Isaza, J.E., Kurtz, S.M. Biomechanical evaluation of a spherical lumbar interbody device at varying levels of subsidence. SAS Journal, 2010 *in press*

Rundell, SA, Day, JS, Isaza, JE, Siskey, R, Macdonald, D, Kurtz, SM. Derivation of clinically relevant boundary conditions suitable for evaluation of chronic impingement of lumbar total disc replacement: Application to standard development. J of ASTM Int, 2010 *in review*

Rundell, SA, Day, JS, Isaza, JE, Guillory, S, Kurtz, SM. Lumbar total disc replacement impingement sensitivity to disc height distraction, spinal sagittal orientation, implant position, and implant lordosis. Spine, 2010 *in review*

Ong KL, Rundell S, Liepins I, Laurent R, Markel D, Kurtz S. Biomechanical modeling of acetabular component polyethylene stresses, fracture risk, and wear rate during press-fit implantation. J Orthop Res 2009; 27(11):1467–1472.

Rundell SA, Guerin HL, Auerbach JD, Kurtz SM. Effect of nucleus replacement device properties on lumbar spine mechanics. Spine 2009; 34(19):2022–2032.

Rundell SA, Auerbach JD, Balderston RA, Kurtz SM. Total disc replacement positioning affects facet contact forces and vertebral body strains. Spine 2008; 33(23):2510–2517.

Baars DC, Rundell SA, Haut RC. Treatment with non-ionic surfactant poloxamer P188 reduces tunnel positive cells in bovine chondral explants exposed to injurious unconfined compression. Biomech Model Mechanobiol 2006; 5(2–3):133–139.

Jex CT, Wan CJ, Rundell S, Haut RC, MacDonald B, Wertheimer SJ. Analysis of three types of fixation of the Weil osteotomy. Foot Ankle Surgery 2006; 45(1):13–19, 2006.

Rundell SA, Haut RC. Exposure to a standard culture medium alters the response of cartilage explants to injurious unconfined compression. J Biomech 2005; 26, July.

Rundell SA, Baars DC, Phillips DM, Haut RC. The limitation of acute necrosis in retro-patellar cartilage after a severe blunt impact to the in vivo rabbit patello-femoral joint. J Orthopaedic Res 2005; 23(6):1363–1369.

Rundell SA. Investigation of the acute injury response of articular cartilage *in vitro* and *in vivo*: Analysis of various therapeutic treatments. M.S. Thesis, Michigan State University, 2005.

I. Appendix A

The development, verification, and validation of a finite element model of the lumbar spine

Steve Rundell

BME 999 Ph.D. Dissertation Research
Advisor: Steve Kurtz, Ph.D.

Intact Model Creation

The current model of the lumbar spine was created from a quantitative computed tomography (QCT) scan of a cadaveric specimen. Semi-automatic image segmentation techniques (Analyze, AnalyzeDirect, Inc., Lenexa, KS) were used to extract detailed, specimen specific surfaces corresponding to the major vertebral body structures from the QCT data. These surfaces were then imported into the commercial finite element mesh generation program, HyperMesh (Altair Inc., Troy, MI). The vertebral bodies were meshed with quadratic tetrahedron elements (Figure I-1) (Figure I-2).

Bony Structures

The 3D CAD surfaces generated by Analyze were exported in STL file format. This is essentially a shell finite element mesh. However, there are usually many problems with the surfaces and they need to be cleaned up. Primarily, the surfaces will have small "holes", i.e., the surfaces don't create an enclosed volume. Hypermesh has many tools for cleaning up the mesh. Typically, this process involves a combination of deleting the elements in bad areas, and recreating new elements to fill the holes.

After the surfaces have been cleaned up it is time to remesh the entire surface. The 2-D tab in Hypermesh has an automesh feature that will create a mesh from an existing finite element mesh. If the entire vertebral body is selected to remesh at once it will not work. Small sections of the vertebral body need to be done one at a

time. Then, once you have a good shell mesh of the surface in all triangular elements, Hypermesh can create a 3D tetrahedron mesh.

Discs

The geometry for the discs cannot be obtained from the QCT image data. Surfaces were generated in between the vertebral body surfaces to represent the discs. Bony landmarks were used to approximate the appropriate location of the annulus and nucleus. Surfaces for the outer annulus and outer nucleus were created. These were then imported into TrueGrid (XYZ Scientific, Livermore, CA). The discs were meshed with brick (hexahedron) elements. Theses meshes were then imported into hypermesh. A mesh of approximately 90 degree triangles was created on the face of the discs maintaining the nodal locations. These elements were then tied into the vertebral bodies and used to create the elements of the vertebral bodies. This insured node compatibility between the tetrahedron vertebrae and the hexahedron discs.

Ligaments

Ligaments were created using spring elements. This was done very simply in Hypermesh by choosing the two nodes that represent the ends.

Contact

A frictionless sliding contact was defined at the facet joints. Segment sets were defined on the external faces of the elements for all of the facet surfaces. A standard penalty based contact algorithm was used to define the contact of these surfaces.

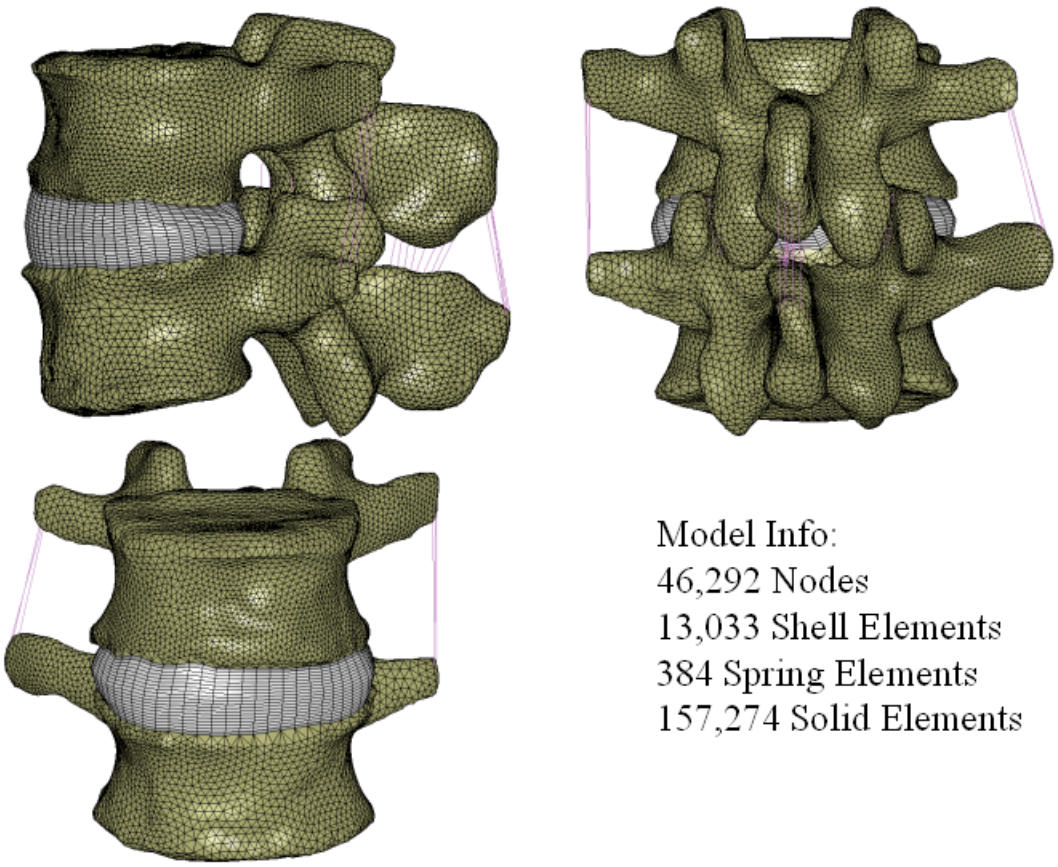

Figure I-1. Graphic depicting the completed finite element model of an L3-L4 motion segment

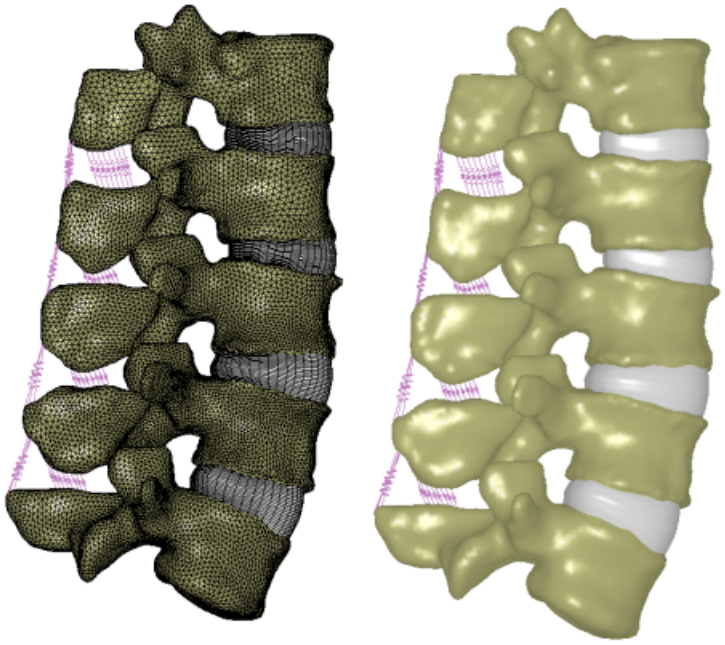

Figure I-2. Graphic depicting a finite element mesh of the lumbar spine L1 to L5

MATERIAL PROPERTIES

Cancellous Bone

Material models for the cancellous bone in the vertebral body are commonly modeled as transversely isotropic [1, 2], but many models have used a linear elastic relationship [3, 4]. Finite element models of the isolated vertebral body use a bone mineral density (BMD) to elastic modulus relationship derived from quantitative computed tomography (QCT) [5, 6]. However, to the knowledge of the author, there are no models of lumbar motion segments that apply material properties to the cancellous bone based on QCT data.

The current model uses a BMD-modulus relationship reported by Morgan et al. in 2003. This study evaluated the BMD-modulus relationship at several anatomical

locations including the vertebra (T10-L5). They derived a relationship of $E=A(density)^B$, where A=4730 and B =1.56 (values from Table 2 in Morgan et al., 2003). This data was used in concert with data from Ulrich et al. (2003) in order to determine the orthotropic properties. Ulrich reports ratios of the moduli in all of the principal coordinates. The material is essentially transversely isotropic with the superior-inferior direction having the greatest modulus.

Cancellous bone properties were assigned to the model based on bone mineral density as obtained from the QCT data. Custom software (QCTMap.c) was written at Exponent to apply the measured Hounsfield numbers (QCT values) to the nodal points within the finite element mesh using temperatures as proxy for density. The quantitative relationships between bone mineral density and elastic modulus in cancellous vertebral bone, as reported by Morgan et al., and Ulrich et al., were utilized to define a nonlinear relationship between temperature (Hounsfield number) and orthotropic elastic modulus. This technique allows spatially variant (inhomogeneous), orthotropic properties to be defined for the cancellous bone in the vertebral body (Figure 1).

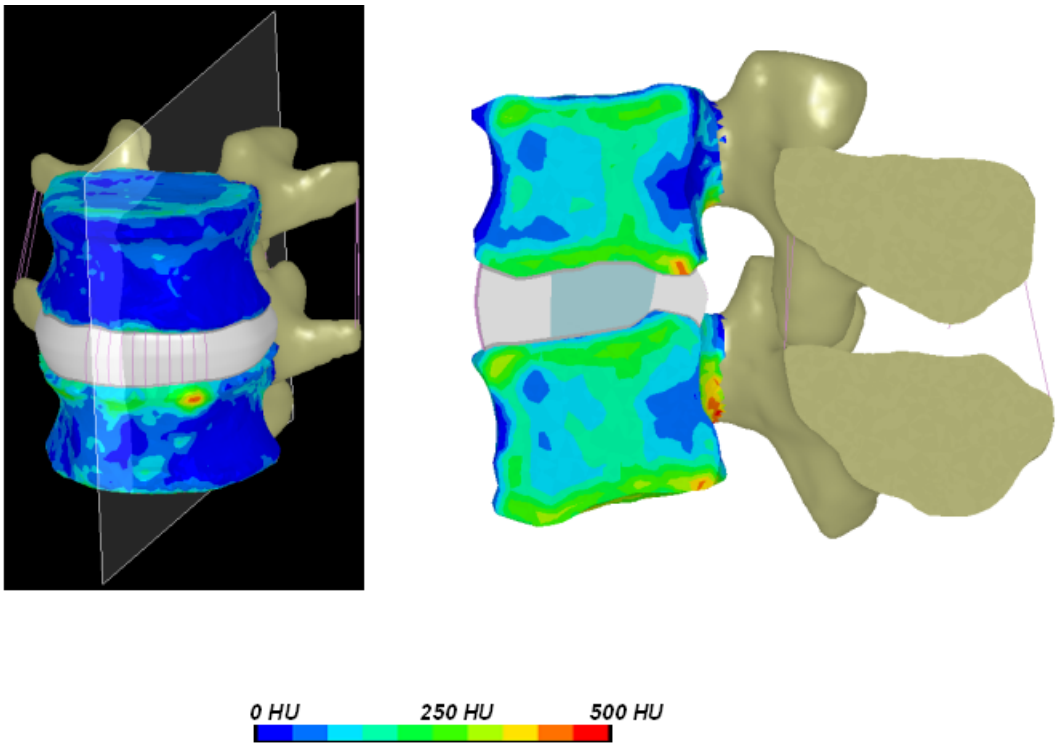

Figure I-3. Images depicting a contour map of the Hounsfield Units within the vertebral bodies of the L3-L4 motion segment finite element model

Cortical Bone and Bony Endplate

Cortical bone around the vertebral bodies was modeled by plating the solid elements of the vertebral body with shell elements. Recently, some models have used a transeversely isotropic material model for cortical bone [7, 8]. However several models use a linear elastic isotropic model. The current model used isotropic material properties that have been well documented in the literature (cortex = 12 GPa and endplate = 1 GPa) [9, 10].

Cartilage Endplate

A single layer of elements (approximately 0.5 mm thick) were defined as cartilage endplates. The material was modeled as linear elastic with a modulus of 24 and Poisson's ratio of 0.4 (Noailly et al. 2005).

Posterior Elements

The posterior elements were modeled as linear elastic with a modulus of 3500 MPa and a Poisson's ratio of 0.25 according to Shirazi-Adl 1986 [11].

Annulus Fibrosus

The AF consists of an incompressible ground substance and collagen fibers running circumferentially at approximately 60 degrees to the endplates. Typically, the AF has been modeled with either a linear or hyper elastic ground substance and nonlinear springs attached at the solid element nodes running in the direction of the collagen fibers [12-14]. A recent calibration study determined material properties for the annulus fibrosus based on results from cadaveric studies. This study indicated an approximate modulus of the ground substance of 1.36 MPa with a Poisson's ratio of 0.46. Therefore the current model used these values and modeled the annulus fibrosus ground substance as linear elastic. The collagen fibers were modeled with fabric elements that plated the circumferential layers of the annulus. The stress vs strain relationship for the collagen fibers were also given in the calibration study and were used for the current model.

Nucleus Pulposus

Currently, the nucleus is typically modeled using an incompressible fluid material [1, 2, 12-15]. However, some modelers are using fluid elements with a bulk modulus of 1667 MPa [12], while others are using a Mooney-Rivlin material law (c1=0.18 and c2=0.03). It is not clear where the bulk modulus for the fluid elements comes from. All references given to justify the selection of this bulk modulus refer to other finite element model studies. The Mooney Rivlin values given were calibrated based on experimental range of motion [16]. Models from both schools have been validated, however, the Mooney Rivlin model has not been validated using intradiscal pressure. Therefore, The current model will use fluid elements with a bulk modulus of 1667 MPa and be compared with experimental intradiscal pressures.

*MAT_001 or *MAT_ELASTIC_FLUID[2] will be used to model the nucleus. This material requires the input of a bulk modulus in place of a Young's modulus and Poisson's ration.

[2] LS-Dyna note - The hourglassing control used for fluid elements appears to artificially stiffen these elements significantly. Although the material appears to not be hourglassing the hourglass energy becomes much larger than the internal energy. To verify this, output a matsum file and look at the hourglassing energy in just the nucleus (*DATABASE_MATSUM). In order to prevent this issue all together, fluid elements should be modeled with element formulation 2 (a fully integrated element – see Dyna keyword manual for more details regarding element formulation). A fully integrated element has no spurious energy states and therefore precludes the concerns associated with hourglassing.

Ligaments

A large variety of spinal ligament material properties have been reported in the literature [11, 17-21]. Stiffness of the various ligaments varies substantially between these studies. For example, Neumann et al, reported a force of 600 N at approximately 2% strain in the ALL compared to 50N at 20% strain reported by Shirazi-Adl. A recent study examined the affects of varying ligament stiffnesses on a finite element model of L3-L4[22]. This study demonstrated that, in terms of intersegmental range of motion, utilization of the stiffest or least stiff properties yielded results that agreed reasonably well with experimental results.

A study by Rohlmann et al. (2006) [23]evaluated the affects of a degenerated disc using a finite element model of an L3-L4 motion segmenet. This study utilized the values of Nolte et al. (1990) and demonstrated range of motions that agreed very well with experimental results and provided a sigmoidal motion response characteristic typical of in vitro study results. Therefore, nonlinear properties for the ligaments reported by Nolte et al. (1990) were used for the current model. Nolte fits experimental data of ligament mechanical testing with an exponential relationship [F = a*(exp (b*(strain-c))-1)]. Where F is the force, a, b, and c are parameters determined by curve-fitting the experimental data, and the strain is the change in length of the ligament along its collagen fiber direction divided by its original length. A spreadsheet was created to allow for implementation of these properties into dyna (bone and ligs.xls). An example of the material and curve are below:

```
$FLAVUM,,,,,,
*MAT_NONLINEAR_ELASTIC_DISCRETE_BEAM
102,0.000000001,102

*DEFINE_CURVE
$ the 0.25 value scales the forces - this depends on the number of
$ springs used to represent the ligament - this example has a total of
$ 4 springs hence the value of 0.25
102,0,0,0.25,0,0,0
-1,-1.5
0,-1.485
0.5,-0.58
1,1.26
1.5,5.059
2,12.853
2.5,28.857
3,61.72
3.5,129.20
4,267.775
```

The force values are scaled by the number of springs that are used to represent that ligament by the scale factor in *DEFINE_CURVE. The formulas used to define the force vs. displacement data are described in Nolte et al., 1990 and Rohlmann et al 2006.

A study by Schmidt et al. [24]calibrated the ligament properties in order to better match in vitro experimental testing. They provided the properties for these ligaments in graph form. The values were extracted from these graphs and used to generate a second set of material property data for the ligaments. Use of these ligament properties resulted in

References

1. Noailly, J., Wilke, H., Planell, J.A., Lacroix, D., *How does the geometry affect the internal biomechanics of a lumbar spine bi-segment fintie element model? Consequences on the validation process.* Journal of Biomechanics, 2007. **40**(11): p. 2414.
2. Rohlmann, A., Burra, N.K., Zander, T., Bergmann, G., *Comparison of the effects of bilateral posterior dynamic and rigid fixation devices on the loads in the*

lumbar spine: a finite element analysis. European Spine Journal, 2007. **Ahead of Print**.

3. Chen, B.H., Natarajan, R.N., An, H.S., Andersson, G.B.J., *Comparison of biomechanical response to surgical procedures used for cervical radiculopathy: Posterior keyhole foraminotomy versus anterior foraminotomy and discectomy versus anterior discectomy with fusion.* Journal of Spinal Disorders, 2001. **14**(1): p. 17-20.
4. Wang, X., Dumas, G.A., *Simulation of bone adaptive remodeling using a stochastic process as loading history.* Journal of Biomechanics, 2002. **35**: p. 375-380.
5. Buckley, J.M., Leang, D.C., Keaveny, T.M., *Sensitivity of vertebral compressive strength to endplate loading distribution.* Journal of Biomechanical Engineering, 2006. **128**: p. 641-646.
6. Eswaran, S.K., Gupta, A., Keaveny, T.M., *Locations of bone tissue at high risk of initial failure during compressive loading of the human vertebral body.* Bone, 2007. **IN PRESS**.
7. Noailly, J., D. Lacroix, and J.A. Planell, *Finite element study of a novel intervertebral disc substitute.* Spine, 2005. **30**(20): p. 2257-64.
8. Noailly, J., et al., *How does the geometry affect the internal biomechanics of a lumbar spine bi-segment finite element model? Consequences on the validation process.* J Biomech, 2007. **40**(11): p. 2414-25.
9. Kumaresan, S., et al., *Contribution of disc degeneration to osteophyte formation in the cervical spine: a biomechanical investigation.* J Orthop Res, 2001. **19**(5): p. 977-84.
10. Silva, M.J., T.M. Keaveny, and W.C. Hayes, *Load sharing between the shell and centrum in the lumbar vertebral body.* Spine, 1997. **22**(2): p. 140-50.
11. Shirazi-Adl, A., A.M. Ahmed, and S.C. Shrivastava, *Mechanical response of a lumbar motion segment in axial torque alone and combined with compression.* Spine, 1986. **11**(9): p. 914-27.
12. Kumaresan, S., Yoganandan, N., Pintar, F.A., Maiman, D., Goel, V.K., *Contribution of disc degeneration to osteophyte formation in the cervical spine: a biomechanical investigation.* Journal of Orthopaedic Research, 2001. **19**: p. 977-984.
13. Rohlmann, A., Zander, T., Schmidt, H., Wilke, H., Bergmann, G., *Analysis of the influence of disc degeneration on the mechanical behaviour of a lumbar motion segment using the finite element method.* Journal of Biomechanics, 2006. **39**(13): p. 2484-2490.
14. Schmidt, H., Heuer, F., Drumm, J., Klezl, Z., Claes, L., Wilke, H., *Application of a calibration method provides more realistic results for a finite element model of a lumbar spinal segment.* Clinical Biomechanics, 2007. **22**(4): p. 377-384.
15. Noailly, J., Lacroix, D., Planell, J.A., *Finite element study of a novel intervertebral disc substitute.* Spine, 2005. **30**(20): p. 2257-2264.
16. Schmidt H, H.F., Simon U, Kettler A, Rohlmann A, Claes L, Wilke HJ., *Application of a new calibration method for a three-dimensional finite element*

model of a human lumbar annulus fibrosus. Clinical Biomechanics, 2006. **21**(4): p. 337-344.
17. Chazal, J., et al., *Biomechanical properties of spinal ligaments and a histological study of the supraspinal ligament in traction.* J Biomech, 1985. **18**(3): p. 167-76.
18. Neumann, P., et al., *Mechanical properties of the human lumbar anterior longitudinal ligament.* J Biomech, 1992. **25**(10): p. 1185-94.
19. Pintar, F.A., et al., *Biomechanical properties of human lumbar spine ligaments.* J Biomech, 1992. **25**(11): p. 1351-6.
20. Goel, V.K., et al., *Interlaminar shear stresses and laminae separation in a disc. Finite element analysis of the L3-L4 motion segment subjected to axial compressive loads.* Spine, 1995. **20**(6): p. 689-98.
21. White, A.A., Panjabi, M.M.,, *Clinical Biomechanics of the Spine, 2nd ed.*1990, Philadelphia-Toronto: J.B. Lippincott Company.
22. Zander, T., A. Rohlmann, and G. Bergmann, *Influence of ligament stiffness on the mechanical behavior of a functional spinal unit.* J Biomech, 2004. **37**(7): p. 1107-11.
23. Rohlmann, A., et al., *Analysis of the influence of disc degeneration on the mechanical behaviour of a lumbar motion segment using the finite element method.* J Biomech, 2006. **39**(13): p. 2484-90.
24. Schmidt, H., et al., *Application of a calibration method provides more realistic results for a finite element model of a lumbar spinal segment.* Clin Biomech (Bristol, Avon), 2007. **22**(4): p. 377-84.
25. Frei H, O.T., Rathonyi GC, Nolte LP., *The Effect of Nucleotomy on Lumbar Spine Mechanics in Compression and Shear Loading.* Spine, 2001. **26**(19): p. 2080-2089.
26. Niosi CA, Z.Q., Wilson DC, Keynan O, Wilson DR, Oxland TR., *Biomechanical characterization of the three-dimensional kinematic behaviour of the Dynesys dynamic stabilization system: an in vitro study.* Eur Spine J, 2005. **15**(6): p. 913-922.

II. Appendix B – Example Input File

The following is an input text file for an intact model of L3-L4 being subjected to 1000 N of compression:

```
*KEYWORD
*TITLE
Intact Compression
$$$$$$$$$$$$$$$$$$$$$$$$$$$$$$$$$$$$$$$$$$$$$$$$$$$$$$$$$$$$$$$$$$$$$$$$$$$$$$$$
$
$ general control - used for number of cpus and structural only (no thermal)
$               also used to help control energies
$
$$$$$$$$$$$$$$$$$$$$$$$$$$$$$$$$$$$$$$$$$$$$$$$$$$$$$$$$$$$$$$$$$$$$$$$$$$$$$$$$
*CONTROL_PARALLEL
2,0,0,0
*CONTROL_SOLUTION
0
*CONTROL_ENERGY
2,
$$$$$$$$$$$$$$$$$$$$$$$$$$$$$$$$$$$$$$$$$$$$$$$$$$$$$$$$$$$$$$$$$$$$$$$$$$$$$$$$
$ Explicit control - determines time step and termination time
$$$$$$$$$$$$$$$$$$$$$$$$$$$$$$$$$$$$$$$$$$$$$$$$$$$$$$$$$$$$$$$$$$$$$$$$$$$$$$$$
*CONTROL_TERMINATION
0.03,0,0.0,0.0,0.0
*CONTROL_TIMESTEP
0.0,0.8,0,0.0,-7.00E-07,0,0,0
$$$$$$$$$$$$$$$$$$$$$$$$$$$$$$$$$$$$$$$$$$$$$$$$$$$$$$$$$$$$$$$$$$$$$$$$$$$$$$$$
$
$ database cards - matsum and glstat used to verify solution accuracy
$
$$$$$$$$$$$$$$$$$$$$$$$$$$$$$$$$$$$$$$$$$$$$$$$$$$$$$$$$$$$$$$$$$$$$$$$$$$$$$$$$
*DATABASE_BINARY_D3PLOT
0.01
*DATABASE_BINARY_INTFOR
0.01
*DATABASE_MATSUM
0.0005,3
*DATABASE_GLSTAT
0.0005,3
*DATABASE_RCFORC
0.0005,3
*DATABASE_RBDOUT
```

```
0.0005,3
$$$$$$$$$$$$$$$$$$$$$$$$$$$$$$$$$$$$$$$$$$$$$$$$$$$$$$$$$$$$$$$$$$$$$$$$$$$$$$$
$
$ system damping - values less than this don't sufficiently damp the system
$
$$$$$$$$$$$$$$$$$$$$$$$$$$$$$$$$$$$$$$$$$$$$$$$$$$$$$$$$$$$$$$$$$$$$$$$$$$$$$$$
*DAMPING_GLOBAL
0,153.25
$$$$$$$$$$$$$$$$$$$$$$$$$$$$$$$$$$$$$$$$$$$$$$$$$$$$$$$$$$$$$$$$$$$$$$$$$$$$$$$
$
$ include files - this brings in all of the necessary files... like the mesh
$
$$$$$$$$$$$$$$$$$$$$$$$$$$$$$$$$$$$$$$$$$$$$$$$$$$$$$$$$$$$$$$$$$$$$$$$$$$$$$$$
*INCLUDE
l3-4.k
*INCLUDE
mats.k
*INCLUDE
ligs.k
*INCLUDE
l3-4-temps.k
$$$$$$$$$$$$$$$$$$$$$$$$$$$$$$$$$$$$$$$$$$$$$$$$$$$$$$$$$$$$$$$$$$$$$$$$$$$$$$$
$
$ Loading conditions
$
$$$$$$$$$$$$$$$$$$$$$$$$$$$$$$$$$$$$$$$$$$$$$$$$$$$$$$$$$$$$$$$$$$$$$$$$$$$$$$$
$ 1000 N Compressive Load
*LOAD_SEGMENT_SET
11,3,1,0
*DEFINE_CURVE
3,0,0.0,0.0,0.0,0.0,0
0.0,0.0
0.005,1.6
1,1.6
$$$$$$$$$$$$$$$$$$$$$$$$$$$$$$$$$$$$$$$$$$$$$$$$$$$$$$$$$$$$$$$$$$$$$$$$$$$$$$$
$
$ Boundary conditions
$
$$$$$$$$$$$$$$$$$$$$$$$$$$$$$$$$$$$$$$$$$$$$$$$$$$$$$$$$$$$$$$$$$$$$$$$$$$$$$$$
*BOUNDARY_SPC_SET
1,,1,1,1
*CONTACT_AUTOMATIC_SURFACE_TO_SURFACE
5,6,0,0,,,1,1
0.0,0.0,0.0,0.0,0.0,0,0.0,0.0
0.0,0.0,0.0,0.0,0.0,0.0,0.0,0.0
```

0.0,0.0,0
*END

III. Appendix C – Example material property input file

```
*KEYWORD
$
$ MATERIAL CARDS
$
$ Units are from LS-DYNA course manual
$ mass = ton
$ length = mm
$ time = s
$ force = N
$ stress = MPa
$ energy = N-mm
$
$$$$$$$$$$$$$$$$$$$$$$$$$$$$$$$$$$$$$$$$$$$$$$$$$$$$$$$$$$$$$$$$$$$$$$$$
$
$   Intervertebral Disc
$
$
$$$$$$$$$$$$$$$$$$$$$$$$$$$$$$$$$$$$$$$$$$$$$$$$$$$$$$$$$$$$$$$$$$$$$$$$
*MAT_ELASTIC
2,1.0E-09,1.36,0.45,,,
*HOURGLASS
2,1,0,0,0.0,0.0
*SECTION_SOLID
2,2,0
*PART
L3/4 AF
2,2,2,0,2,0,0,0
$
$ DEFINITION OF MATERIAL     103
$
$*MAT_ELASTIC
$1,1.0e-09,4.0,0.48,,,
*MAT_ELASTIC_FLUID
1,1.000E-09,,,,,1667E+00
0.1,1.0E+20
*SECTION_SOLID
1,2,0
*PART
L3/4 NP
1,1,1,0,,0,0,0
*MAT_FABRIC
29,1.000E-09,1.0,1.0,1.0,0.0,0.0,0.0
```

```
0.0,0.0,0.0,1.0,0.0,0.0,0.0,0.5
0.0,0.0,0.0,0.0,0.0,4.0
0.0,0.0,0.0,0.0,0.0,0.0
0.0,0.0,0.0,0.0,0.0,0.0
30,29
*HOURGLASS
29,0,0.0,0,0.0,0.0
*SECTION_SHELL
29,1,0.0,3.0,0.0,0.0,1
0.07E+00,0.07E+00,0.07E+00,0.07E+00,0.0
0,90,0
$ Ea is the inf-sup direction
$ these curves are based on the Schmidt calibration study
*DEFINE_CURVE
30,0,0.0,0.0,0.0,0.0,0
0.0,0.0
0.013,0.75
0.06,25
0.1,35
0.2,45
$ Eb is the circumferential direction
*DEFINE_CURVE
29,0,0.0,0.0,0.0,0.0,0
0.0,0.0
0.013,1.3
0.06,43.3
0.1,60.62
0.2,78
*PART
L3/4 AF
28,29,29,0,29,0,0,0
*PART
L3/4 AF
29,29,29,0,29,0,0,0
*PART
L3/4 AF
30,29,29,0,29,0,0,0
*PART
L3/4 AF
31,29,29,0,29,0,0,0
*PART
L3/4 AF
32,29,29,0,29,0,0,0
*PART
L3/4 AF
```

```
33,29,29,0,29,0,0,0
*PART
L3/4 AF
34,29,29,0,29,0,0,0
*PART
L3/4 AF
35,29,29,0,29,0,0,0
$$$$$$$$$$$$$$$$$$$$$$$$$$$$$$$$$$$$$$$$$$$$$$$$$$$$$$$$$$$$$$$$$$$$$$$$$$$
$
$   Ligaments
$
$$$$$$$$$$$$$$$$$$$$$$$$$$$$$$$$$$$$$$$$$$$$$$$$$$$$$$$$$$$$$$$$$$$$$$$$$$$
*SECTION_BEAM
100,6,,,,2.0,

*PART
ALL
18,100,100
*PART
PLL
19,100,101
*PART
flavum
20,100,102
*PART
ISL
23,100,103
*PART
SSL
24,100,104
*PART
CAPS
21,100,105
*PART
ITL
22,100,106
$$$$$$$$$$$$$$$$$$$$$$$$$$$$$$$$$$$$$$$$$$$$$$$$$$$$$$$$$$$$$$$$$$$$$$$$$$$
$
$   Endplates
$
$$$$$$$$$$$$$$$$$$$$$$$$$$$$$$$$$$$$$$$$$$$$$$$$$$$$$$$$$$$$$$$$$$$$$$$$$$$
$
$ cartilage endplate (used by Noailly 2005 and 2007)
*MAT_ELASTIC
4,1.0e-09,24,0.4,,,
```

```
*HOURGLASS
4,6,0.5,0,0.0,0.0
*SECTION_SOLID
4,1,0
*PART
cartilage endplate
4,4,4,0,4,0,0,0
$
$ bony endplate
*MAT_ELASTIC
25,1.874E-09,1E+03,0.2,,,
*HOURGLASS
25,1,0.0,0,0.0,0.0
*SECTION_SHELL
25,1,0.0,3.0,0.0,0.0,0
2.5E-01,2.5E-01,2.5E-01,2.5E-01,0.0
*PART
S1 Superior Endplate
25,25,25,0,25,0,0,0
$$$$$$$$$$$$$$$$$$$$$$$$$$$$$$$$$$$$$$$$$$$$$$$$$$$$$$$$$$$$$$$$$$$$$$$$
$
$   Cortex and Cancellous bone
$
$$$$$$$$$$$$$$$$$$$$$$$$$$$$$$$$$$$$$$$$$$$$$$$$$$$$$$$$$$$$$$$$$$$$$$$$
$
$ posterior elements from Shirazi-Adl 1986
$
*MAT_ELASTIC
3,1.500E-09,3.5E3,0.3,,,
*HOURGLASS
3,1,0,0,0.0,0.0
*SECTION_SOLID
3,10,0
*PART
Posterior Elements
3,3,3,0,3,0,0,0
$
$ cortical bone
$
*MAT_ELASTIC
26,1.874E-09,12E+03,0.3,,,
*HOURGLASS
26,1,0.0,0,0.0,0.0
*SECTION_SHELL
26,1,0.0,3.0,0.0,0.0,0
```

```
0.4,0.4,0.4,0.4,0.0
*PART
Cortex
26,26,26,0,26,0,0,0
$
$ L4 vertebral body cancellous bone
*MAT_TEMPERATURE_DEPENDENT_ORTHOTROPIC
17,1.200E-09,2.0
$ first unit vector is the medial to lateral direction and the second is anterior-posterior
,,,0.992,0.12,-0.001
,,,-0.132,0.953,-0.269
21.0,14.4,50.0,0.226,0.399,0.381
0.0,0.0,0.0,7.65,9.15,6.55,-2000.0
21.0,14.4,50.0,0.226,0.399,0.381
0.0,0.0,0.0,7.65,9.15,6.55,-900.0
21.0,14.4,50.0,0.226,0.399,0.381
0.0,0.0,0.0,7.65,9.15,6.55,-800.0
21.0,14.4,50.0,0.226,0.399,0.381
0.0,0.0,0.0,7.65,9.15,6.55,-700.0
21.0,14.4,50.0,0.226,0.399,0.381
0.0,0.0,0.0,7.65,9.15,6.55,-600.0
21.0,14.4,50.0,0.226,0.399,0.381
0.0,0.0,0.0,7.65,9.15,6.55,-500.0
21.0,14.4,50.0,0.226,0.399,0.381
0.0,0.0,0.0,7.65,9.15,6.55,-400.0
21.0,14.4,50.0,0.226,0.399,0.381
0.0,0.0,0.0,7.65,9.15,6.55,-300.0
21.0,14.4,50.0,0.226,0.399,0.381
0.0,0.0,0.0,7.65,9.15,6.55,-200.0
21.0,14.4,50.0,0.226,0.399,0.381
0.0,0.0,0.0,7.65,9.15,6.55,-100.0
21.0,14.4,50.0,0.226,0.399,0.381
0.0,0.0,0.0,7.65,9.15,6.55,0.0
37.9,25.9,90.3,0.226,0.399,0.381
0.0,0.0,0.0,13.8,16.5,11.8,100.0
118.0,80.6,281.0,0.226,0.399,0.381
0.0,0.0,0.0,43.0,51.4,36.8,200.0
226.0,154.0,538.0,0.226,0.399,0.381
0.0,0.0,0.0,82.3,98.5,70.5,300.0
357.0,244.0,850.0,0.226,0.399,0.381
0.0,0.0,0.0,130.0,156.0,111.0,400.0
508.0,347.0,1210.0,0.226,0.399,0.381
0.0,0.0,0.0,185.0,222.0,159.0,500.0
678.0,463.0,1610.0,0.226,0.399,0.381
0.0,0.0,0.0,247.0,295.0,211.0,600.0
```

864.0,591.0,2060.0,0.226,0.399,0.381
0.0,0.0,0.0,315.0,377.0,270.0,700.0
1070.0,729.0,2540.0,0.226,0.399,0.381
0.0,0.0,0.0,389.0,465.0,333.0,800.0
1280.0,877.0,3060.0,0.226,0.399,0.381
0.0,0.0,0.0,468.0,559.0,400.0,900.0
1510.0,1030.0,3610.0,0.226,0.399,0.381
0.0,0.0,0.0,552.0,660.0,472.0,1000.0
1760.0,1200.0,4190.0,0.226,0.399,0.381
0.0,0.0,0.0,641.0,766.0,549.0,1100.0
2020.0,1380.0,4800.0,0.226,0.399,0.381
0.0,0.0,0.0,734.0,879.0,629.0,1200.0
2290.0,1560.0,5440.0,0.226,0.399,0.381
0.0,0.0,0.0,833.0,996.0,713.0,1300.0
2570.0,1750.0,6110.0,0.226,0.399,0.381
0.0,0.0,0.0,935.0,1120.0,801.0,1400.0
2860.0,1950.0,6810.0,0.226,0.399,0.381
0.0,0.0,0.0,1040.0,1250.0,892.0,1500.0
3170.0,2160.0,7540.0,0.226,0.399,0.381
0.0,0.0,0.0,1150.0,1380.0,987.0,1600.0
3480.0,2380.0,829.0,0.226,0.399,0.381
0.0,0.0,0.0,1270.0,1520.0,1090.0,1700.0
3810.0,2600.0,9060.0,0.226,0.399,0.381
0.0,0.0,0.0,1390.0,1660.0,1190.0,1800.0
4140.0,2830.0,9860.0,0.226,0.399,0.381
0.0,0.0,0.0,1510.0,1800.0,1290.0,1900.0
4490.0,3070.0,10700.0,0.226,0.399,0.381
0.0,0.0,0.0,1640.0,1960.0,1400.0,2000.0
4840.0,3310.0,11500.0,0.226,0.399,0.381
0.0,0.0,0.0,1760.0,2110.0,1510.0,2100.0
5210.0,3560.0,12400.0,0.226,0.399,0.381
0.0,0.0,0.0,1900.0,2270.0,1630.0,2200.0
5590.0,3820.0,13300.0,0.226,0.399,0.381
0.0,0.0,0.0,2030.0,2430.0,1740.0,2300.0
5970.0,4080.0,14200.0,0.226,0.399,0.381
0.0,0.0,0.0,2170.0,2600.0,1860.0,2400.0
6360.0,4350.0,15200.0,0.226,0.399,0.381
0.0,0.0,0.0,2320.0,2770.0,1990.0,2500.0
6770.0,4620.0,16100,0.226,0.399,0.381
0.0,0.0,0.0,2470.0,2950.0,2110.0,2600.0
7180.0,4910.0,17100.0,0.226,0.399,0.381
0.0,0.0,0.0,2.610.0,3130.0,2240.0,2700.0
7600.0,5190.0,18100.0,0.226,0.399,0.381
0.0,0.0,0.0,2770.0,3310.0,2370.0,2800.0
8030.0,5480.0,19100,0.226,0.399,0.381

0.0,0.0,0.0,2920.0,3500.0,2500.0,2900.0
8460.0,5780.0,20200.0,0.226,0.399,0.381
0.0,0.0,0.0,3080.0,3690.0,2640.0,3000.0
8910.0,6090.0,21200.0,0.226,0.399,0.381
0.0,0.0,0.0,3250.0,3880.0,2780.0,3100.0
9360.0,6400.0,22300.0,0.226,0.399,0.381
0.0,0.0,0.0,3410.0,4080.0,2920.0,3200.0
9820.0,6710.0,23400.0,0.226,0.399,0.381
0.0,0.0,0.0,3580.0,4280.0,3060.0,3300.0
10300.0,7030.0,24500.0,0.226,0.399,0.381
0.0,0.0,0.0,3750.0,4480.0,3210.0,3400.0
10800.0,7360.0,25600.0,0.226,0.399,0.381
0.0,0.0,0.0,3920.0,4690.0,3360.0,3500.0
11300.0,7690.0,26800.0,0.226,0.399,0.381
0.0,0.0,0.0,4100.0,4900.0,3510.0,3600.0
18800.0,12800.0,44800.0,0.226,0.399,0.381
0.0,0.0,0.0,6850.0,8190.0,5860.0,5000.0
$ L3
*MAT_TEMPERATURE_DEPENDENT_ORTHOTROPIC
16,1.200E-09,2.0
$ first unit vector is the medial to lateral direction and the second is anterior-posterior
,,,0.99,0.136,-0.017
,,,-0.072,0.996,-0.053
21.0,14.4,50.0,0.226,0.399,0.381
0.0,0.0,0.0,7.65,9.15,6.55,-2000.0
21.0,14.4,50.0,0.226,0.399,0.381
0.0,0.0,0.0,7.65,9.15,6.55,-900.0
21.0,14.4,50.0,0.226,0.399,0.381
0.0,0.0,0.0,7.65,9.15,6.55,-800.0
21.0,14.4,50.0,0.226,0.399,0.381
0.0,0.0,0.0,7.65,9.15,6.55,-700.0
21.0,14.4,50.0,0.226,0.399,0.381
0.0,0.0,0.0,7.65,9.15,6.55,-600.0
21.0,14.4,50.0,0.226,0.399,0.381
0.0,0.0,0.0,7.65,9.15,6.55,-500.0
21.0,14.4,50.0,0.226,0.399,0.381
0.0,0.0,0.0,7.65,9.15,6.55,-400.0
21.0,14.4,50.0,0.226,0.399,0.381
0.0,0.0,0.0,7.65,9.15,6.55,-300.0
21.0,14.4,50.0,0.226,0.399,0.381
0.0,0.0,0.0,7.65,9.15,6.55,-200.0
21.0,14.4,50.0,0.226,0.399,0.381
0.0,0.0,0.0,7.65,9.15,6.55,-100.0
21.0,14.4,50.0,0.226,0.399,0.381
0.0,0.0,0.0,7.65,9.15,6.55,0.0

37.9,25.9,90.3,0.226,0.399,0.381
0.0,0.0,0.0,13.8,16.5,11.8,100.0
118.0,80.6,281.0,0.226,0.399,0.381
0.0,0.0,0.0,43.0,51.4,36.8,200.0
226.0,154.0,538.0,0.226,0.399,0.381
0.0,0.0,0.0,82.3,98.5,70.5,300.0
357.0,244.0,850.0,0.226,0.399,0.381
0.0,0.0,0.0,130.0,156.0,111.0,400.0
508.0,347.0,1210.0,0.226,0.399,0.381
0.0,0.0,0.0,185.0,222.0,159.0,500.0
678.0,463.0,1610.0,0.226,0.399,0.381
0.0,0.0,0.0,247.0,295.0,211.0,600.0
864.0,591.0,2060.0,0.226,0.399,0.381
0.0,0.0,0.0,315.0,377.0,270.0,700.0
1070.0,729.0,2540.0,0.226,0.399,0.381
0.0,0.0,0.0,389.0,465.0,333.0,800.0
1280.0,877.0,3060.0,0.226,0.399,0.381
0.0,0.0,0.0,468.0,559.0,400.0,900.0
1510.0,1030.0,3610.0,0.226,0.399,0.381
0.0,0.0,0.0,552.0,660.0,472.0,1000.0
1760.0,1200.0,4190.0,0.226,0.399,0.381
0.0,0.0,0.0,641.0,766.0,549.0,1100.0
2020.0,1380.0,4800.0,0.226,0.399,0.381
0.0,0.0,0.0,734.0,879.0,629.0,1200.0
2290.0,1560.0,5440.0,0.226,0.399,0.381
0.0,0.0,0.0,833.0,996.0,713.0,1300.0
2570.0,1750.0,6110.0,0.226,0.399,0.381
0.0,0.0,0.0,935.0,1120.0,801.0,1400.0
2860.0,1950.0,6810.0,0.226,0.399,0.381
0.0,0.0,0.0,1040.0,1250.0,892.0,1500.0
3170.0,2160.0,7540.0,0.226,0.399,0.381
0.0,0.0,0.0,1150.0,1380.0,987.0,1600.0
3480.0,2380.0,829.0,0.226,0.399,0.381
0.0,0.0,0.0,1270.0,1520.0,1090.0,1700.0
3810.0,2600.0,9060.0,0.226,0.399,0.381
0.0,0.0,0.0,1390.0,1660.0,1190.0,1800.0
4140.0,2830.0,9860.0,0.226,0.399,0.381
0.0,0.0,0.0,1510.0,1800.0,1290.0,1900.0
4490.0,3070.0,10700.0,0.226,0.399,0.381
0.0,0.0,0.0,1640.0,1960.0,1400.0,2000.0
4840.0,3310.0,11500.0,0.226,0.399,0.381
0.0,0.0,0.0,1760.0,2110.0,1510.0,2100.0
5210.0,3560.0,12400.0,0.226,0.399,0.381
0.0,0.0,0.0,1900.0,2270.0,1630.0,2200.0
5590.0,3820.0,13300.0,0.226,0.399,0.381

```
0.0,0.0,0.0,2030.0,2430.0,1740.0,2300.0
5970.0,4080.0,14200.0,0.226,0.399,0.381
0.0,0.0,0.0,2170.0,2600.0,1860.0,2400.0
6360.0,4350.0,15200.0,0.226,0.399,0.381
0.0,0.0,0.0,2320.0,2770.0,1990.0,2500.0
6770.0,4620.0,16100,0.226,0.399,0.381
0.0,0.0,0.0,2470.0,2950.0,2110.0,2600.0
7180.0,4910.0,17100.0,0.226,0.399,0.381
0.0,0.0,0.0,2.610.0,3130.0,2240.0,2700.0
7600.0,5190.0,18100.0,0.226,0.399,0.381
0.0,0.0,0.0,2770.0,3310.0,2370.0,2800.0
8030.0,5480.0,19100,0.226,0.399,0.381
0.0,0.0,0.0,2920.0,3500.0,2500.0,2900.0
8460.0,5780.0,20200.0,0.226,0.399,0.381
0.0,0.0,0.0,3080.0,3690.0,2640.0,3000.0
8910.0,6090.0,21200.0,0.226,0.399,0.381
0.0,0.0,0.0,3250.0,3880.0,2780.0,3100.0
9360.0,6400.0,22300.0,0.226,0.399,0.381
0.0,0.0,0.0,3410.0,4080.0,2920.0,3200.0
9820.0,6710.0,23400.0,0.226,0.399,0.381
0.0,0.0,0.0,3580.0,4280.0,3060.0,3300.0
10300.0,7030.0,24500.0,0.226,0.399,0.381
0.0,0.0,0.0,3750.0,4480.0,3210.0,3400.0
10800.0,7360.0,25600.0,0.226,0.399,0.381
0.0,0.0,0.0,3920.0,4690.0,3360.0,3500.0
11300.0,7690.0,26800.0,0.226,0.399,0.381
0.0,0.0,0.0,4100.0,4900.0,3510.0,3600.0
18800.0,12800.0,44800.0,0.226,0.399,0.381
0.0,0.0,0.0,6850.0,8190.0,5860.0,5000.0
*HOURGLASS
16,6,0.5,0,0.0,0.0
*SECTION_SOLID
16,10,0
*PART
L4 QCT Based Modulus
17,16,16,0,16,0,0,0
*PART
L3 QCT Based Modulus
16,16,16,0,16,0,0,0
$$$$$$$$$$$$$$$$$$$$$$$$$$$$$$$$$$$$$$$$$$$$$$$$$$$$$$$$$$$$$$$$$$$$$$$$
$  Rigid Bodies
$$$$$$$$$$$$$$$$$$$$$$$$$$$$$$$$$$$$$$$$$$$$$$$$$$$$$$$$$$$$$$$$$$$$$$$$
*MAT_RIGID
27,1.04E-09,3.5E+03,0.2,,,
1,0,4
```

```
*SECTION_SHELL
27,1,0.0,3.0,0.0,0.0,0
0.1,0.1,0.1,0.1,0.0
*PART
Rigid L3
27,27,27,0,,0,0,0
$ALL,
*MAT_GENERAL_NONLINEAR_1DOF_DISCRETE_BEAM
100,1e-9,,0
100

*DEFINE_CURVE
100,0,0,0.0909,0,0,0
-0.001,-0.0005
0,0
0.001,25
0.005,56.18
0.01,73.429
0.015,95.04
0.02,122.13
0.025,156.08
0.03,198.63
0.035,251.9
0.04,318.795
0.045,402.55
0.05,507.523
0.055,639.07
0.06,803.952
0.065,1010.5
0.07,1269.54
0.075,1594.0
0.08,2000.83
0.085,2510.5
0.09,3149.44
0.095,3950.0
0.1,4953.522
$PLL,,
*MAT_GENERAL_NONLINEAR_1DOF_DISCRETE_BEAM
101,1e-9,,0
101

*DEFINE_CURVE
101,0,0,0.14285,0,0,0
-0.01,-0.00005
```

```
0,0
0.08,1.724
0.09,10.97
0.1,29.279
0.11,65.47
0.12,137.0
0.13,278.62
0.14,558.61
0.15,1112.34
0.16,2207.45
0.17,4373.27
0.18,8656.65
0.19,17127.92
$FLAVUM,,,,,,
*MAT_GENERAL_NONLINEAR_1DOF_DISCRETE_BEAM
102,1e-9,,0
102

*DEFINE_CURVE
102,0,0,0.25,0,0,0
-1,-0.00005
0,0
1,1.26
1.5,5.05
2,12.85
2.5,28.85
3,61.72
3.5,129.20
4,267.775
4.5,552.3
5,1136.59
5.5,2336.3
6,4799.96
6.5,9858.73
7,20246
7.5,41576
$ISL,
*MAT_GENERAL_NONLINEAR_1DOF_DISCRETE_BEAM
103,1e-9,,0
103

*DEFINE_CURVE
103,0,0,0.125,0,0,0
-1,-0.0001
0,0
```

```
2.25,2.017
2.5,8.59
2.75,20.94
3,44.14
3.25,87.73
3.5,169.59
3.75,323.35
4,612.16
4.25,1154.65
4.5,2173.63
4.75,4087.6
$SSL,,,,,,
*MAT_GENERAL_NONLINEAR_1DOF_DISCRETE_BEAM
104,1e-9,,0
104

*DEFINE_CURVE
104,0,0,0.25,0,0,0
-1,-0.001
0,0
3,1.84
4,14.6
5,34.22
6,64.23
7,110.17
8,180.53
9,288.29
10,453.32
11,706.061
12,1093.11
13,1685.87
14,2593.65
15,3983.89
16,6112.98
$CAPS,,,,,,
*MAT_GENERAL_NONLINEAR_1DOF_DISCRETE_BEAM
105,1e-9,,0
105

*DEFINE_CURVE
105,0,0,0.1,0,0,0
-0.1,-0.001
0,0
2.4,10
2.7,15
```

```
3.1,20
3.3,30
3.6,50
3.85,80
4,120
4.1,150
4.25,200
$ITL,,,,,,
*MAT_GENERAL_NONLINEAR_1DOF_DISCRETE_BEAM
106,1e-9,,0
106

*DEFINE_CURVE
106,0,0,0.3333,0,0,0
-10,-0.01
0,0
10,1.78
20,6.1
30,12.4
40,21
50,34.8
60,53
70,81
80,121
90,179
100,263
110,384
120,560
130,813
140,1180
150,1711
160,2479
170,3590
*END
```

IV. Appendix D. Raw Data

Validation

Bone Strain

	Left Rim	Left Endplate	Central Endplate	Right Endplate	Right Rim
FEA (intact)	529.0335292	1023.68764	1895.92822	1003.878238	515.022176
Experimental (intact)	283	868	1803	700	283
min	192	137	1014	273	215
max	711	4497	3227	2548	463
min from median	91	731	789	427	68
max from median	428	3629	1424	1848	180

	Posterior Endplate	Central Endplate	Anterior Endplate	Anterior Rim
FEA (intact)	417.8	1895.9	1026.8	615.5
Experimental (intact)	636	1803	1017	543
min	464	1014	176	431
max	2032	3227	3168	916
min from median	172	789	841	112
max from median	1396	1424	2151	373

Facet Contact Force

	Facet Contact Force (N)		
	FEM	Niosi 2008	Std. Dev
Axial Rotation	162.417	55	18
Extension	68.8418	27	10
Flexion	0	4	4
Lateral Bending	34.394	16	14

Kinematics

	Niosi w/ CFL		Niosi no CFL		FEM w/ CFL	FEM no CFL
	RoM	Std Dev	RoM	Std Dev		
Axial Rotation	1.2	0.5	2.1	0.9	1.6	2.1
Extension	2.4	0.9	3.3	1.5	2.3	2.3
Flexion	4.4	2.0	3.7	1.5	3.6	3.5
Lateral Bending	2.4	1.2	3.8	1.4	1.8	1.9

Chapter 1

Rotation Data

Flexion	RoM (radians)	RoM (degrees)
Intact	0.074998	4.297068872
0.1	0.082281	4.714354034
1	0.077995	4.468784323
4	0.073109	4.188837144
100	0.055825	3.198536891
Extension	RoM (radians)	RoM (degrees)
Intact	0.065205	3.735971303
0.1	0.073419	4.206598836
1	0.066998	3.838702636
4	0.059028	3.382055273
100	0.037876	2.170134945
Axial Rotation	RoM (radians)	RoM (degrees)
Intact	0.030041	1.721222512
0.1	0.032105	1.839481001
1	0.028792	1.649660084
4	0.024703	1.415377641
100	0.011336	0.649504957
Lateral Bending	RoM (radians)	RoM (degrees)
Intact	0.047693	2.732607612
0.1	0.043227	2.476724661
1	0.041322	2.367576201
4	0.038092	2.182510833
100	0.025826	1.479720802

Facet Contact Force Data

	Facet Contact Force (N)				
	Flexion	**Extension**	**Axial Rotation**	**Lateral Bending**	**Compression**
Intact	0	149.2	165.1	57.2	32.3
0.1 MPa	0	147.7	158	49.3	30.1
1 MPa	0	155.7	165.6	61.6	33.3
4 MPa	0	158.3	166.3	66.7	39
100 MPa	0	142.6	157.4	55.8	19.5

Disc Shear Strain Data

	Flexion	**Extension**	**Axial Rotation**	**Lateral Bending**	**Compression**
Intact	38%	54%	51%	53%	50%
0.1 MPa	61%	75%	78%	68%	74%
1 MPa	38%	52%	34%	40%	35%
4 MPa	32%	42%	28%	34%	28%
100 MPa	17%	20%	10%	18%	10%

Center of Rotation

Axial Rotation

	I	j	k	X	Y	Z	Theta (rads)	Theta (degs)
"01"	-0.046264	-0.011506	0.99886	50.834	99.555	0	0.037678	2.15879038
"1"	-0.033135	-0.01539	0.99933	46.366	98.434	0	0.032987	1.890015879
"4"	-0.033763	-0.015959	0.9993	46.094	96.274	0	0.027978	1.603021319
"100"	-0.093916	-0.017809	0.99542	63.092	80.49	0	0.012155	0.6964302
Intact	-0.032943	-0.016678	0.99932	46.512	97.24	0	0.03449	1.976131435

Extension

	I	j	k	X	Y	Z	Theta (rads)	Theta (degs)
"01"	0.99999	-0.0033072	-1.29E-05	0	65.848	225.28	0.060056	3.440955334
"1"	0.99996	-0.0083627	0.0024244	0	64.856	226.26	0.051263	2.937153545
"4"	0.99995	-0.0093486	-0.0025663	0	64.839	223.5	0.052736	3.021550228
"100"	0.99995	-0.0084833	-0.0042788	0	63.61	220.07	0.031332	1.795191364
Intact	0.9999	-0.014237	0.00071992	0	63.4	225.89	0.042231	2.419658065

Flexion

	I	j	k	X	Y	Z	Theta (rads)	Theta (degs)
"01"	-0.99998	0.0056481	0.00063991	0	64.01	215.97	0.083472	4.782593308
"1"	-0.99999	0.0048052	0.001921	0	63.007	216.18	0.077617	4.447126518
"4"	-0.99999	0.0035534	-0.0011219	0	62.588	216.64	0.063331	3.628599012
"100"	-0.99999	0.0040312	-0.00152	0	63.191	215.35	0.046915	2.688031496
Intact	-1	0.0017826	0.00073818	0	62.874	217.63	0.081822	4.688055271

Lateral Bending

	I	j	k	X	Y	Z	Theta (rads)	Theta (degs)
"01"	-0.0027094	0.99998	6.29E-03	44.29	0	211.22	0.04027	2.307301041
"1"	-0.011265	0.99993	0.0044273	45.728	0	210.67	0.037435	2.144867506
"4"	-0.010267	0.99992	0.0074407	46.077	0	210.06	0.03527	2.020822143
"100"	-0.02708	0.99963	-0.0012093	47.718	0	214.1	0.022546	1.291790645
Intact	-0.0097292	0.99995	0.0037657	46.76	0	208.31	0.044413	2.544677456

Chpater 2

Kinematics

	Axial Rotation	Extension	Lateral Bending	Flexion
Intact	2.53	3.21	2.34	3.93
0 mm	4.55	5.45	3.50	4.31
2 mm	2.72	4.22	2.62	3.77
4 mm	1.73	3.11	2.17	3.58
4mm friction		2.71		3.40

Facet Contact Force

	Axial Rotation	Extension	Lateral Bending	Flexion
Intact	148.206	77.3619	22.5241	0
0 mm	124.131	45.716	11.7451	0
2 mm	152.078	50.1747	14.2836	0
4 mm	161.723	103.865	25.6539	0
4mm friction		82.3		0

Chapter 3

RoM

	Intact	**Posterior**	**Anterior**
axial rotation	1.56	5.38	3.96
extension	2.27	11.48	4.43
flexion	3.61	7.97	10.79
lateral bending	1.76	4.53	2.75

FCF

	Intact	Posterior	Anterior
axial rotation	158.80	221.40	162.90
extension	94.10	7.69	95.27
flexion	3.10	336.81	269.51
lateral bending	45.60	136.56	11.30

Chapter 4

Intact Results

ES Force	RoM	Disc Normal Force	Disc Shear Force	Peak von Mises Stress (Mpa)
0	0.06	443.61	106.97	0.47
25	0.05	406.19	94.06	0.40
50	0.03	393.45	74.47	0.32
75	0.02	398.00	58.74	0.26
100	0.00	409.59	40.92	0.26
125	-0.01	424.15	23.21	0.30

Facet Contact Forces

Facet Contact Resultant

	Intact	Mobile 0mm	Mobile 3mm	Fixed 0mm	Fixed 3mm
125	146.27	218.20	217.96	172.78	122.03
100	168.03	189.76	199.29	150.31	70.00
75	145.65	168.65	145.98	187.25	137.74
50	126.41	134.11	88.04	268.95	165.31
25	104.80	112.84	58.65	281.86	185.38
0	85.87	103.44	17.25	285.42	194.79

y forces

	Intact	Mobile 0mm	Mobile 3mm	Fixed 0mm	Fixed 3mm
125.00	131.61	162.79	190.58	135.12	107.20
100.00	149.81	160.14	188.97	136.95	65.75
75.00	131.41	157.52	139.70	177.88	129.25

50.00	116.65	126.19	82.94	250.31	154.89
25.00	96.19	102.91	54.85	256.08	172.48
0.00	78.62	94.12	0.00	261.06	181.18

z forces

	Intact	Mobile 0mm	Mobile 3mm	Fixed 0mm	Fixed 3mm
125.00	63.34	142.22	105.50	105.20	57.42
100.00	75.47	100.86	63.19	61.65	23.97
75.00	62.35	59.60	42.36	57.61	47.41
50.00	48.34	45.41	29.53	98.37	57.31
25.00	41.23	45.94	20.51	117.74	67.43
0.00	34.39	42.83	16.85	115.37	70.99

Kinematics

Sagittal Rotation

	Intact	Mobile 0mm	Mobile 3mm	Fixed 0mm	Fixed 3mm
125	-0.62	-0.34	-4.10	-0.27	-7.61
100	0.21	0.19	-3.83	0.45	1.88
75	1.11	0.87	-1.12	1.57	3.96
50	1.99	4.14	3.48	3.65	4.60
25	2.86	5.01	4.41	4.78	5.00
0	3.67	5.35	4.86	5.10	5.24

A-P Translation

	Intact	Mobile 0mm	Mobile 3mm	Fixed 0mm	Fixed 3mm
125	-0.13764	-0.2222	-2.7456	-0.13235	-6.5798
100	0.57314	0.31564	-2.5053	0.57177	2.2711
75	1.3276	0.94634	-0.088402	1.6011	4.1473
50	2.0403	3.523	3.7035	3.4079	4.7442
25	2.7131	4.1746	4.4349	4.3445	5.1143
0	3.3058	4.438	4.7931	4.5976	5.3308

Chapter 5

Retrieval Clinical Data

Implant	Level	Dome Wear (mm)	Wear Rate (mm/yr)	Maximum Rim Thickness	Rim Penetration (mm)	Rim Penetration Rate (mm/y)
BR 002	L4/L5	0.391	0.176	1.760	0.028	0.013
Maa 010	L5/S1	0.371	0.044	4.802	0.019	0.002
Maa 018	L4/L5	0.333	0.031	2.929	0.059	0.006
Maa 022	L4/L5	0.216	0.041	2.976	0.386	0.073
Maa 023	L5/S1	0.228	0.049	2.958	0.028	0.006
Maa 025	L4/L5	0.613	0.045	4.752	0.098	0.007
Maa 027	L3/L4	0.205	0.050	1.891	0.358	0.088
Maa 032	L5/S1	0.369	0.035	2.885	0.274	0.026
Maa 033	L5/S1	0.157	0.025	1.880	0.026	0.004
Maa 034	L5/S1	0.223	0.025	2.914	0.064	0.007

Implant	PE Locked? (Chronic Impingement)	Any sign of Impingement?	Max Dome OI	Max Rim C	Implantation Time (years)	Facet A-P Force
BR 002	Yes	No	0.865	2.178	2.219	86.078
Maa 010	No	Yes	0.488	3.610	8.471	33.915
Maa 018	Yes	No	0.386	1.624	10.578	22.668
Maa 022	Yes	No	0.562	2.881	5.279	59.852
Maa 023	No	Yes	0.207	0.878	4.611	34.888
Maa 025	Yes	No	0.641	2.251	13.627	29.974
Maa 027	Yes	No	0.537	5.900	4.074	118.734
Maa 032	Yes	No	0.561	6.908	10.460	40.589
Maa 033	No	Yes	0.226	2.452	6.414	25.697
Maa 034	Yes	No	0.248	1.294	8.781	77.843

Finite Element Model Results

Implant	Facet A-P Force	Disc A-P	Facet Inf-Sup	Disc Inf-Sup	Facet Resultant	Disc Resultar	A-P translation	Inf-Sup translation
BR 002	86.078	-47.863	72.801	484.620	113.117	486.979	-3.665	-1.840
Maa 010	33.915	-167.711	16.278	485.006	42.225	513.325	1.524	-0.789
Maa 018	22.668	-89.542	29.734	445.051	39.195	454.041	-1.617	-1.262
Maa 022	59.852	-118.013	69.925	477.796	100.585	492.550	-2.417	-1.679
Maa 023	34.888	-196.551	27.299	511.862	50.186	548.585	2.630	-0.563
Maa 025	29.974	-29.123	19.757	490.121	36.129	490.990	-1.912	-1.314
Maa 027	118.734	-70.440	95.803	460.256	152.591	465.708	-2.614	-2.301
Maa 032	40.589	-172.830	95.207	429.919	113.488	464.557	-3.498	-1.702
Maa 033	25.697	-162.558	41.257	482.447	61.917	509.734	-2.023	-1.186
Maa 034	77.843	-241.770	99.659	408.484	139.497	476.716	-3.112	-1.239

Implant	Extensio	Rotation (degrees)	Total Lordosis from FEM	Total Lordosis from X-Ray	%differenc e	Angular Difference	Peak First Princ Strain
BR 002	-0.117	-6.677	0.523	12.590	-23.058	-12.067	0.041
Maa 010	-0.010	-0.593	13.807	16.000	-0.159	-2.193	0.005
Maa 018	-0.085	-4.862	2.338	9.800	-3.192	-7.462	0.032
Maa 022	-0.100	-5.728	1.472	22.110	-14.024	-20.638	0.112
Maa 023	0.066	3.790	18.190	11.200	0.384	6.990	0.003
Maa 025	-0.088	-5.025	2.175	9.860	-3.534	-7.685	0.012
Maa 027	-0.104	-5.938	1.262	15.310	-11.127	-14.048	0.050
Maa 032	-0.156	-8.913	5.487	20.500	-2.736	-15.013	0.035
Maa 033	-0.110	-6.286	8.114	17.300	-1.132	-9.186	0.036
Maa 034	-0.135	-7.723	6.677	23.100	-2.460	-16.423	0.055

Implant	Peak Contact Stress Superior	Peak Contact Stress Inferior	%angular difference magnitude	%angular difference magnitude4	Dome heig
BR 002	7.430	8.700	23.058	0.093	8.109
Maa 010	6.710	7.070	0.159	0.067	11.129
Maa 018	4.760	7.050	3.192	0.188	9.167
Maa 022	8.280	7.780	14.024		9.284
Maa 023	4.460	5.610	0.384	0.056	9.272
Maa 025	8.260	4.410	3.534	0.193	10.887
Maa 027	10.520	8.320	11.127	0.165	8.295
Maa 032	6.050	6.470	2.736	0.121	9.131
Maa 033	5.970	8.560	1.132	0.164	8.343
Maa 034	6.590	4.920	2.460	0.044	9.277

Implant	Disc height Distraction	Erector Spinae Force (N)	Peak von Mises Strain	Local Core Normal	Local Core Transverse
BR 002	2.700	300.000	0.044	-487.529	45.803
Maa 010	6.000	275.000	0.005	-514.157	1.375
Maa 018	3.700	225.000	0.035	-460.360	25.048
Maa 022	3.700	300.000	0.119	-502.338	96.999
Maa 023	4.000	295.000	0.005	-549.515	1.103
Maa 025	5.200	250.000	0.014	-488.148	47.169
Maa 027	2.700	300.000	0.056	-462.299	68.898
Maa 032	4.000	300.000	0.040	-459.637	46.160
Maa 033	3.000	300.000	0.039	-512.995	22.311
Maa 034	4.000	300.000	0.061	-473.762	35.463

Implant	Local Core Resultant
BR 002	489.676
Maa 010	514.159
Maa 018	461.041
Maa 022	511.617
Maa 023	549.516
Maa 025	490.421
Maa 027	467.405
Maa 032	461.949
Maa 033	513.480
Maa 034	475.087

Disc Height Distraction

Implant Name	Dome Height	Max height of implant	Distraction of FE Model (mm)
BR-002	8.5	13.1	**2.7**
Maa010	11.5	16.1	**6**
Maa018	9.5	14.1	**3.7**
Maa022	9.5	14.1	**3.7**
Maa023	9.5	14.1	**4**
Maa025	11	15.6	**5.2**
Maa027	8.5	13.1	**2.7**
Maa032	9.5	14.1	**4**
Maa033	8.5	13.1	**3**
Maa034	9.5	14.1	**4**

Implant Size

Name	Endplate Size	Height (mm)	File	Level
BR 002	3	8.11	chariteno18.prt.3	L4/L5
Maa 010	3	11.13	chariteno9.prt.2	L5/S1
Maa 018	3	9.17	chariteno8.prt.4	L4/L5
Maa 022	3	9.28	chariteno8.prt.4	L4/L5

Maa 023	3	9.27	chariteno8.prt.4	L5/S1
Maa 025	3	10.89	chariteno9.prt.2	L4/L5
Maa 027	4	8.30	chariteno20.prt.2	L3/L4
Maa 032	3	9.13	chariteno8.prt.4	L5/S1
Maa 033	4	8.34	chariteno20.prt.2	L5/S1
Maa 034	3	9.2768	chariteno8.prt.4	L5/S1

Footplate Angles

Implant	EP 1	EP 2
BR-002	0	7.5
Maa-010	0	0
Maa-018	0	0
Maa-022	0	5
Maa-025	0	0
Maa-027	0	0
Maa-032	5	5
Maa-033	0	7.5
Maa-034	5	5
Maa-023	7.5	0

Chapter 6

Summary tables within chapter 6 contained all of the extracted data